Hybrid Trigeneration

Thermally Activated Heat Pump Technologies

Luke Bannar-Martin

Design Engineering Group
Department of Mechanical Engineering
Imperial College London

A Thesis submitted to Imperial College London in partial fulfillment for the degree of Doctor of Philosophy and Diploma of Imperial College

September 13, 2015

Declaration

I declare that the work reported in this Thesis was conducted by me at Imperial College London and has not been submitted in part, or in whole, for any other qualifications.

Acknowledgements

I wish to record my thanks to Professor Peter R.N. Childs, Head of the School of Design Engineering of Imperial College London, for his constant enthusiasm and guidance as my supervisor. I also wish to express my sincere thanks to the Royal Commission for the Exhibition of 1851 for their unwavering support of this research. I would also like to extend my thanks the Climate Knowledge and Innovation Community for their support of the research and the excellent opportunities they afforded to me. Finally, I would like to thank all those who have helped along the way; there are simply too many names to list.

Abstract

This Thesis describes a theoretical approach to the design and analysis of concepts in the field of trigeneration, which is the combined generation of electricity, hot water and chilled water from a single prime mover. The continuously increasing demand for cooling in modern buildings and cities due to economic expansion, which is further compounded by the effects of climate change, means that there is a tremendous opportunity for new concepts in the fields of trigeneration, refrigeration and heat pump cycles and technologies. It is this opportunity which forms the context and primary aim for the research presented within this Thesis, which is to identify high performance heat pump cycle concepts.

A thorough review of trigeneration systems, controls and operational strategies is presented, which demonstrates their energetical benefits in terms of Primary Energy Consumption (PEC) and Energy Utilisation Factor (EUF). This is followed by a review of the state of the art in absorption chiller cycles, adsorption chiller cycles and R744 (carbon dioxide) Mechanical Vapour Compression (MVC) heat pump cycles. To fulfil the main aim of this research, the focus of the review is in multi - stage / multi - effect absorption and adsorption chillers, hybrid compression - absorption chillers and high temperature R744 heat pump and supercritical Brayton cycles.

A number of novel absorption heat pump cycle concepts are modeled and analysed, the most advanced of which being: a double - stage / triple - effect ammonia - water absorption heat pump cycle, and a triple - stage / triple - effect lithium bromide - water compression - absorption heat pump cycle. Under certain operating

parameters, these cycles are capable of achieving a Coefficient Of Performance (COP) in cooling of upto 2.0. However, they are not believed to represent the best opportunity for further research due to: the inability for simultaneous heat and coolth production; potential corrosion problems resulting from the high temperatures; the extremely high volumetric flowrate of steam required through compressors; the significant body of research which has explored almost all avenues for innovations in absorption heat pump cycles.

A novel thermally activated transcritical R744 heat pump cycle is developed, which combines the principles of both the Brayton cycle and reverse Rankine cycle. The cycle is designed to utilise relatively hot gas turbine exhaust ($\sim 500°C$) gases to produce low temperature hot water and chilled water for domestic hot water and space cooling, respectively. The cycle itself achieves a COP of 1.58 and 2.41 in cooling and heating respectively with a maximum inlet temperature of 350 °C. A Coefficient of Performance in cooling of 1.58 is comparable to a triple - stage / triple - effect lithium bromide - water absorption heat pump cycle. The principal advantage of the novel cycle is that it simultaneously produces hot water ($\sim 65°C$), while absorption chillers are not capable of producing heat and coolth simultaneously.

Certain components of the novel R744 heat pump cycle are analysed in detail, including: R744 heat exchangers, R744 two - phase ejector, R744 compressor and work expanders. A design and calculation methodology is presented with the purpose of forming the continuation of this research from a Technology Readiness Level[1] of 2 (technology concept and / or application formulated) to a Technology Readiness Level of 3 (analytical and experimental critical function and / or characteristic proof - of - concept).

[1]Technology Readiness Level is a widely used concept to estimate the maturity of specific technologies

Acronyms

CCGT Combined Cycle Gas Turbine.

CCHP Combined Cooling, Heating & Power.

CCP Combined Cooling & Power.

CFC ChloroFluoroCarbon.

CHP Combined Heat & Power.

COP Coefficient Of Performance.

CSP Concentrated Solar Power.

DHW Domestic Hot Water.

DSG Direct Steam Generation.

EES Engineering Equation Solver.

EHR Exhaust Heat Recovery.

EHRSG Exhaust Heat Recovery Steam Generator.

ELF Electric Load Following.

EUF Energy Utilisation Factor.

FESR Fuel Energy Savings Ratio.

GAX Generator - Absorber Exchange.

GAXAC Generator Absorber Exchange Absorption Compression.

GWP Global Warming Potential.

HC HydroCarbon.

HCFC HydroChloroFluoroCarbon.

HFC HydroFluoroCarbon.

HLF Hybrid Load Following.

HX Heat Exchanger.

LTHW Low Temperature Hot Water.

MTHW Medium Temperature Hot Water.

MVC Mechanical Vapour Compression.

ODP Ozone Depletion Potential.

ORC Organic Rankine Cycle.

PEC Primary Energy Consumption.

PGU Primary Generation Unit.

S-CO2 Supercritical Carbon Dioxide.

SCP Specific Cooling Production.

TLF Thermal Load Following.

VLTHW Very Low Temperature Hot Water.

VRA Vapour Recompression Absorber.

Subscripts

$_{c}$ Cooling.

$_{h}$ Heating.

$_{m}$ Mechanical.

$_{PEC}$ Primary Energy Consumption.

$_{th}$ Thermal.

Refrigerants

CH_3OH - LiBr Methanol & Lithium Bromide.

CH_3OH - LiCl Methanol & Lithium Chloride.

CH_3OH - TEGDME Methanol / TetraEthyleneGlycol-DiMethylEther.

H_2O-LiBr:LiI:$LiNO_3$-LiCl Water / Lithium Bromide : Lithium Iodide : Lithium Nitrate : Lithiurm Cloride (5 : 1 : 1 : 2).

H_2O - NH_3 Water & Ammonia.

LiBr - H_2O Lithium Bromide Water.

R115 Chloropentafluoroethane.

R12 Dichlorodifluoromethane.

R125 Pentafluoroethane.

R134a 1,1,1,2-Tetrafluoroethane.

R143a 1,1,1-Trifluoroethane.

R22 Difluoromonochloromethane.

R22 - TEGDME R22 / TetraEthyleneGlycol-DiMethylEther.

R290a Propane.

R32 Difluoromethane.

R407c 23 % R32 / 25 % R125 / 52 % R134a.

R410a 50 % R125 / 50 % R32.

R502 51.2 % R115 / 48.8 % R22.

R507 50 % R125 / 50 % R143a.

R600a Isobutane.

R717 Ammonia.

R744 Carbon Dioxide.

R744a Nitrous Oxide.

TFE - TEGDME TriFluoroEthanol / TetraEthyleneGlycol-DiMethylEther.

Symbols

Nu = Nusselt Number ($\frac{hL}{k}$).

Pr = Prandtl Number ($\frac{\nu}{\alpha}$).

Re = Reynolds Number ($\frac{vL}{\nu}$).

$\Omega = \frac{\dot{Q}_{generator}}{\dot{W}_{pump}}$ (i.e the ratio of external heat input to the generator and external mechanical input to the solution pump).

$\Phi = \frac{\dot{Q}_{solution,recuperation}}{\dot{Q}_{rectifier,recuperation}}$ (i.e. the ratio of recuperated heat from the solution heat exchanger and the recuperated heat from the rectifier (relevant to H_2O - NH_3 absorption heat pumps)).

$\Psi = \frac{\dot{m}_{refrigerant\ \ produced}}{\dot{m}_{strong\ \ solution}}$ (i.e. the ratio of mass flow rate of refrigerant in the absorption chiller and the mass flow rate of solution exiting the absorber and returning to the generator).

$\Theta = 1 - \frac{Q_{gen.,in}}{Q_{gen.,in} + Q_{solution\ hx} + Q_{rect.,out}}$ (i.e. the proportion generator heat input which is internally recuperated (relevant to H_2O - NH_3 absorption heat pumps)).

f = Friction factor.

$x = \frac{m_{refrigerant}}{m_{solution}}$ (i.e. the proportion of the fluid which passes through the condenser and evaporator in an ammonia - water absorption heat pump which is the refrigerant, ammonia).

Contents

List of Figures

Chapter 1

Review of Trigeneration Systems

1.1 Context

It is estimated that residential, commercial and industrial air conditioning consumes approximately 1×10^{12} kWh of electricity annually worldwide [1]. The effect of climate change is expected to increase worldwide air conditioning demand by 72% by the year 2100 [2]. This statistic is independent from increases in air conditioning demand resulting from societal changes, economic changes and changes in building design, use and thermal efficiency. The prospective economic development of Asia and Africa, in particular, will have a profound effect on the demand for air conditioning. Upper estimates predict a global increase in air conditioning demand to rise to 1×10^{13} kWh [1]. It is well documented in the media of this day that China and India experience regular and significant shortfalls in electricity supply during hot periods. This commonly results in brownouts and blackouts, factory closures, disconnection of residential supples, and loss of economic output.

Conversely, worldwide heating demand is expected to decrease by 34% over the same period of time as a result of climate change. There is therefore significant scope and opportunity for new cooling technologies, and the integration of heating and cooling technologies to deliver increased efficiencies and primary energy savings; this is the basis for, and focus of, this Thesis.

1.2 Trigeneration Systems

The term trigeneration, or Combined Cooling, Heating & Power (CCHP), implies the simultaneous production of electricity, heating and cooling from a single energy source. Trigeneration is a concept born from the ideal of fully utilising the available energy from a power generation system, typically achieved through the recuperation of exhaust heat from the Primary Generation Unit (PGU). Given the relative difficulty of transmitting heating and cooling flows compared to electricity, trigeneration systems are solely used in distributed power generation systems.

Crucial in the design and optimsation of trigeneration systems is the matching of economical, energetical and environmental factors; commonly referred to as the *'3 - E Trilemma'* [3].

A review of trigeneration systems is given by Wu and Wang[4], which gives a high level analysis of the performance and financial aspects of cogeneration and trigeneration systems, PGUs, absorption and adsorption chiller working fluids. It also provides a summary and commentary of the nature cogeneration and trigeneration systems all all scales across the USA, Europe and Asia. The trigeneration system review presented within this Chapter includes an overview of Trigeneration system design, operation and control strategies, as well as a brief overview of subsystems: Primary Generation Units (PGUs), thermal storage devices.

1.2.1 Trigeneration Subsystems

A typical trigeneration system will comprise of these basic subsystems; a Primary Generation Unit (PGU), an Exhaust Heat Recovery (EHR) device and a chilling device. Almost without exception further subsystems are necessary to ensure energetic feasibility, and these may include; an electrical storage device, a hot / cold thermal storage device, an auxiliary boiler, a secondary heat pump (mechanically activated to supplement thermally activated - See Chapter 3) and the wider electrical grid. When a trigeneration system has two subsystems for producing the same energy flow, the system is referred to as a hybrid trigeneration system.

Primary Generation Unit

Suitable PGUs for trigeneration applications include: Rankine cycle devices, internal combustion engines (both liquid and gas fueled), open and closed cycle gas turbines, fuel cells, concentrated solar driven Brayton and Rankine cycle devices.

Steam Turbine A principal design consideration when selecting steam turbines is whether the steam exit pressure is higher or lower than atmospheric

pressure, the former of which is commonly referred to as a backpressure turbine and the latter a condensing turbine. A backpressure turbine enables steam at an intermediate pressure to be produced for other uses, whilst a condensing turbine allows electrical and thermal power outputs to be varied. Steam turbines are very reliable and have an extremely long life if corrected maintained. However, slow response time, low conversion efficiency at smaller scale and poor part load performance severly limit their use in distributed trigeneration systems.

Internal Combustion Engines Commonplace in systems below 1 MW_e, reciprocating engines are split into two categories: compression ignition and spark ignition, which typically use diesel and gas. They are a very flexible power source, with fast start up and excellent partial load efficiency. However, they are complex and require frequent maintenance, which means that their availability is lower than the other PGUs mentioned. Further, it is difficult to fully utilise the various heat sources and diverse temperature levels in the context of a trigeneration system.

Gas Turbines Whilst gas turbines are often used as the PGU in large scale Combined Heat & Power (CHP), their use in systems below $\sim$5 MW_e is uneconomical due to their low high cost per kW_e. Gas turbines typically have lower capital and maintenance costs than reciprocating engines, as well as more affordable NO_x emissions control systems, which are vital for installation in emissions controlled zones. With exhaust temperatures around 500 °C, there is significant scope for subsequent processes (*e.g.* high temperature Organic Rankine Cycle (ORC) systems, multi-stage absorption chillers, phase change thermal storage). Much like steam turbines, gas turbines also suffer from poor part load performance and slower response time than reciprocating engines, as well as significantly diminished performance at higher ambient temperatures and lower ambient pressures.

Fuel Cells Fuel cells pose an interesting prospect for PGUs in a distributed generation system, particularly in large cities where emissions and noise control is vital. Fuel cells are quiet, compact and require very little maintenance. There are five major fuel cell technologies [5], the most mature of which are based on a phosphoric acid electrolyte; however, fuel cells based upon a solid oxide electrolyte, typically a yttrium stabilised zirconia, show great promise in CHP and CCHP applications due to their high efficiency and operational temperatures (600 - 1,000 °C). Potential fuels for these types of fuel cell are numerous and include hydrogen, natural or biogas and alcohols.

Chilling Device

This is presented in Chapter 2.

Thermal Storage Device

Sensible Sensible heat storage refers to thermal storage systems where the storage media does not undergo any chemical of phase related changes; energy stored is simply the product of the mass, specific heat and the temperature difference ($Q_{sens.} = \int_{T_1}^{T_2} m \cdot c_p(T) \cdot \mathrm{d}T$). Suitable storage mediums are greatly influenced by a number of properties, including: thermal conductivity, thermal diffusivity, heat loss coefficient, operational temperatures, vapour pressure, chemical compatibility and cost. Sensible heat storage media can be categorised as either solid or liquid, and single or dual media [6].

In solid medium systems the media is usually packed in beds and a heat transfer fluid passes through the beds; this is known as a dual storage system. Layering the storage medium in strata (packed beds) promotes thermal stratification, which is advantageous because it allows for a high level of thermal control. For example, the hot strata is in discharging mode when cold fluid is passing through, and the cold strata is in charging mode when hot fluid is passing through. One major problem with dual storage stratified systems is the large pressure drop and

consequent required pumping power consumption, resulting from passing the heat transfer fluid through the beds [7].

In liquid medium systems it is possible for the thermal stratification of the storage media to be maintained passively . In order to utilize this characteristic, the hot fluid must enter the storage vessel at the top (during charging), whilst the cold fluid must exit the storage vessel at the bottom (during discharging). This type of storage is known as thermocline and relies upon the density differences between the hot and cold fluid, due to thermal expansion. The storage medium itself has a large implication on the design of the storage system.

In single medium systems the storage medium itself circulates through the charging heat exchanger directly. Single medium systems can operate with one or two tanks. Dual tank systems utilise a cold tank for the cold fluid being discharged and a hot tank for the hot fluid being charged. The flow rate of hot and cold fluid is controlled, such that during periods of high demand and low heat supply the cold fluid has a high flow rate and the hot fluid has a low flow rate implying the storage system is in a pure discharging mode. Single tank systems are known as thermocline storage systems and, as previously explained, operate as a result of density variations in the hot and cold fluid. Extensive research into thermocline storage has been conducted by Kandari et al.[8].

The principal characteristic of the dual media storage system is that the storage medium is stationary and does not circulate around the plant. The storage medium can be a solid or liquid undergoing sensible heating, or a phase change material. Typically, the heat transfer fluid passes directly through the storage media, although for solid medium the heat is usually transferred by a heat exchanger and not direct contact. There are however some major drawbacks with dual media systems [6]. Firstly, when the system is discharging the storage material naturally cools down which causes the temperature of the heat transfer to decrease increasing the thermal inertia of the system, reducing the speed at which the system can switch from discharging back to charging. Secondly, the

thermal conductivity capabilities of the storage media/HTF must be sufficient to satisfy the internal heat transfer requirements, in order to charge or discharge at an acceptable rate. A poor thermal conductive material can result in greatly reduced performance and high thermal gradients across the media, a potentially serious problem with some solid media.

Sensible liquid storage mediums in use today and under research are predominantly oils and salts [6, 7, 9–11]. Salts have the advantage of low cost, but most exhibit a high freezing point, which means that parasitic heating may be required to present them from freezing during periods of low storage demand. Typical salts used for heat storage include nitrate, nitrite and carbonate salts. Synthetic and silicone oils are also used, which these come at a higher cost. Synthetic oils are also hazardous, which place restrictions on their use in certain environments.

Latent The underlying concept of latent heat thermal storage is to utilise the large amount of energy required in forcing a material to undergo a phase change ; ie. heat of vaporization, heat of fusion or heat of a solid-solid crystalline transformation. When latent heat themal storage is chosen over sensible heat storage the result could be a significantly smaller storage system, without the negative effects of temperature glide associated with sensible heat storage. The difficulties with latent heat storage systems lie around the heat transfer mechanisms, transport mechanisms and the properties of the storage medium itself; research has shown that the performance of medium degrades quite rapidly after only a small number of freeze-melt cycles [6, 10]. A number of recent studies have focused on methods of enhancing heat transfer through the addition of finds, multitubes, insertion/dispersion of high thermal conductivity materials and micro/macro encapsulation [12].

A comprehensive list of potential Phase Change Materials (PCM) for use in thermal storage systems is given by Agyenim et al. [12] and Sharma et al [13]. Considerable research into latent heat thermal storage has focused on applications in domestic space heating and cooling, with common PCMs including: paraffin,

salts, wax, n-octadecane and stearic acid [10, 14]. Very few studies into medium temperature latent heat thermal storage for absorption chiller space exist.

RedOx & Thermochemical RedOx, or reduction and oxidation, reactions can be used as an extremely effective method of storing thermal energy, and have therefore become the focus of significant amounts of research into thermal storage techniques [3, 6, 13, 15]. During charging, thermal energy is essentially converted into chemical bonds via a reduction reaction, whilst during discharging thermal energy is released via an oxidation reaction. RedOx thermal storage has not been demonstrated at a commercial level and only recently at a prototype level due to the complex fundamental challenges which must be overcome.

There are an almost limitless number of materials which could potentially be used in a RedOx thermal storage systems, including: hydroxides, carbonates and metal oxides, and mixtures thereof. There are two fundamental design concepts governing the operation of RedOx thermal storage reactors; direct and indirect heat exchange. Direct heat exchange involves the flow of heat transfer fluid, typically the gaseous reactant and/or an inert gas, through the storage media. Indirect heat exchange means that the hot/cold fluid passes through an external heat exchanger.

The performance of indirectly heated reactors is significantly hampered by the poor thermal conductivity of the fixed bed, which in the case of calcium hydroxide ($Ca(OH)_2$) has been measured to be below 1 W/m.K [16]. This results in poor conversion (oxidation) of the media during discharging. Hence, this is an area which requires rigorous research and development to ensure the successful deployment of indirectly heated RedOx thermal storage systems.

Directly heated reactors negate the effects of poor thermal conductivity associated with indirectly heated reactors [16], due to the direct mixing of the hot/cold fluid with the media. However, this in turn creates other issues which must be addressed; mass transfer, pressure gradients, reaction rates and thermal capacity of the hot/cold feed stream. It is noted by Van Essen et al. [15] that

for an optimal heat storage media the rate of chemical reaction must be considerably higher than the rate of heat transport, a view echoed by Schaube [16]. Although an increase in reaction rate serves to improve the reactor conversion performance, its effect is limited by the thermal capacitance of the feed stream. To overcome this phenomenon the mass flow of feed stream has to be increased in accordance with the heat generated by the reactor (provided the system is in discharging / hydration / oxidation). The increased flow rate through the reactor leads to an increase in pressure drop over the fixed bed reaction zone, which in turn implies in a higher pumping power is required.

Metal oxide based heat storage has been highlighted by Wong and Brown [17]; ten potential multivalent metal oxides as storage media are considered in this study. The oxides were identified using both feasibility studies and thermodynamic modeling. It was discovered through non-isothermal redox measurements, all ten candidate oxides underwent full thermal reduction under heating with air, but only seven indicated a measurable level of oxidation during cooling. The most promising of these was a mixture of 90 % cobalt oxide and 10 % iron oxide (by mass).

Sorption Absorption thermal storage using NaOH and H_2O has been studied in depth as a method of long term thermal storage. During charging, thermal energy is produced (often by a solar collector) and drives the desorption process, whilst the ground acts a heat sink. During discharging, the ground/ambient air acts as a heat source, whilst the absorption process upgrades the heat source to useful levels for space heating and hot water supply. The theoretical storage density of NaOH is 250 kWh/m^3, and its cost is approximately €250 per m^3 [3]. In order to improve the quality of heat produced during the discharging process, a double-stage cycle has been conceptualised and is due to be created and analysed by Weber and Dorer [18]. It is expected that the addition of the second stage will decrease the storage density, resulting in a much larger and more complex system.

One of the most promising thermochemical storage technologies for space heating applications is the thermochemical accumulator . This is an absorption process which uses a fluid pair operating in the solid, solution and vapour phases. Sorption systems operate with either solution and vapour phases (absorption) or solid and vapour phases (adsorption). TCA systems using LiCl salt and water have achieved an experimental storage density of 253 kWh/m^3, and an experimental cooling COP [1] of 0.46 [19]. However, the very high cost of LiCl (€3500 per m^3) is very prohibitive to the success of this technology.

Sorption storage can also be provided by adsorption chillers, via the desorption and adsorption of a fluid onto a solid surface. The quality of the heat stored can vary dependent upon the number of stages within the cycle and the chosen fluid-pair, but temperatures of below 80°C to above 300°C are possible [3]. The prospect of seasonal sorption heat storage for space heating and cooling was studied by Mottillo, Zmeureanu and Beausoleil-Morrison [20]. The analysed system consisted of a solid oxide fuel cell cogeneration system, coupled to a hot water tank for short-term thermal storage and a sorption storage unit for long-term thermal storage. The author concluded that the sorption storage system successfully provided heat during the winter months which would otherwise come from a back-up boiler, but during the summer months the sorption unit did not store sufficient amounts of thermal energy, as the temperature of the heat source (fuel cell coolant) was not high enough to fully charge the unit.

There are two types of adsorption processes; physical adsorption (physisorption) and chemical adsorption (chemisorption), the former of which is due to Van der Waals forces and the latter valency forces. Examples of physisorption solid-fluid pairs are zeolite-water and silicagel-water. Zeolites are alumina silicates with high micro-porosity, and are fully compliant with all environmental regulations. Zeolite and water sorption storage systems using synthetic zeolites have reached experimental storage densities of 124 kWh/m^3 in heating and 100 kWh/m^3 in

[1] The Coefficient of Performance (COP) is the ratio of the external work input (mechanical or thermal) into the system and the useful cooling or heating effect produced by the system.

cooling, with COPs of 0.9 and 0.86 respectively [3]. Silicagel-water has been shown to reach an experimental storage density of 50 kWh/m^3, although theoretically 200-300 kWh/m^3. Examples of chemisorption pairs are sodium sulphide-water (Na_2S-H2O), magnesium sulphate heptahydrate ($MgSO_4$-$7H_2O$) and iron hydroxide ($Fe(OH)_2$). Sodium hydrate is a highly corrosive substance and operates under a vacuum, and has a measured storage density of 1980 kWh/m^3 in heating and 1300 kWh/m^3 in cooling, with a COP of 0.84 and 0.57, respectively. Magnesium sulphate heptahydrate is promising for solar energy storage, with a storage density of 780 kWh/m^3 and an inlet temperature of 122 °C. $MgSO_4$-$7H_2O$ is non-corrosive and non-toxic but very expensive (€4870 per m^3) [3]. Magnesium sulphate heptahydrate ($MgSO_4 7H_2O$) and iron hydroxide ($Fe(OH)_2$) appear to be the most promising chemisoption pairs, with storage densities an order of magnitude higher than that of conventional hot water storage.

Sorption storage technologies can be further defined in terms of open and closed systems. Open systems operate at atmospheric pressure and the working fluid vapour, typically water, is realised to the environment. In closed systems the regeneration requires a higher temperature, which is useful if the desired storage temperature is high.

1.2.2 Trigeneration System Design

Trigeneration system design is a term used to encompass all factors concerning the basic design of the system: energy inputs, flows, outputs and wastes. This is achieved via individual subsystem design and a top level system design. In a separate system, energetic efficiency is the key performance driver behind the system design, which can be complex in a trigeneration system design due to the interactivity of the different subsystems. Subsystems will often be required to operate at sub - optimal efficiencies, in order to maximise the EUF of the Trigeneration system as a whole.

A theoretical study of a conceptual trigeneration system is documented by

Ameri et al. [21]. The system utilises a micro gas turbine coupled to a Exhaust Heat Recovery Steam Generator (EHRSG) and three further subsystems which achieve the follows tasks: domestic hot water production, winter heating production and summer cooling production. The proposed system has two 'operational modes', in winter mode the system works purely as a CHP plant, whilst in the summer the system works purely as a Combined Cooling & Power (CCP) plant.

In winter mode, the steam produced by the EHRSG directed to a heat exchanger where water is heated for building ambient space heating. In summer mode, the steam produced by the EHRSG is directed to a steam ejector refrigeration cycle, which produces chilled water for building ambient space cooling. In both modes, a proportion of the steam is directed to another heat exchanger for the production of building hot water. Compared to a system consisting of a grid connected centralised power station, a gas boiler and an electrically driven MVC chilling device, the system proposed by Ameri et al. provides a Fuel Energy Savings Ratio (FESR) of between 29 and 33 % and EUF of between 69 and 77 % in the winter (CHP) mode. The corresponding values for FESR and EUF in the summer (CCP) mode are between 18 and 21 %, and 53 and 58 %, respectively. It can be noted that both the FESR and EUF are more favourable in the CHP mode. However, the proposed system requires an auxiliary boiler to achieve the required heating and cooling load in the winter and summer respectively.

A competing analysis of a similar system is put forward by Li et al. [22], with very different results obtained. In typical cogeneration (dedicated CHP systems) and trigeneration studies, the reference case is assumed to be a coal separate production; this is a flaw which provides inaccurate results, due to the intrinsic difference between coal and gas. In this study the reference case features a Combined Cycle Gas Turbine (CCGT) system as the generation method, and high efficiency natural gas boilers as the heating method and high efficiency compression chillers as the cooling method. The trigeneration is as described by Ameri et al. [21], although the ejector refrigeration cycle is replaced by an absorption

chiller (with an associated increase in efficiency). As a result of this viewpoint, the results indicate that under certain conditions the trigeneration system actually has a negative FESR. In scenarios where there is a demand for cooling the proposed systems exhibits a negative FESR almost without exception, whilst the opposite is observed during periods of demand for heating. The values of FESR for trigeneration systems which use gas engines as the PGU range from - 40 % to 5 % in cooling mode and 15 % to 25 % in heating mode. Therefore, one can conclude that the overall annual FESR of trigeneration systems strongly depends on the ratio of heating hours to yearly operation hours, τ.

A range of algorithms used to obtain the optimal system design are well documented in the literature [23–26], including: linear sequential quadratic, non - linear sequential quadratic, tri - commodity simplex, extended power simplex, genetic and Lagrangian relaxation.

A hybrid trigeneration system comprising a PGU, EHR device, auxiliary boiler, absorption chiller and MVC chiller has been optimised using genetic algorithm by Wang. et al [23]. The analysis indicates that the proposed system would, in the absence of the MVC chiller, produce a negative FESR when the average temperature is above a certain threshold. It therefore follows that a system which features both absorption and MVC chillers would require significantly less primary fuel to satisfy the cooling demand. An identical system is proposed by Fumo et al. [27] and analysed for two cities in USA; the results indicating that hybrid trigeneration is more likely to produce a positive FESR in colder climates, where the demand for cooling is less. Due to the low COP of absorption chillers, the system thermal efficiency in electricity - cooling mode is lower than in electricity - cooling mode.

A trigeneration system for total energy provision for a supermarket in the UK is proposed and analysed by Tassou [28]; the system features an 80 kW_e micro - gas turbine with pre - heat, a EHR device and an absorption chiller. The absorption chiller is a commercially available gas - fired ammonia - water chiller (ROBUR

ACR-60LB), with a cooling capacity of 12 kW and a measured COP of between 0.32 and 0.57, for brine outlet temperatures of −11 °C and 3 °C respectively. In supermarkets, approximately 50 % of the electricity is used for refrigeration, whilst 25 % is used for lighting and the remaining 25 % for cooking and ventilation and computer systems [29, 30]. Assuming a conservative COP for the refrigeration systems, this implies that the chilling demand in kW_{th} is three times greater than the total non - refrigeration based kW_e electrical consumption. The price of gas was found to have a notable effect on the system payback period; a change of ± 20 % from the base value alters the payback period by ± 40 %. Further, the gas - to - electricity price ratio ('spark spread'), ζ, has a profound effect on the payback period; when $\zeta = 0.2$ the payback period is 2.7 years, when $\zeta = 0.3$ the payback period is 4.5 years, when $\zeta = 0.4$ the payback period is 13.7 years [28]. The high sensitivity of the economical feasibility of the system to gas prices is most attributed to the very low COP of the absorption chiller, relative to the COP for an equivalent MVC chiller.

1.2.3 Trigeneration Control Strategies

Whilst the selection, specification and sizing of plant is crucial to the energetic and economical feasibility of trigeneration systems, the control strategy used to monitor the interaction and energy flows between each of the subsystems is an equally crucial factor. Given the variability of the demand side and the highly complex and interdependent relationship between subsystems on the supply side, managing and indeed correctly selecting an appropriate control strategy is difficult.

On the demand side, variability is comprised of four components, two external and two internal: seasonal fluctuations and climatic fluctuations representing the external components; diurnal fluctuations and spontaneous fluctuations representing the internal components. Seasonal fluctuations are easily predictable, and are likely to include demand side changes such as an increased heating or

cooling demand and a change in the diurnal pattern of electrical demand, resulting from changes in lighting hours due to longer days or nights. Climatic fluctuations are less easily predictable and are dependent upon the variations in local temperature, which can vary substantially over a period of a few days. Both seasonal and climatic fluctuations are influenced by factors outside of the end user control, these are therefore referred to as external components. Diurnal fluctuations are easily predictable and encompass the changes in demand apparent due to behavioral changes in the users throughout the day. Volatile fluctuations are unpredictable and apparent due to random changes in individual user habits; if the number of users is large, the volatile fluctuations are under most circumstances considerably less in magnitude than the others.

	Relevance		**Characteristic**		
	System Design	**Control Strategy**	**Amplitude**	**Frequency**	**Predictability**
Seasonal	High	Low	High	Low	High
Climatic	High	Medium	High	Medium	Medium
Diurnal	High	Medium	High	Medium	High
Volitile	Medium	High	Low	High	Low

Figure 1.1: Relevance of demand side variability components to systems design and control strategy; and the correlation of each to the amplitude, frequency and predictability of the demand

Figure 1.1 gives an indication of the relevance of demand side variability components to systems design and control strategy and the correlation of each to the amplitude, frequency and predictability of the demand. Lower frequency variations are more relevant to system design; the implication being that in order to handle the effects of large seasonal variations in temperature (*e.g.* humid continental climates, such as New England and Eastern Europe), appropriate system design is crucial. High frequency variations are more relevant to the control strategy; the implication being that in order to handle the effects of anthropological cycles and unpredictabilities, an appropriate control strategy is crucial [26, 31, 32].

A domestic - scale trigeneration system has been created and tested by Miguez et al. [33]. The system comprises a small 2 - stroke petrol engine with a EHR heat exchanger, and a reversible MVC heat pump. The heat pump is reversible such that it can provide both summer cooling demands and compliment the recuperated thermal energy during winter heating demands. There is also a large thermal accumulator (a water tank) and deep cycle storage batteries to act as buffers, to ensure consistent demand matching under a highly variable demand scenario. When the demand side consists of a larger network of users, loads and buildings; whose characteristics are more predictive and can be modeled and controlled; it is possible to reduce the relative size of the buffers. Miguez et al. describe five operational modes:

- Stand-by mode
- Electric generator mode
- Co-generation mode
- Heat pump winter mode
- Heat pump summer mode

Under heat pump summer mode the EUF of the system is poor because all the useful thermal energy is rejected, unless there is thermal demand from either hot water supply or to top - up the thermal accumulator. Further, if the demand for electricity is high, the possibility that the system will become unable to meet the combined electrical and cooling demand becomes a reality; the system becomes energetically unfeasible. The addition of a thermally activated heat pump such as a sorption chiller device would help negate this problem, which could indeed be used in direct substitution of the MVC heat pump. This will be discussed further in Chapter 3.

The most common control strategies are based upon operating the PGU in accordance with the thermal demand (Thermal Load Following (TLF)), and in

accordance with the electrical demand (Electric Load Following (ELF)) [34]. The philosophy behind TLF and ELF is such that the supply of either thermal or electrical energy is aligned to the thermal or electrical demand, respectively. The choice of TLF or ELF is usually affected by the operational characteristics of the PGU, the presence and size of thermal storage and electrical storage systems, and the ability to sell excess electricity to the grid. The cost of fuel and the cost of grid electricity also has a huge implication upon the control strategy [35].

When a TLF strategy is adopted, both CHP and CCHP systems exhibit an increase in EUF [36]. However, due to the low electricity demand to heat demand ratio of most building sectors (typically 0.1 - 0.2 in the domestic sector and 0.4 - 0.6 in the tertiary sector [35]) this almost always results in excess electricity being produced which must be either exported or stored for use at another time. Therefore, when a ELF strategy is adopted, the thermal energy demands are unlikely to be satisfied and supplementary boilers will be necessary.

An alternative operational strategy, a Hybrid Load Following (HLF), is proposed and analysed by Mago and Chamra [36]. Under this solution the ELF strategy is employed under certain conditions, whilst under contrasting conditions the TLF strategy is employed. The philosophy of the HLF strategy is based upon controlling the PGU such that no excess energy is produced, inevitably creating a shortfall of one energy stream which is satisfied either by the grid or a supplementary boiler. Although the model used by Mago and Chamra is heavily simplified, particularly with respect to the relationship between power output and recuperated heat of the PGU, the results indicate an increase EUF and associated operational cost savings.

1.3 Conclusion

Worldwide demand for air conditioning is predicted to increase by 72 % by the year 2100, primarily due to the increase in economic productivity of south east Asia and Africa, which will result in an improvement in living standards and a

consequent increase in demand for air conditioning. It is predicted that this effect will be compounded by climate change. Therefore, the efficient, low carbon and low cost provision of chilled water for air conditioning systems is both a huge challenge and opportunity. Trigeneration (the combined generation of electricity, heating and cooling) is a progression of cogeneration (the combined generation of electricity and heating), which will enable this goal to be reached.

This Chapter has given an overview of trigeneration system design, thermal storage technologies and trigeneration control strategies. Trigeneration has been shown to deliver an improved EUF over a system where electricity, heating and cooling are produced separately [21, 28–30]. The magnitude of the improvement in EUF is primarily dependent upon the performance characteristics of the PGU and the device which converts waste heat into useable coolth. The control of the system is an additional important factor in maximising the EUF [26, 31, 32], and the integration of a thermal storage device can greatly improve the diurnal and seasonal performance of the system. Trigeneration control and operation strategies have been discussed and analysed at length in a number of studies [23, 25, 26, 33, 36, 37], which conclude that the ideal control and operation strategy is dependent upon climatic conditions and the performance parameters of the trigeneration system.

1.4 Aims and Objectives of Thesis

A list of primary aims and objectives for the research documented in this Thesis are given below.

1. Review the literature for interesting innovations in the field of mechanically and thermally activated heat pump cycles. This will include academic journal and conference papers, PhD Theses, patents, commerically available data.

2. Identify the innovations which exhibit a high level of perfomance or the potential to achieve high levels of performance (n.b. COP is the primary performance parameter of interest) given further development.

3. Design, model, analyse and optimise at least 3 thermally activated heat pump cycles. The primary performance parameter is the cycle COP, but consideration will also be given to the operating temperatures and pressures as well as the practicability of the developing the cycle.

4. Develop the design of the most promising heat pump cycle, including performance optimsation and an analysis of the heat pump performance when integrated within a trigeneration system.

5. Develop preliminary design data for specific components within the heat pump cycle to serve as a basis for the continuation of research and development.

Chapter 2

Review of Heat Pump Systems

2.1 Introduction

Heat pumps encompass a wide variety of devices which transfer thermal energy from a cold reservoir to a hot reservoir, as highlighted in Figure 2.1. In this chapter the varying types of refrigerants are discussed, with particular focus given to sorption heat pumps and R744 MVC heat pumps.

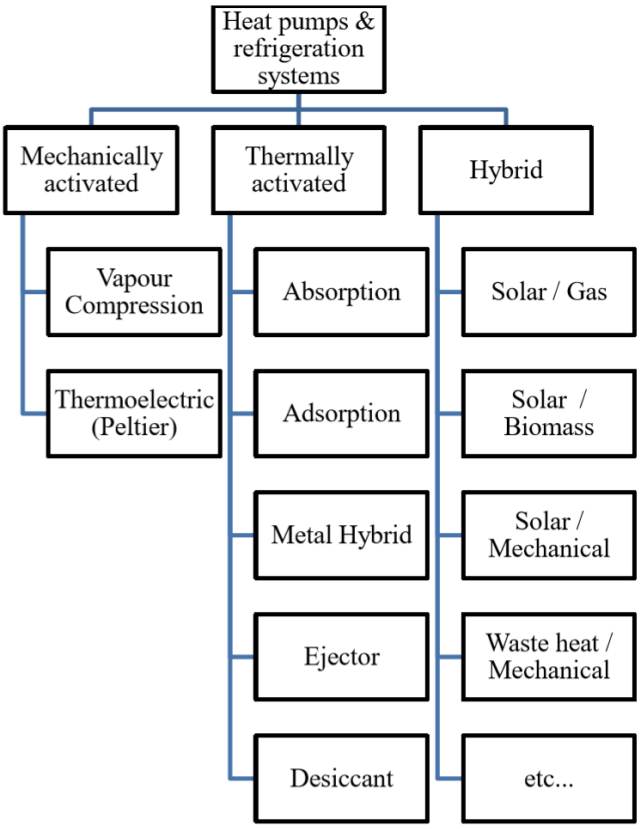

Figure 2.1: Classification of Heat Pump / Refrigeration System

2.2 Refrigerants

2.2.1 Single Component Refrigerants

Single component refrigerants are the most simple type of refrigerants available, comprising a single substance. Refrigerants can be split into two categories: synthetic and natural. Synthetic refrigerants are denoted by 000, 100, 200 or 300

series numbers under ASHRAE Std. 34[1] if they are methane based, ethane based or propane based. Natural refrigerants are either inorganic compounds which are denoted by 700 series numbers, or organic compounds which are denoted by 600 series numbers. Synthetic refrigerants include ChloroFluoroCarbons (CFCs), HydroChloroFluoroCarbons (HCFCs) and HydroFluoroCarbons (HFCs), whilst natural refrigerants include HydroCarbons (HCs), R717 and R744.

CFC

ChloroFluoroCarbons are synthetic man - made substances containing chlorine, fluorine and carbon. Prior to the advent of CFCs, MVC heat pump systems utilised more simple refrigerants such as ammonia, sulphur dioxide, carbon dioxide and chloromethane. It is well documented that CFCs contribute significantly to the depletion of ozone in the upper atmosphere, which led to in the creation of the Montreal Protocol in 1987 to phase out the use of CFC refrigerants. The most common CFC refrigerant was R12, which has an Ozone Depletion Potential (ODP) of 1 and a Global Warming Potential (GWP) of 2400 [38].

HCFC

HydroChloroFluoroCarbons are very similar in structure to CFCs, with the addition of one or more hydrogen atoms. The use of HCFC refrigerants became widespread following the phasing out of CFCs in the 1980s, with refrigerants such as R22 becoming ubiquitous in air conditioning units. HCFCs are less stable than CFCs and break down in the lower atmosphere, prior to reaching the ozone layer. Most HCFC refrigerants have an ODP below 0.1 although GWP levels remain very similar to CFCs. R22 has an ODP of 0.05 and a GWP of 1810 [38]. As of January 1 2010 the production of R22 for charging new systems was be banned, and from January 1 2020 the production and import of all R22 will be banned entirely. Global production and use of HCFC refrigerants, particu-

[1]ASHRAE Standard 34: Designation and Safety Classification of Refrigerants. www.ashrae.org

larly R22, has been buoyant in recent years, owing to the rapid expansion of air conditioning use in China and India [2].

HFC

HydroFluoroCarbons are a further evolution of HCFC refrigerants and do not contain chlorine, which is the prime contributor to ODP in older refrigerants. HFCs are non - toxic and have zero ODP, but do have a high GWP. One of the most common HFC refrigerants is R134a, which is commonplace in domestic and mobile air conditioning systems and has a GWP of 1430. Worldwide regulations controlling the use of HFC refrigerants, such as the 1997 Kyoto Protocol [39] and the 2006 EU MAC directive which controls the use of fluorinated gases with a GWP greater than 150 in mobile air conditioning units [40] are driving innovation in the refrigerant, heat pump and chiller market. It is clear that the age of the chlorinated and fluorinated refrigerants is over, and research efforts must be directed into systems which use alternative working fluids.

HC

Hydrocarbons have properties which make them ideal as refrigerants: they have zero ODP, negligible GWP, low toxicity, are cheap to produce and have desirable thermodynamic characteristics for achieving a high COP. The most commonly used HC refrigerants are R600a and R290a, with GWPs of 4 and 20, respectively. Since HCs are obviously highly flammable, there can be significant restrictions regarding their use in certain applications.

Ammonia - R717

Ammonia is widely used as a refrigerant in large scale refrigeration facilities, and has an ODP and GWP of 0. The thermodynamic properties of R717 are such that it is often considered as a superior alternative to many older synthetic refrigerants [41] because it has a higher heat transfer coefficient and a much higher volumetric

refrigeration capacity. R717 has a very distinctive smell, enabling leakages to be easily detected by personnel and negating the possibility of asphyxiation, which makes it an attractive refrigerant for large industrial facilities. However, R717 is highly toxic and combustible, and is also corrosive towards coppers and alloys containing copper and zinc.

Carbon Dioxide - R744

Carbon dioxide is a non-toxic, incombustible substance with a ODP of 0 and a GWP of 1, which is cheap, easy available, fully compatible with normal lubricants and construction materials and is not required to be recovered at the end of plant life. Due to the high volumetric capacity (approximately five times greater than R22), plant size can be greatly reduced compared to common synthetic refrigerant systems. R744 has a relatively low critical temperature of 31.1 °C, and a relatively high critical pressure of 73.77 bar. The optimum heat rejection pressures are typically around 100 bar, which is significantly higher than for most synthetic refrigerants, however the increased volumetric capacity implies that the potential danger of pipe rupture is somewhat reduced (when considering both pressure and volume as the prime contributers)

Carbon dioxide was first harnessed as a refrigerant by Thaddeus S.C Lowe in 1866 in the production of ice, and the first R744 compressor was designed and built by Windhausen in 1880 [42]. R744 was used extensively in buildings where humans could be exposed to the cooling systems: theatres, hospitals, restaurants. However, the advent of synthetic refrigerants in the 1950s, which could provide a greatly increased COP, resulted in the eventual phasing out of R744. In recent years R744 has been making a comeback, owed in part to policy changes controlling the use of synthetic refrigerants (*e.g.* the Montreal Protocol), and also to an appreciation of the numerous benefits of R744 heat pumps over synthetic refrigerant heat pumps [see Section 1.4].

Nitrous Oxide - R744a

Nitrous oxide has a very similar molecular structure to carbon dioxide and an almost identical molar mass, which results in both gases having very similar thermodynamic properties and characteristics. It is acknowledged that R744a have certain performance advantages over R744 heat pumps, although there are limitations to these. R744a heat pumps exhibit a slightly higher COP_c than R744 heat pump, require a lower pressure ratio and have a higher second law efficiency [43, 44]. R744a also has a much lower triple point than R744 ($-90.82\,°C$ vs $-56.56\,°C$), which enables it to be suitable for use at very low temperatures. However, R744a has a GWP or 298, has a lower volumetric heating and cooling capacity, and begins to decompose at temperatures above $300\,°C$.

2.2.2 Multi Component Refrigerants

Multi component refrigerants contain two or more refrigerants, and may be described as either azeotropic, zeotropic and near - azeotropic.

An azeotropic mixture is a combination of two or more refrigerants, which all have the same concentration of liquid and vapour phase at a given pressure and temperature. Azeotropic refrigerants are often suitable for low temperature cooling, as they tend to have a lower triple point and vapouration temperature then their constituents A common azeotropic refrigerant, and indeed exception to the previous rule, is R507, which is a blend of R143a and R125 ($50:50$ by mass). Azeotropic refrigerants are denoted by 500 series numbers under ASHRAE Std. 34[2].

Very few azeotropic refrigerants exist, and in most instances a blended refrigerant is a near - azeotropic mixture. Common examples including R502 (a mix of R115 and R22) and R410a (a mix of R125 and R32). Near azeotropic refrigerants experience undesirable characteristics such as temperature glide and a very non-

[2]ASHRAE Standard 34: Designation and Safety Classification of Refrigerants. www.ashrae.org

linear relationship between temperature and enthalpy. The former degrades the overall COP of the by effecting the linearity of the evaporator temperature, whilst the latter can result in undesirable temperature pinches in heat exchangers.

A zeotropic mixture is a combination of two or more refrigerants, whose liquid and vapour concentrations are never equal. Most blended refrigerants are zeotropes to a varying degree, which results in systems using them experiencing temperature glides in the evaporator and condenser to varying degrees. R410a (a near - azeotropic refrigerant) typically experiences a temperature glide of 0.5 °C, whilst the glide for R407c (a blend of R32, R125 and R134a) is about 4 °C. The temperature glide is apparant due to differences between the bubble and dew temperatures of the two fluids. Zeotropic and near-azeotropic refrigerants are denoted by 400 series numbers under ASHRAE Std. 34.

Zeotropic mixtures are used in absorption chillers because the two fluids have vastly different vapour pressures, which enables a desorption and resorption process of the refrigerant to the absorbent. Over 40 different refrigerant and 200 absorbents are discussed in the literature [4]. The two most common working fluid pairs (LiBr - H_2O and H_2O - NH_3) are highlighted below, although others include: R22 - TEGDME, CH_3OH - LiBr ad CH_3OH - LiCl [45].

Lithium Bromide - Water

Lithium bromide and water (LiBr - H_2O) is one of the most common working fluid pairs in absorption chillers, with lithium bromide serving as the absorbent and water as the refrigerant. Absorption chillers which utilise LiBr - H_2O are capable of operating at high temperatures, albeit with inhibitors to control corrosion in the generator. LiBr - H_2O can be used in multi-stage absorption chillers, which are capable of much of a higher COP [46–49]. In order to sufficiently cool the absorber and condenser, a cooling tower is typically required. Due to crystallisation of lithium bromide at relatively high temperatures, LiBr - H_2O chillers are not able to provide low temperature cooling.

Water - Ammonia

Water and ammonia (H_2O - NH_3) is another common working fluid pair in absorption chillers, with water serving as the absorbent and ammonia as the refrigerant. H_2O - NH_3 is a less zeotropic mixture than H_2O - NH_3, which results in the quality of ammonia refrigerant exiting the generator being low. The presence of water in the ammonia circuit leads to a very significant temperature glide in the condenser and evaporator. In order to counteract this a rectifier is located following the generator, which allows the entrained water vapour to condense untit such a point that the ammonia quality is sufficient (usually greater than 0.995 [50, 51]). H_2O - NH_3 chillers do not suffer from crystallisation problems in the absorber, and are therefore capable of providing cooling at very low temperatures, therefore H_2O - NH_3 are often used as the bottoming cycle to a LiBr - H_2O chiller [52, 53].

2.3 Absorption Heat Pumps

Absorption heat pumps are commonly referred to as absorption chillers, due to their predominant use as a way of converting low - to - mid grade waste heat into cooling. Absorption chillers use a zeotropic mixture as the working fluid, where one fluid is the refrigerant and the other the absorbent. In its most simplest form, the absorption cycle process can be described as a desorption - condensation - expansion - evaporation - absorption - compression process. A simplistic process flow diagram of this process in given in Figure 2.2.

Absorption chillers are a very well established technology, but compared to MVC heat pumps have a relatively small market share. There are a number of potential reasons for this: the relatively high COP of MVC heat pumps, the simplicity of MVC heat pumps, the abundance and widespread availability of cheap electricity, the increased size and weight of absorption heat pumps. In distributed CCHP systems the PGU exhaust stream is a potential high grade

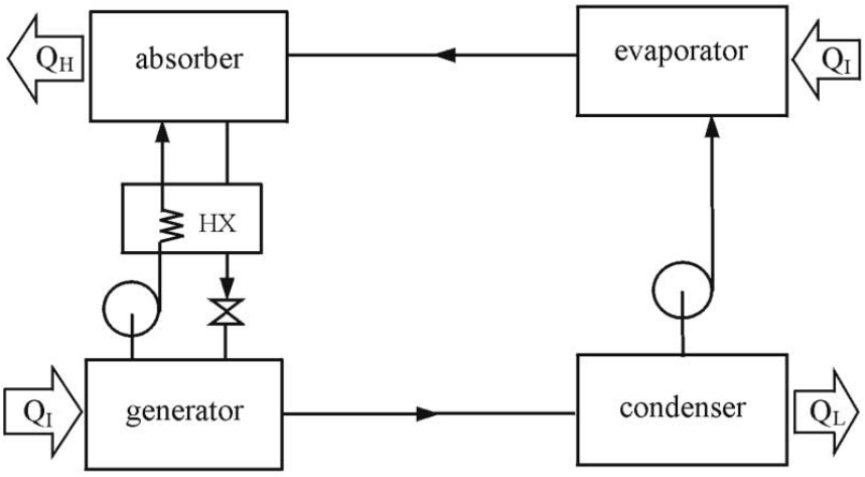

Figure 2.2: Basic process flow diagram of a typical single-stage absorption chiller

heat source, which can be used to drive high efficiency multi - effect absorption chillers.

2.3.1 Multi - Stage / Multi - Effect

Single - stage, single - effect absorption chillers tend to achieve a COP_c of around 0.7, with a associated generation (desorption) temperature of around 80 °C [45]. Double - stage, double - effect absorption chillers have corresponding values of around 1.2 and 150 °C, whilst triple - stage, triple - effect chillers achieve figures of around 1.6 and > 200 °C [48]. The limitation in the maximum number of stages is the inhibition of corrosion in the high temperature generator as the generation temperature and pressure increases. A further complication is the increased level of complexity, which can make successfully controlling the system very difficult [47].

In multi - stage absorption chillers the working fluids pass through a number of generators, each operating at differing pressure levels, which greatly increases the mass proportion of refrigerant produced relative to the mass flow of solution, Ψ. An 'effect' refers to the process of transferring heat from one part of the cycle to another; all multi - stage chillers are also multi - effect chillers. For LiBr - H_2O chillers, multiple cycles are cascaded and share a single absorber, the thermal

energy from the hot refrigerant generated in the upper cycle is used to drive the generator of the cycle below it; in some systems the refrigerant condenses during this process. Monitoring and control of temperature pinch is key in ensuring exergetic efficiency. There are three possible flow configurations in multi - stage cascade chillers: series flow, reverse flow and parallel flow.

In series flow configuration, the strong[3] refrigerant / absorbent solution exiting the absorber flows into the high temperature generator (through a series of solution - to - solution Heat Exchangers (HXs)). The weaker solution exiting the upper generator passes into the generator below, and so on, until the strong solution outlet of the low temperature generator which flows back into the absorber. In reverse flow configuration, the wet solution passes to the lower generator first and finishes at the high temperature generator. In parallel flow configuration, the wet solution passes is split and passes through each generator independently, the mass flow ratio of which is vital, and returns directly to the absorber. The performance characteristics of each configuration as a function of the absorber inlet solution concentration has been discussed by Kaita [47]. Parallel flow configuration achieves the highest COP_c throughout the range of absorber inlet conditions, whilst series flow achieves the lowest COP_c. The difference is more profound when the absorber inlet solution is weaker, whilst when the solution is strong all configurations provide a similar and higher COP_c, implying that if the generators are efficient in producing refrigerant the choice of configuration is unimportant.

A similar study by Aghdam, Ranjbar and Mahmoudi [54] concluded that series flow is capable of achieving a higher COP_c than parallel flow, provided that the evaporator pressure and generation temperature are favourable (both being high). Series flow exhibits a less constant COP_c than parallel flow over the range of evaporator pressures and generation temperatures considered. In both configurations, the generation temperature (ranging from 180 °C to 210 °C) has much less profound effect on COP_c than the evaporator pressure. The implication

[3] 'Strong' implies that the mass proportion of refrigerant in the solution is low, ie. it is strong in absorbent

is that the minimising temperature pinch in the evaporator is more vital than in the generator.

An analysis of a steam driven microscale double - stage LiBr - H_2O chiller, operating with parallel flow configuration has been presented by [55]. It was founds that the high temperature generator produces approximately 60 % of the refrigerant, whilst the low temperature generator produces 40 %; this ratio remains consistent regardless of the cooling output.

The number of effects in an absorption chiller can, and often does, exceed the number of stages in the chiller, an example of which is the double - stage, triple - effect H_2O - NH_3 'Kangaroo' cycle proposed by Shelton, Jacob and Schaefer [56]. A very similar concept was patented by DeVault in 1995 [53].

The kangaroo cycle features two independent cycles: a high pressure outer cycle operating at 200 °C, and a low pressure inner cycle driven by the heat rejected by the heat of absorption and heat of condensation from the upper cycle. Its name is derived from idea that the inner cycle is within the pouch of the outer cycle, a phenomenon manifested through observation of the Duhring plot in Figure 2.3. The pressure of the working fluid pair is plotted on the ordinate axis, and the inverse of temperature is plotted on the abscissa. The cycle evaporators are represented in the lower left portion of the plot, whilst the inner generator is represented by the upper right portion of the red curve and the outer generator by the upper right portion of the green curve. The left side of the plot represents the part of the cycle which is predominantly ammonia refrigerant (*i.e.* $x = 0.99$), whilst the right side of the plot is the sorbent rich mixed fluid (*i.e.* $x = 0.2$). This cycle is capable of achieving a COP_c of 1.50 when $T_{amb} = 30\,°C$, although the performance is highly sensitive to the T_{amb}, with COP_c dropping to 1.15 when $T_{amb} = 35\,°C$.

The COP_c of the double - stage triple - effect H_2O - NH_3 'Kangaroo' cycle is much greater than the COP_c of an equivalent double - stage double - effect LiBr - H_2O cascaded cycle [55]. A similar system is proposed in a patent registered to

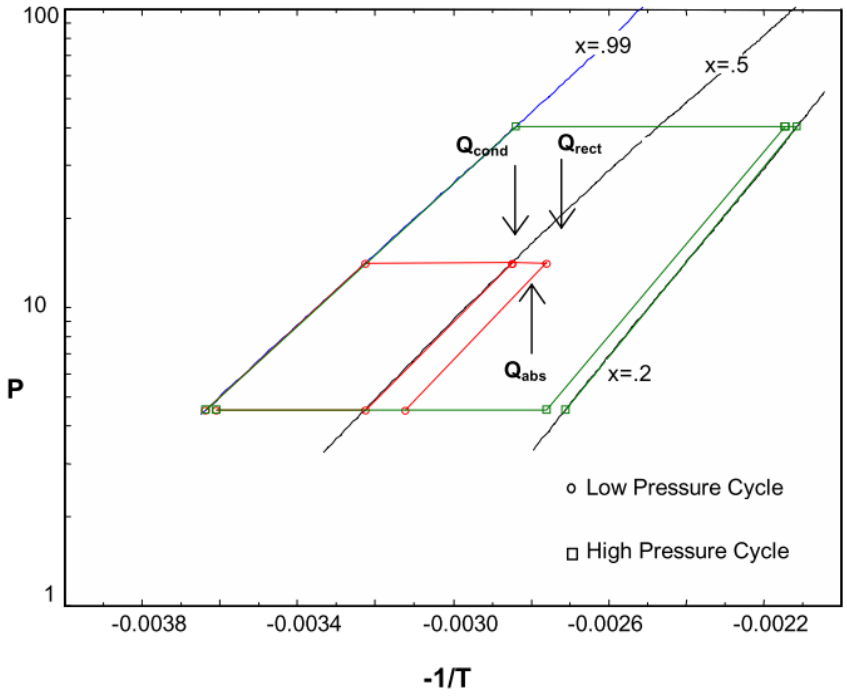

Figure 2.3: Dühring plot - Kangaroo cycle [56]

DeVault [53]. The proposed system differs from the aforementioned 'Kangaroo' cycle in that the inner loop is effectively a double-stage cascade cycle (i.e. two generators and condensers), which implies a dual stage condenser is required in the outer loop

Numerous multi-stage and multi-effect absorption chiller cycles using non-standard working fluids have been proposed in the literature, including: a double-stage absorption / compression cycle using CH_3OH-TEGDME and TFE-TEGDME [57], CH_3OH-LiBr [45], CH_3OH-LiCl [45] and H_2O-LiBr:LiI:$LiNO_3$-LiCl [58].

2.3.2 Generator-Absorber Exchange Cycles

GAX cycles recycle some of the low grade heat available in the absorber and use it to drive a portion of generator [59]. This is made possible by a temperature overlap between the hot side of the absorber and cold side of the generator. When combined with solution HX transferring thermal energy from the strong solution exiting the generator to the weak solution exiting the absorber, a high proportion

of the thermal energy supplied to the desorption process is internally recycled heat. This provides a reduction in external heat requirements and increases the COP of the cycle. The basic principal of the GAX cycle is highlighted on a Dühring plot in Figure 2.4.

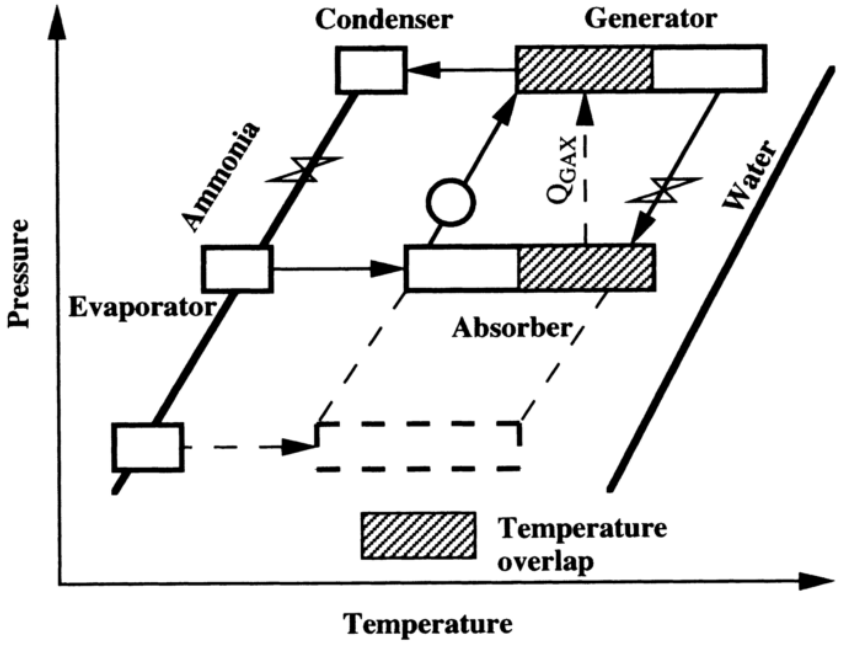

Figure 2.4: Basic GAX cycle

A computational analysis of four very similar H_2O - NH_3 GAX cycles has been documented by Park, Koo and Kang[59]. The cycles each feature three stages within the absorber and three stages with the generator. In the generator the high stage is the driven by external heat, the middle stage by the strong solution exiting the high stage generator, and the low stage by the high stage absorber. In the absorber, the high stage is cooled by the low stage generator, the middle stage by the weak solution exiting the high stage absorber, and the high stage by an external heat sink.

The difference between the four different cycles is the sequence and method of heat rejection, and the parallelisation of the middle and low stage absorbers. Three cycles are capable of providing simultaneous heating and cooling, whilst one is capable of providing cooling only. The COP_c as a function of hot water outlet temperature is shown in Figure 2.5. This demonstrates that a COP_c of

approximately 1 is achievable under the best operating conditions (lowest hot water outlet temperature), but the cycle can only really be considered as a pure cooling mode cycle under this scenario. For simultaneous heating and cooling (i.e. hot water outlet temperature $> 50\,^{\circ}\mathrm{C}$) the best configuration achieves a COP_c of approximately 0.85.

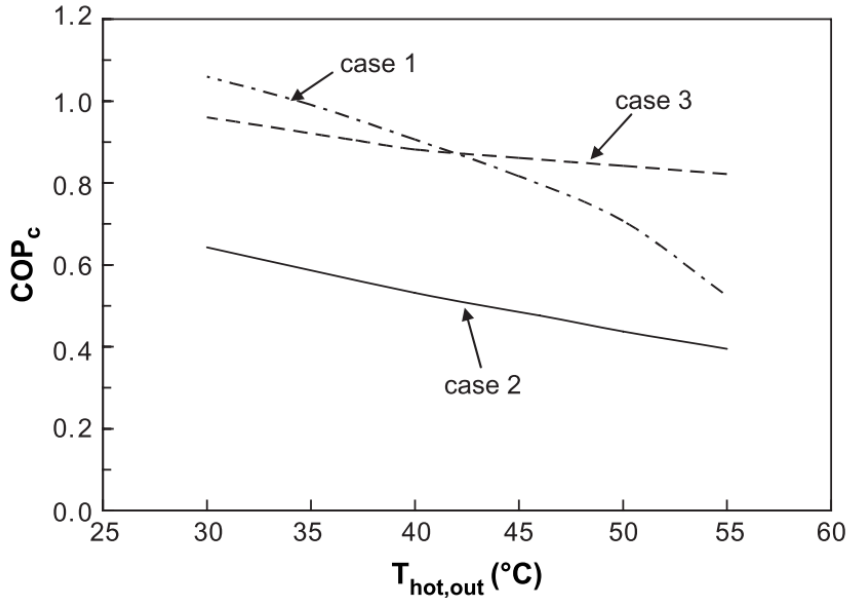

Figure 2.5: Basic GAX cycle[59]

An advanced GAX cycle, developed by Kang et al., included the addition of a fourth 'waste heat' stage within the generator [60]. It was found that the generator outlet temperature could be reduced whilst simultaneously increasing the COP for all scenarios. However, when considering the enthalpy of the waste heat in the calculation of COP, the COP was lower than a standard GAX cycles in almost all scenarios.

A further modification to the standard GAX cycle is the Generator Absorber Exchange Absorption Compression (GAXAC) cycle [61]. Hybridised absorption chiller cycles are well documented [62–66], but hybrid GAX absorption chillers cycles are a relatively unknown concept. Kang, Hong and Park [67] analysed four slightly different GAXAC cycles. The differences in the cycles was the of the location of the compressor unit on the refrigerant side absorber inlet and refrigerant side generator outlet. The aim of the former is to create a wide

temperature overlap between absorber and generator, and/or a lower evaporation temperature. The aim of the latter is to reduce the generation temperature (via a reduction in the generator pressure), and/or to increase the condenser temperature for hot water production. The highest COP_c calculated was 1.24 and was achieved in the former case, 85 % of energy input was thermal and 15 % isentropic compression work. COP_c increases as a function of absorber pressure, by as much as 24 % over the standard GAX cycle (albeit with an assumed 100 % compressor isentropic efficiency).

2.3.3 Vapour Recompression Absorption Cycles

The Vapour Recompression Absorber (VRA) is a noteworthy modification to the basic absorption chiller cycle, which aims to increase the refrigerant production rate and therefore the cycle COP [68, 69]. The VRA effectively adds a third stage to a double stage cycle. It achieves two things: an increase in the strength of the solution entering the absorber, and a decrease in the strength of the solution entering the upper generator. When compared to a conventional triple effect LiBr - H_2O absorption chiller cycle, the double effect LiBr - H_2O VRA absorpton chiller cycle offers simplification, a reduction in upper generator temperature and a potential decrease in the overall size of the system. The addition of the VRA has been demonstrated to theoretically increase COP_c by 8 % and reduces the upper generator temperature by around 5 °C. Whilst no laboratory study has been identified within the literature, a patent for the concept does exist [70]

2.4 Adsorption Pumps

Adsorption heat pumps are devices which generally utilise a low grade heat source to provide a cooling effect, with the potential for a subsequent heating effect. Adsorption chillers operate using the same basic process as absorption chillers: desorption, condensation, throttling, evaporation, adsorption, pumping. The ma-

jor difference is that the sorbent is in the solid phase and the sorbate / refrigerant adheres to the surface, rather than permeating it. This consequence of this is that in the adsorption / desorption process there is no change in the density of the sorbent (in the absorption process there is an decrease in the density of the sorbent as it absorbs the sorbate).

There are two types of adsorption processes: physical adsorption (physisorption) and chemical adsorption (chemisorption), the former of which is due to Van der Waals forces and the latter valency forces [3]. Due to the fact that the sorbent is a solid and cannot be easily transported, the desorption and adsorption processes both occur in the same location (i.e. the generator is the adsorber and vice versa). This poses a problem in that multiple desorption / adsorption chambers / beds are required to maintain a quasi - continuous operation, with a control system required to switch between the processes at the appropriate moment.

2.4.1 Multi - bed adsorption chiller

In order to maintain a quasi-continuous operation, a minimum of two sorption beds are required, however, for performance reasons more than two beds are often used. A theoretical study of a three - bed silica - gel adsorption chiller was conducted, as reported in [28]. With a driving temperature of 80 °C, a coolant temperature of 30 °C, and a chilled water temperature of 6 °C, the adsorption chiller achieves a COP_c of 0.38. The three - bed cycle is shown to have more stable performance than a two - bed cycle throughout an entire sorption / desorption cycle, where a third 'dormant' bed can be used to provide a steady chilled water output. The addition of a third bed represents an increase in capital cost, but will extend the operational lifetime of the chiller. One could argue that the addition of a fourth or fifth bed could provide a further increase in performance, but this is a concept which has not been widely presented in the literature.

2.4.2 Multi - stage adsorption chiller

Of further interest are multi - stage adsorption chillers, which, like multi - bed adsorption chillers, feature more than the a single bed. However, unlike multi - bed adsorption chillers, which have multiple beds arranged in a parallel formation, multi - stage adsorption chillers have multiple beds arranged in a series formation. Multi - stage adsorption chillers allow for lower driving temperatures, as demonstrated by Saha, Akisawa and Kashiwagi using a double - parallel and double - series silica gel and water chiller [71]. This can be advantageous in many scenarios, most notably when the driving source is low temperature solar energy; the system achieves a COP_c of 0.36 with a driving temperature of just 55 °C, coolant temperature of 30 °C and delivered chilled water temperature of around 7 °C.

A triple - stage metal hydride adsorption chiller utilising different working fluids in each stage was analysed by Li et al. [72]. The sorbent of the high temperature bed was $NiCL_2$, and the sorbents of the medium and low temperature bes were $MnCL_2$ and $SrCL_2$, respectively; the sorbate in each bed was NH_3. The system achieved a theoretical COP_c of between 0.75 and 0.97, given a driving temperature of 250 °C. Compared to a cascade triple - stage absorption chiller, the proposed adsorption chiller does not suffer from the corrosion or crystallisation problems but has a greatly diminished performance and potential operational issues with the freezing of the metal hydrides. A thorough review of metal hydride adsorption chiller systems is presented by Muthukumar and Groll [73].

2.5 R744 MVC Heat Pumps

The vast majority of heat pumps in use are electrically activated [2] and thus fall into the MVC category. The MVC heat pump industry is continually in a state of change due to the continually evolving political restraints regarding refrigerants. In recent years, R744 has risen to the fore as a prime refrigerant [42, 74–77]. It

is also considered a prime candidate for future power conversion cycles [78–81], in particular concentrated solar power applications [82–85]

The transcritical R744 heat pump, depicted in Figure 2.6, is ubiquitous due to the requirement for a heat rejection temperature greater than 31 °C in almost all scenarios. The resulting high compressor outlet temperature gives rise to the possibility for combined heating and cooling, and is explored by Sarkar, Bhattacharyya and Ram Gopal in the context of a dairy plant requiring chilling at 4 °C and heating at 73 °C [76, 86]. The analyses indicated that such a system is well suited to high heating temperatures but modest cold temperatures [86].

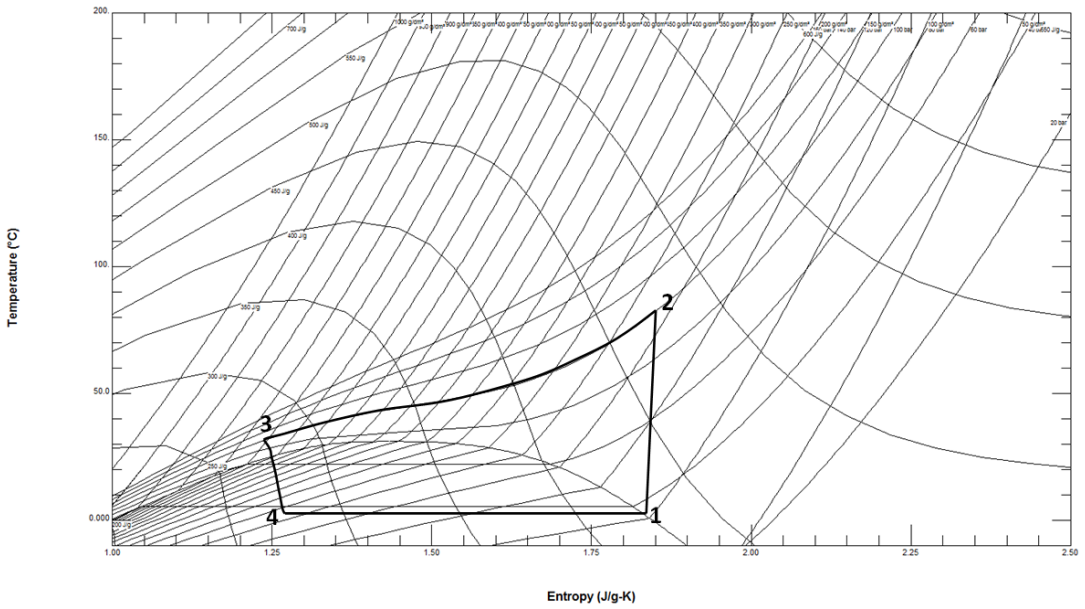

Figure 2.6: Temperature - Entropy plot of a basic transcritical R744 heat pump cycle

The replacement of an isothermal condenser with an anisothermal gas cooler results in a significant temperature glide, which, combined with the close proximity to the critical point, gives rise to significant thermophysical fluid property changes along the gas cooler. Therefore, simple heat exchanger models (*e.g.* LMTD) cannot be used with R744. Figure 2.7 shows the variation of C_p as a function of temperature for pressures close to the critical pressure, one notes the pronounced peak in C_p when the when the critical pressure and temperature intersect. At higher pressures, the peak is more subdued and is shifted towards

higher temperatures (the opposite being true for lower pressures). The significant increase in C_p close to the critical point gives rise to pronounced pinch points in heat exchangers.

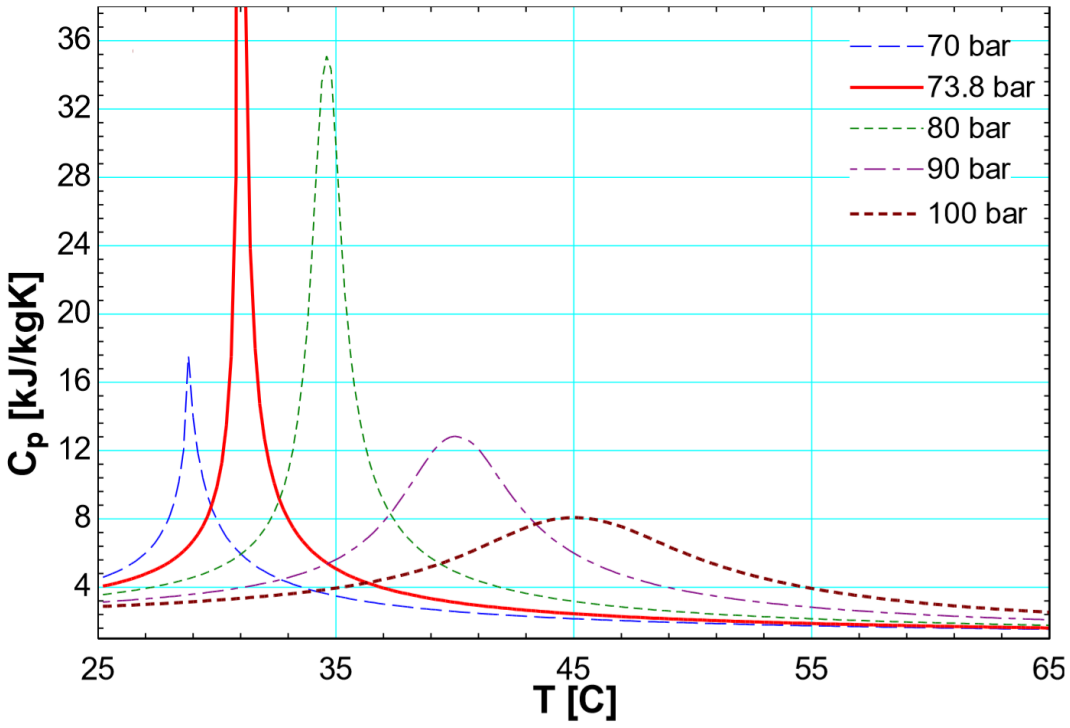

Figure 2.7: C_p as a function of temperature for R744 at various pressures

Due to the high pressure of the cooled R744 exiting the gas cooler it is both possible and desirable to extract work from the fluid using a work expansion device or an ejector [42, 87, 88]. The addition of an ejector to the cycle increases the COP by between 7 and 18 % relative to the basic cycle depicted in Figure 2.6. The ejector combines the high pressure supercritical / superheated vapour R744 at the gas cooler outlet with the low pressure saturated vapour R744 at the evaporator outlet , producing a fluid at an intermediate pressure in the saturated region. The addition of the ejector reduces the exergetic losses associated with the isenthalpic expansion of a valve, thus reducing the pressure ratio of the compressor whilst not increasing the evaporation temperature, and increases the refrigerant flow rate through the evaporator. Expanders can achieve a similar (∼15 % when $\eta_{turb,is} = 60\%$ [42]), if not greater (∼40 % with a triple - stage expander and dual - stage compressor [88]) boost in COP to ejectors.

2.6 Supercritical Carbon Dioxide Brayton Cycle

Although Supercritical Carbon Dioxide (S-CO2) was first investigated as a working fluid in the late 1960's, Brayton cycles operating with S-CO2 is a relatively new concept, with no commercial plant currently existing or currently being built. Research into carbon dioxide Brayton cycles has experienced a significant increase in recent years, due in part to a resurgence in the nuclear power industry. Carbon dioxide is a fluid which can be used to both cool the reactor core and as a working fluid for the power cycle [79], thus potentially eliminating the need for two separate fluid loops. When compared to the helium S-CO2 provides several advantages over the the helium and steam indirect cycles. Thermoeconomic analyses have indicated that the S-CO2 cycle could provide cost savings of 30 % over the steam indirect cycle and 15 % over the helium cycle [79].

The part-flow S-CO2 closed gas turbine cycle, proposed by [81], features an additional compressor and heat recuperator as well as a part-flow valve to regulate the flow to each compression stage. With a turbine inlet pressure and temperature of 200 bar and 525 °C respectively, a thermal to mechanical efficiency of 45 % is achievable. It is estimated that due to the presence of a pinch point within the recuperator, the conventional closed Brayton cycle suffers from a reduction in conversion efficiency of around 7 % (absolute). The part flow cycle aims to reduce the pinch effect, with 6 % (absolute) of the lost efficiency recoverable at optimal conditions. Futher, it is suggested that the adiabatic efficiency of the compressor and temperature effectiveness of the recuperator are not sensitive to efficiency and, as such, the S-CO2 cycle is viable in distributed generation scenarios where small capacities are required [81].

The recompression S-CO2 cycle with reheating proposed by [79] is a futher evolution of the part-flow cycle, featuring the addition of a second reactor loop and low pressure turbine. This cycle is theoretically capable of a maximum thermal to

mechanical conversion efficiency of 45.3 %, assuming a turbine inlet temperature of 550 °C (42.4 % for a turbine inlet temperature of 480 °C) [79]. The addition of reheating provides a maximum efficiency improvement of 3.5 % at optimum conditions over the non-reheating case. Futher, it is noted that the "energetic efficiency increases monotonically with increase in turbine inlet temperature" [79]. Whether the advantages proposed by the recompression S-CO2 cycle outweigh the extra complexity and capital cost of the secondary turbine, compressor, heat recuperator and reactor loop remain unknown.

A prototype test rig operating the S-CO2 simple Brayton cycle has been developed by Sandia National Laboratories [78]. The test rig is designed to produce 10 kW of mechanical power. The centrifugal compressor unit has a rotor of radius 19 mm, rotational speed of 75,000 rpm, pressure ratio of 1.8, mass flow rate of 3.5 kg/s and exit blade height of 1.7 mm. Due to the extreme fluctuations in thermophysical properties of carbon dioxide around the critical point, the density of the fluid entering the compressor is between 65 - 80% the density of water in liquid state. Coupled to the very low enthalpy change across the compressor, this results in rather unique compressor design characteristics. The turbo - compressor unit is noted as reaching energetic 'break even' when the turbine inlet temperature is 60 °C [78]. Sandia National Laboratories are planning on subsequently developing and testing a 10 MW system.

A prospect of utilising S-CO2 in Concentrated Solar Power (CSP) systems has been considered in a number of different studies [82–84, 89]. The majority of operational parabolic trough CSP plants use synthetic oils as the heat transfer fluid, which is used to produce steam either directly or indirectly (if thermal storage is present) for the turbine. A smaller minority of parabolic trough CSP plants use Direct Steam Generation (DSG), where the steam is produced and superheated directly in the collector tubes. Both of these methods have a number of drawbacks, which can potentially be eradicated through the use of the S-CO2 Brayton cycle. Synthetic oils are expensive, highly flammable, are limited to a maximum

temperature of around 400 °C and over time degrade to their constituent parts which reduces plant efficiency. DSG plants experience a phase change in the collector tubes, which adds complexity to the design and control of the system. Besides mitigating all of these drawbacks, a S-CO2 Brayton cycle has a much smaller power block and can use forced air cooling far more effectively - condensing water requirements for standard CSP systems places significant restraints on suitable sites. Indeed, the S-CO2 simple Brayton cycle has a theoretical efficiency which surpasses that of the superheated steam Rankine cycle at turbine inlet temperatures above approximately 450 °C and the supercritical steam Rankine cycle at above approximately 550 °C.

Possibly the greatest challenge facing S-CO2 parabolic trough CSP systems, besides the closed Brayton cycle itself - which is being actively researched for next generation nuclear plants, is the high pressure S-CO2 piping system running through the collector fields or power tower receiver. The very high pressure fluid combined with the distance that the fluid must travel brings technical challenges with the collectors tubes themselves, which ordinarily carry high density oil and low pressure (not low density fluid at very high pressure). The next biggest challenge is the integration of thermal storage technologies, *e.g.* two-tank molten salt systems versus packed-bed thermocline systems [82]. High pressure thermal storage vessels require very thick walls and are limited in diameter, a low pressure molton salt thermal storage vessel could be used but this would require a S-CO2 - to - molten salt heat exchanger – these do not currently exist [82]. A prototype low temperature evacuated tube S-CO2 solar collector system has been created and tested [83], where comparisons between R744 and other refrigerants are made in the context of CSP. The prototype evacuated tubes consist of an outer glass envelope, and inner glass selectively coated tube, inside of which is an aluminium fin housing two small steel tubes which carry the pressurised carbon dioxide at 120 bar. The collectors were capable of heating the CO_2 to 165 °C, which the author predicts would correspond to a power generation efficiency of 25 % and

a heat recovery efficiency of 65 % - this appears optimistic, and will have to be verified.

A S-CO2 CSP system using a central receiver tower has been proposed by Chacartegui et al. [89]. Three cycles are proposed: a basic closed S-CO2 Brayton cycle, a part-flow recompression closed S-CO2 Brayton cycle, and a topping basic closed S-CO2 Brayton cycle with a bottoming ORC. Central receiver tower systems hold many advantages of parabolic trough systems when S-CO2 is the working fluid. The high pressure associated with S-CO2 is best if kept refined to a single location for cost, performance and safety reasons, as would be the case in a central receiver tower. In a parabolic trough system the highly pressurised fluid would be sent around the entire field, which would require no doubt expensive receiver tubes, and result in notable pressure and heat losses around the field, as well as present an increased safety hazard. Further, the concentration of the incident radiation is considerably higher in central receiver towers than it is for parabolic troughs - the implication being that central receiver towers are capable of producing extremely high temperatures at the focal point. Higher temperatures allow for considerably higher thermal to mechanical conversion efficiencies to be achieved. At a turbine inlet temperature of 450 °C a supercritical steam Rankine cycle is capable of a conversion efficiency of approximately 43 % whilst a S-CO2 closed Brayton cycle is capable of a theoretical conversion efficiency of approximately 40 %, at a turbine inlet temperature of 950 °C a S-CO2 closed Brayton cycle is capable of a theoretical conversion efficiency of approximately 55 % [82], which is well above the maximum conversion efficiency and turbine inlet temperature possible in a supercritical steam Rankine cycle.

2.7 Conclusions

This Chapter provided a general review of literature relating to thermally activated heat pumps for integration into trigeneration systems. A review of refrigerants, single component and multi component, zeotropic and azeotropic is given.

Natural refrigerants such as R744 and R717 have been identified as featuring heavily in research over the past decade, owing to a continued move towards low GWP and low ODP refrigerants, driven in part by the Montreal protocol. The use of highly zeotropic refrigerant mixtures, such as LiBr - H_2O and H_2O - NH_3, in thermally activated absorption heat pumps has been discussed, and a number of concepts and recent advances to increase the COP have been presented. These include: multi - stage / multi - effect cycles, generator - absorber exchanger cycles and vapour recompression cycles. Triple - stage triple - effect absorption chillers are capable of achieving a COP_c of approximately 1.6, but suffer from corrosion in the upper generator due to the high temperatures [48]. The COP is both a function of the upper generation temperature, chilled water temperature, load conditions and the flow arrangement. It is demonstrated by Kaita that the parallel flow configuration achieves the highest COP for all absorber and generator conditions considered [47].

A brief review of multi - bed and multi - stage adsorption heat pumps, and sorbent and sorbate pairs demonstrates that COP of this technology is still far below that of absorption heat pumps. The Chapter closes with a review of R744 Mechanical Vapour Compression (MVC) heat pumps along with a review advances Supercritical Carbon Dioxide (S-CO2) power cycle concepts. It is evident from the review of literature that there is a small scope for innovations in multi - stage multi - effect absorption heat pump cycle design, and a significant scope for innovations in R744 heat pump cycle design. Therefore, the analysis of multi - stage multi - effect absorption heat pump cycle and R744 heat pump cycle concepts form the key contributions to research presented within this Thesis.

An overview of some common heat pump cycles found within the literature is contained within Table 2.1.

Type of Technology	Working Fluids	Comment	Typical range of COP
Adsorption	Silica gel - water	Three bed, non-regenerative. Hot water inlet T = 85 °C, coolant water inlet T = 30 °C, chilled water inlet / outlet T = 14 / 6 °C	0.7 [90]
Adsorption	Activated carbon - CO_2	-	0.083 [91]
Adsorption	Zeolite - water	Double-bed with heat regeneration. Ambient temperatures ranged from 27 °C to 38 °C, Specific Cooling Production (SCP) was 36 W/kg and could be increased to 106 W/kg whilst sacrificing COP (0.7)	1.0 - 1.6 [92]
Adsorption	Silica gel - water	Triple-bed. Designed for low driving temperature operation	0.43 [90]
Adsorption	$NiCl_2$ - NH_3	Single-stage. Ideal COP	0.38 [72]
Adsorption	$MnCl_2$ - NH_3	Single-stage. Ideal COP	0.45 [72]
Adsorption	$MnCl_2$ / $NiCl_2$ - NH_3	Double-stage. Evaporation temperature of -10 °C, condensation temperature of 40 °C	0.6 [92]
Adsorption	$SrCl_2$ / $FeCl_2$ - NH_3	Double-stage. Evaporation temperature of -10 °C, condensation temperature of 40 °C	0.7 [92]
Adsorption	$NiCl_2$ / $SrCl_2$ - NH_3	Double-stage. Ideal COP	0.75 [72]
Adsorption	$MnCl_2$ / $SrCl_2$ - NH_3	Doule-stage. Ideal COP	0.95 [72]
Adsorption	$NiCl_2$ - $MnCl_2$ - $SrCl_2$ - NH_3	Triple-stage. Ideal COP	1.10 [72]
Absorption / Compression	H_2O-NH_3	GAXAC cycle	1.185 [61]
Absorption / Ejector	LiBr - H_2O	Single stage absorption cycle utilising a steam ejector to simulate a GAXAC-style cycle	1.013 [93]
Absorption	H_2O-NH_3	Double stage triple effect 'Kangaroo' cycle. T_{amb} ranging from 28 °C to 35 °C	1.15 - 1.55 [56]
Absorption	LiBr - H_2O	Theoretical study of a 16 kW steam driven double effect chiller. Performance is heavily dependant upon ambient conditions	1.03 [55]
Absorption	H_2O - NH_3	GAX cycle utilising four operational modes. COP_c quoted is for T_{amb} of 40 °C	0.55, 0.85, 0.9 [59]
Absorption	LiBr - H_2O	Three stage triple effect chiller in parallel or series flow configuration. Generator temperature around 200 °C	1.7 [54]
Absorption	H_2O:NaOH - NH_3	Single stage cycle. Addition of NaOH increases COP_c by around 15 %	0.6 [94]

Table 2.1: List of various absorption and adsorption cycles and relevant data

Chapter 3

Absorption Heat Pump Cycle Concepts

3.1 Absorption Heat Pump Cycle Concepts

3.1.1 Introduction

Absorption heat pumps are typically used in CCHP systems (discussed in §2.2) as chillers to produce chilled water for space cooling, dehumidification and process chilled water. As mentioned previously, the technoeconomic feasibility of the such systems is generally very dependent upon climatic conditions. The most common type of absorption heat pumps, LiBr - H_2O and H_2O - NH_3, achieve COP_c of ∼0.7 in a single - stage configuration, ∼1.2 in a double - stage configuration, and ∼1.7 in a triple - stage configuration (LiBr - H_2O only). In this Chapter, a number of high performance and hybrid absorption heat pump cycles are conceptualised, analysed and discussed.

These cycles are modeled and simulated using Engineering Equation Solver (EES)[1]. It is assumed that all processes are adiabatic and reversible, with the exception of the pump, which is modeled using an appropriate pumping efficiency. Ambient temperature is specified as 30 °C. Evaporator refrigerant inlet temperature is specified as 4 °C, which, given a standard chilled water flow / return of 6 / 12 °C, implies a ΔT_{min} in the evaporator of 2 °C. In all other HXs, ΔT_{min} is specified at 4 °C.

3.1.2 H_2O - NH_3 Kangaroo Cycle

The Kangaroo Cycle, as mentioned in §2.3.1, is a H_2O - NH_3 multiple effect cycle, where each stage is independent, but thermally coupled to the others. Six cycles are presented in this chapter: single - stage / single - effect V.1 & V.2, double - stage / triple - effect V.1 & V.2 and triple - stage / quintuple - effect V.1 & V.2.

Rectifier The purpose of the rectifier is to increase refrigerant mass fraction (x) from that which leaves the generator to that which is deemed sufficient to negate

[1] http://www.fchart.com/ees/

an unacceptable thermal gradient (temperature glide) in the evaporator. Typically a mass fraction (x) 0.995 kg/kg is deemed acceptable [51, 61, 95, 96], and this research indicates that this value results in a temperature glide of between 5 & 6 °C in the evaporator. Higher values of x require significantly increased plant size, can lead to condensation of refrigerant in the rectifier (hence, reduction of refrigerant mass flow), and provide minimal performance gain. Indeed, temperature glide in evaporators is rarely an issue, provided a direct exchange evaporator is specified. Without rectification, the evaporator temperature glide is in excess of 25 °C, which is highly undesirable.

The rectifier can take a number of physical forms, but the main design choice is how heat is removed from the low refrigerant mass fraction generator outlet vapour, external heat rejection or internal heat rejection. With external heat rejection, the rectifier simply rejects heat to an external sink, potentially via dry cooling or wet cooling, the former of which would create a electrical load on the system, and the latter of which would require a continuous water source or, if recirculation is used, a coolant circuit and associated subsystems. Internal heat rejection has none of the drawbacks of external, and actually has a positive impact upon COP by reducing the generator's requirement for heat. The mid quality refrigerant / sorbent solution exiting the absorber is either passed through the solution HX and then the rectifier (V.1) or passed through the rectifier and then the solution HX (V.2). Recuperation via the rectifier accounts for around 13 % of internally recuperated heat.

Based upon Figure 3.1 the rectifier is modeled under the constraints of equations 3.1, 3.2 and 3.3.

$$m_1 = m_2 + m_3 \tag{3.1}$$

$$m_1 x_1 = m_2 x_{2=x_f} + m_3 x_{3=x_g} \tag{3.2}$$

$$m_1 h_1 = m_2 h_{2=h_f} + m_3 x_{3=h_g} + m_9^{H_2O+NH_3 mixture} h_9 - m_{10}^{H_2O+NH_3 mixture} h_{10} \quad (3.3)$$

Generator The generator produces refrigerant vapour and weak sorbent solution via an endothermic reaction, using an input of strong sorbent solution from the absorber and weak sorbent solution returned from the rectifier. Depending on the conditions, the refrigerant vapour has a value of x of around 0.98, with a quality (q) slightly below the saturated vapour line. The weak sorbent solution outlet is the highest temperature flow of the cycle, and has a typical mass fraction of around 0.38.

In the single - stage cycle the generator, or in the case of multiple - stage cycles the upper generator, is driven by an external heat source, which is likely to be a heat transfer fluid which passes through the generator and is itself heated by an external source. In the lower generators of multiple - stage cycles the generators are driven either by the condenser or absorber from the upper cycle. In the case of the former the condenser runs directly through the generator, whilst in the case of the latter an intermediate heat transfer medium is required. Heat pipes could be used as an effective way of transferring the heat from absorber to generator. The minimum ΔT of upper condenser / absorber temperature to lower generator is 10 °C.

Based upon Figure 3.1 the generator is modeled under the constraints of equations 3.7, 3.8 and 3.9.

$$m_1 = m_2 + m_{10} - m_{11} \quad (3.4)$$

$$m_1 h_1 = m_2 h_1 + m_{10} h_{10} - m_{11} h_{11} + m_{21} h_{21} - m_{22} h_{22} \quad (3.5)$$

$$m_1 x_1 = m_2 x_{2=x_f} + m_{10} h_{10} - m_{10} h_{10} \quad (3.6)$$

Absorber The absorber produces strong sorbent solution via an exothermic reaction, using an input of weak sorbent solution from the generator and refrigerant vapour from the evaporator. The absorber is modeled to produce a Δx of 0.1, which typically equates to a refrigerant to solution mass flow rate ratio (Ψ) of around 0.19. An increase in Ψ would decrease the pump work, but would require a larger absorber; given that the pump work is less than 1 % of the energy supplied to the cycle, increasing Ψ is typically not desirable.

$$m_7 = m_6 + m_{13} \tag{3.7}$$

$$m_7 h_7 = m_6 h_6 + m_{13} h_{13} \tag{3.8}$$

$$m_7 x_7 = m_6 x_6 + m_6 h_{10} - m_{10} h_{10} \tag{3.9}$$

Single - Stage / Single - Effect

The single - stage / single - effect H_2O - NH_3 absorption heat V.1 and V.2 are depicted in Figures 3.1 and 3.2; Tables 3.1 and 3.2 show corresponding data for the state points under the operational criteria specified prior. The generation temperature is allowed to 'float' in order to obtain the highest possible value for COP.

V.1 This cycle, with the solution HX situated at the solution pump outlet, achieves a theoretical maximum COP_c[2] of 0.725, given a generation temperature of 105 °C. This implies a heating fluid outlet temperature of approximately 115 °C; the inlet temperature depending upon the C_p and $\dot{m}$ of the fluid. The ratio of the mass flow rate of refrigerant in the evaporator and the mass flow rate of solution exiting the absorber (Ψ) is 0.191 kg/kg. The ratio of generator heat input to

[2] COP_c is defined as the ratio of thermal energy input into the cycle to the production of useful coolth within the evaporator(s)

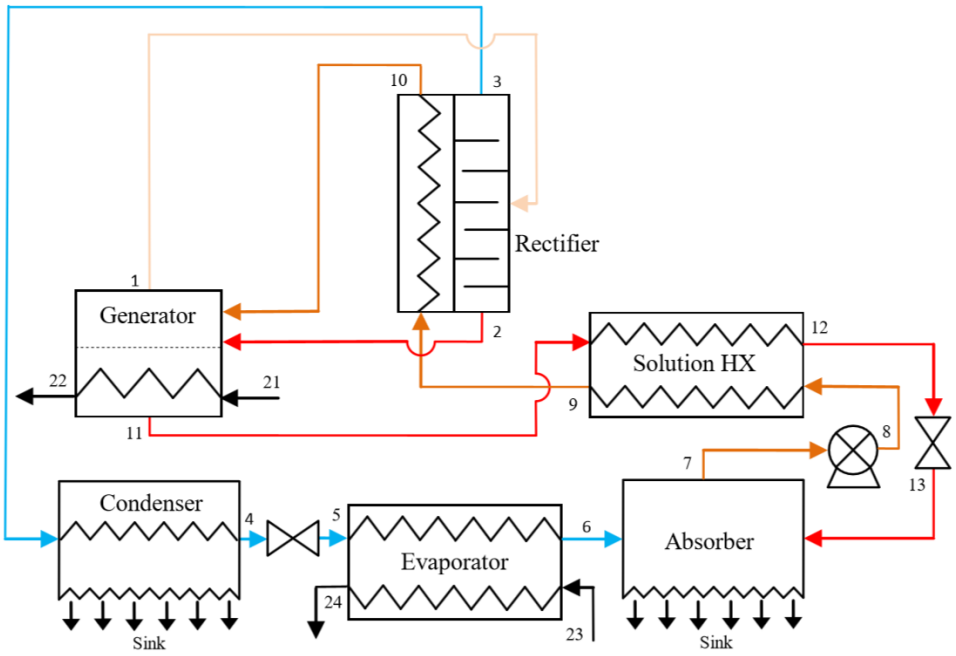

Figure 3.1: 1 - Stage / 1 - Effect H_2O - NH_3 V.1 absorption heat pump cycle process flow diagram

pump work (Ω) is 99.4.

State Point	h (kJ/kg)	P (bar)	m (kg/s)	T (°C)	s (kJ/kgK)	x (kg/kg)
1	1446	15.13	1	85.3	4.64	0.9812
2	147.1	15.13	0.03494	85.3	1.06	0.4745
3	1299	15.13	0.9651	44.8	4.20	0.9995
4	185.7	15.13	0.9651	39.0	0.642	0.9995
5	185.7	5.155	0.9651	5.00	0.679	0.9995
6	1281	5.155	0.9651	10.5	4.60	0.9995
7	-38.94	5.155	6.031	44.8	0.508	0.4745
8	-36.51	15.13	6.031	45.1	0.512	0.4745
9	176.0	15.13	6.031	86.9	1.14	0.4745
10	207.1	15.13	6.031	88.6	1.22	0.4745
11	249.7	15.13	5.066	105.3	1.32	0.3745
12	-3.259	15.13	5.066	49.1	0.595	0.3745
13	-3.259	5.155	5.066	49.3	0.599	0.3745

Table 3.1: State properties - 1 - Stage / 1 - Effect H_2O - NH_3 V.1 cycle

V.2 This cycle, with the rectifier is situated at the solution pump outlet and solution HX is situated following the rectifier, achieves a theoretical maximum COP_c of 0.680, given a generation temperature of 98 °C; implying a heating fluid outlet temperature of 108 °C. Ψ is 0.205 kg/kg and Ω is 111.4.

There is a marginal increase in both Ψ and Ω when progressing from V.1 to

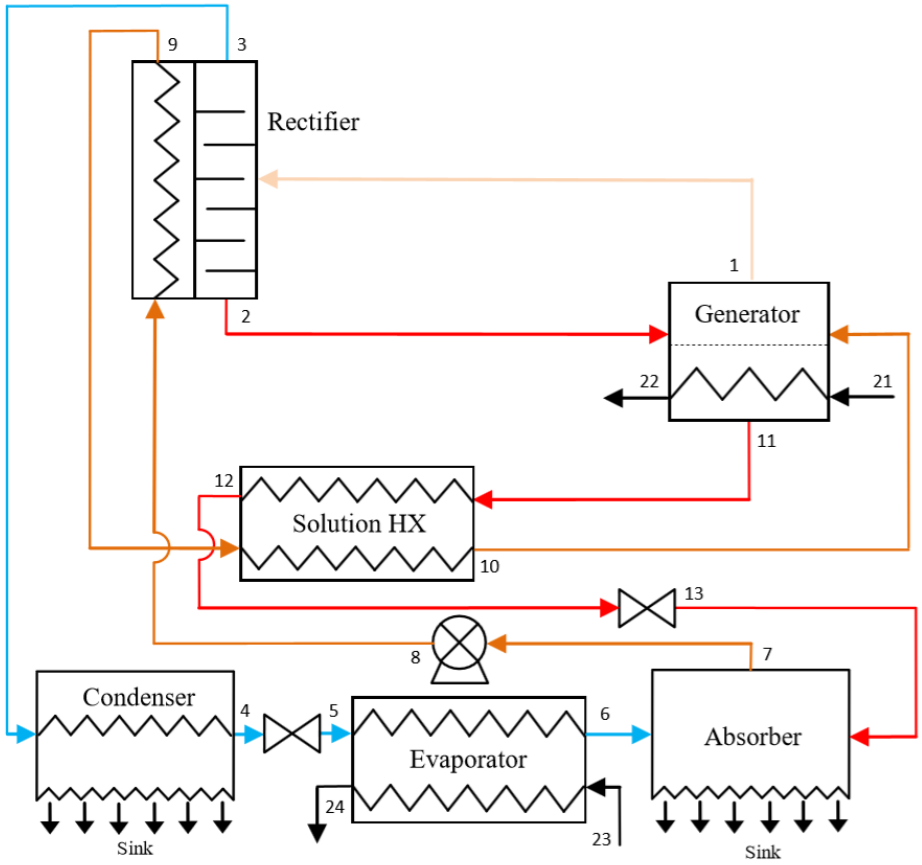

Figure 3.2: 1 - stage / 1 - effect H_2O - NH_3 V.2 absorption heat pump cycle process flow diagram

V.2. This indicates that V.2 produces more refrigerant vapour in the generator than V.1, although the COP_c is marginally lower. The generator temperature in V.2 is lower than V.1, which is the cause of the marginal decrease in COP_c despite the higher Ψ.

The ratio of recuperated heat from the solution HX to the rectifer (Φ) is 6.83 for V.1, whilst for V.2 it is 6.76. The similar values for Φ indicate that the order of recuperation bears little effect upon the relative source of the recuperated heat; the predominant factor being the heat available, and the refrigerant mass fraction, x, of the fluid entering the rectifier.

The proportion of generator heat input which is internally recuperated (Θ) is 0.502 for V.1 and 0.432 for V.2. The substantially lower Φ in V.2 is the predominant cause of the reduction in COP_c; a reduction in internally recuperated heat, due to the exergy of the weak sorbent solution entering the solution HX

State Point	h (kJ/kg)	P (bar)	m (kg/s)	T (°C)	s (kJ/kgK)	x (kg/kg)
1	1425	15.13	1.000	78.9	4.58	0.9880
2	119.3	15.13	0.02348	78.9	0.973	0.5112
3	1299	15.13	0.9765	44.8	4.20	0.9995
4	185.7	15.13	0.9765	39.0	0.642	0.9995
5	185.7	5.155	0.9765	5.00	0.679	0.9995
6	1281	5.155	0.9765	10.5	4.60	0.9995
7	-64.64	5.155	5.745	39.0	0.423	0.5112
8	-62.18	15.13	5.745	39.4	0.427	0.5112
9	-5.36	15.13	5.745	45.3	0.512	0.5112
10	146.2	15.13	5.745	80.2	1.05	0.5112
11	207.9	15.13	4.768	97.6	1.22	0.4112
12	-10.83	15.13	4.768	49.3	0.585	0.4112
13	-10.83	5.155	4.768	49.5	0.588	0.4112

Table 3.2: State properties - 1 - Stage / 1 - Effect H_2O - NH_3 V.2 cycle

hot side, means that more heat must be supplied from external sources to the generator. The order of rectifier and solution HX in V.2 results in a decreased 2nd Law efficiency and unnecessary exergy destruction. It also leads to a hitting of the minimum ΔT_{min}[3] at the cold end of the solution HX, indicating that the potential level of heat recuperation is restricted; whilst in V.1 the equivalent temperature pinch is 4.19 °C, the cycle is not restricted by the ΔT_{min}.

Double - Stage / Triple - Effect

The double - stage / triple - effect H_2O - NH_3 absorption heat pump V.1 and V.2 are depicted in Figures 3.3 and 3.4; Tables 3.3 and 3.4 show corresponding data for the state points under the operational criteria specified prior.

V.1 This cycle features two separate but thermally coupled single - stage cycles, depicted in Figure 3.3. The upper cycle (Figure 3.3a), is thermally activated by an external source and much the same as the single - stage V1 cycle depicted in Figure 3.1. The primary difference being an increase in temperature of the external heat source (Point 51), resulting in increased temperatures and pressures throughout the cycle. The upper condenser and upper absorber are both cooled by the two generators in the lower cycle (Figure 3.3b). The specific means by

[3] ΔT_{min} refers to the minimum pinch temperature, or temperature difference between the two fluid flows in a heat exchanger

which heat is transferred is not included in this analysis; direct heat exchange is possible, although indirect exchange via an active system such as a circulated heat transfer fluid, or a passive system such as heat pipes would simplify system design and control. In order to accommodate any heat transfer method, a minimum temperature pinch between the lower generator(s) and upper absorber / condenser of 10 °C has been specified. The fluid entering both the upper and lowers evaporator is throttled to the same pressure, thus both produce a cooling effect of the same temperature, but not necessarily the same magnitude.

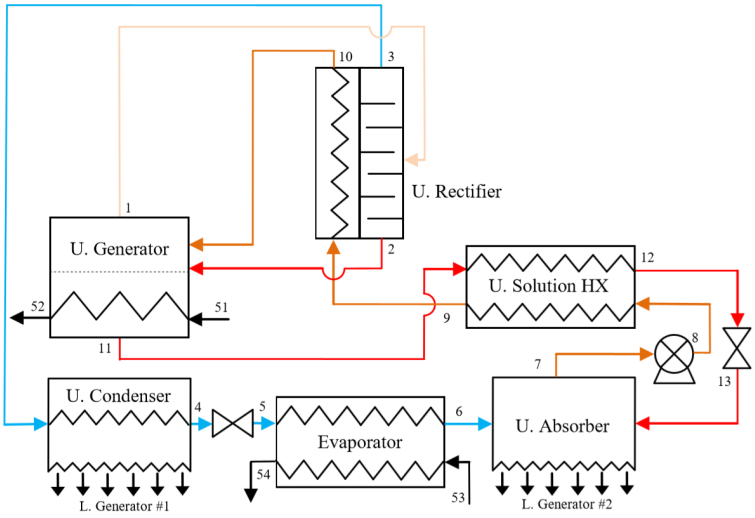

(a) Upper Cycle

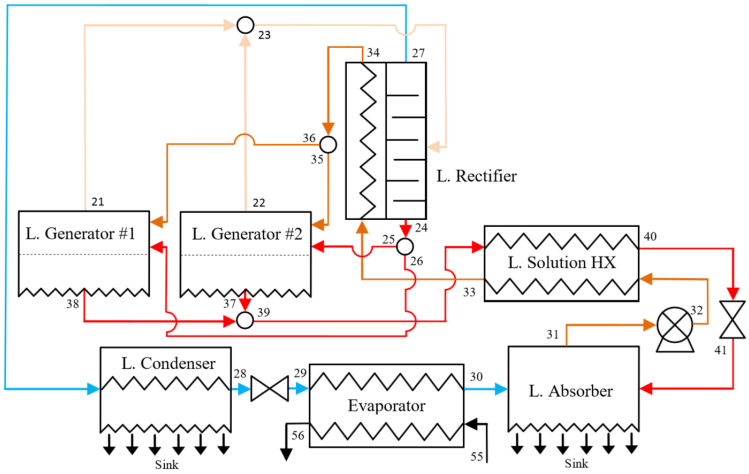

(b) Lower Cycle

Figure 3.3: 2 - stage / 3 - effect H_2O - NH_3 V.1 absorption heat pump cycle process flow diagram

This cycle achieves a COP_c of 1.765, given an upper generation temperature

of 224 °C; thus implying a heating fluid outlet temperature of approximately 234 °C. The upper cycle has a Ψ of 0.131 kg/kg, and the lower cycle has a Ψ of 0.217 kg/kg.

State Point	h (kJ/kg)	P (bar)	m (kg/s)	T (°C)	s (kJ/kgK)	x (kg/kg)
1	1957	47.52	0.602	200.5	5.241	0.6975
2	755	47.52	0.239	200.5	2.428	0.2386
3	1247	47.52	0.363	87.3	3.675	0.9995
4	434	47.52	0.363	86.0	1.363	0.9995
5	434	4.97	0.363	4.0	1.571	0.9995
6	1280	4.97	0.363	9.6	4.610	0.9995
7	228	4.97	3.127	90.1	1.182	0.2386
8	238	47.52	3.127	91.8	1.195	0.2386
9	764	47.52	3.127	201.0	2.449	0.2386
10	939	47.52	3.127	210.2	2.811	0.2386
11	908	47.52	2.763	224.4	2.661	0.1386
12	313	47.52	2.763	95.74	1.285	0.1386
13	313	4.97	2.763	96.4	1.297	0.1386
14	1399	13.12	0.630	68.7	4.563	0.9915
15	74	13.12	0.011	68.7	0.838	0.5377
16	1298	13.12	0.619	40.9	4.563	0.9995
17	161	13.12	0.619	34.0	0.564	0.9995
18	161	4.97	0.619	4.0	0.592	0.9995
19	1280	4.97	0.619	9.6	4.610	0.9995
20	-85	4.97	3.478	34.0	0.350	0.5377
21	-83	13.12	3.478	34.3	0.353	0.5377
22	94	13.12	3.478	69.6	0.896	0.5377
23	116	13.12	3.478	70.6	0.960	0.5377
24	152	13.12	2.859	86.1	1.047	0.4377
25	-64	13.12	2.859	38.3	0.423	0.4377
26	-64	4.97	2.859	38.5	0.426	0.4377

Table 3.3: State properties - 2 - Stage / 3 - Effect H_2O - NH_3 V.1 cycle

V.2 This cycle is similar to V.1, but the position of the rectifier and solution HX in both the upper and lower cycles has been altered. The rectifiers are now situated following the absorber strong sorbent solution outlet, whilst the solution heat exchanger follows on from the rectifier. A schematic of the double - effect triple - effect cycle is shown in Figure 3.4.

This cycle achieves a COP_c of 1.422, given an upper generator temperature of 187 °C; thus implying a heating fluid outlet temperature of approximately 197 °C. The upper cycle has a Ψ of 0.147 kg/kg, and the lower cycle has a Ψ of 0.217 kg/kg. When compared to the values for Ψ achieved by V.1, this represents a small increase in generation efficiency in the upper cycle, whilst the generation

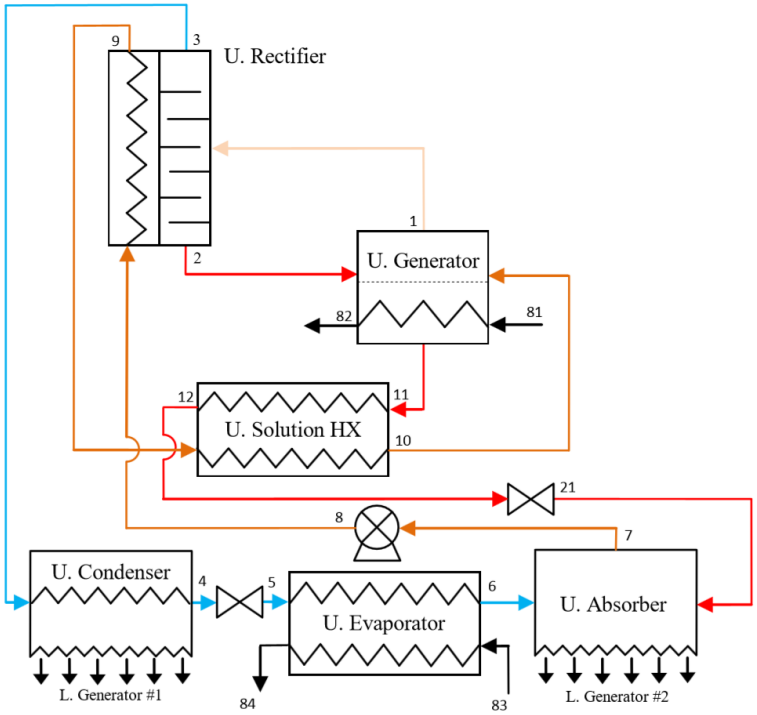

(a) Upper Cycle

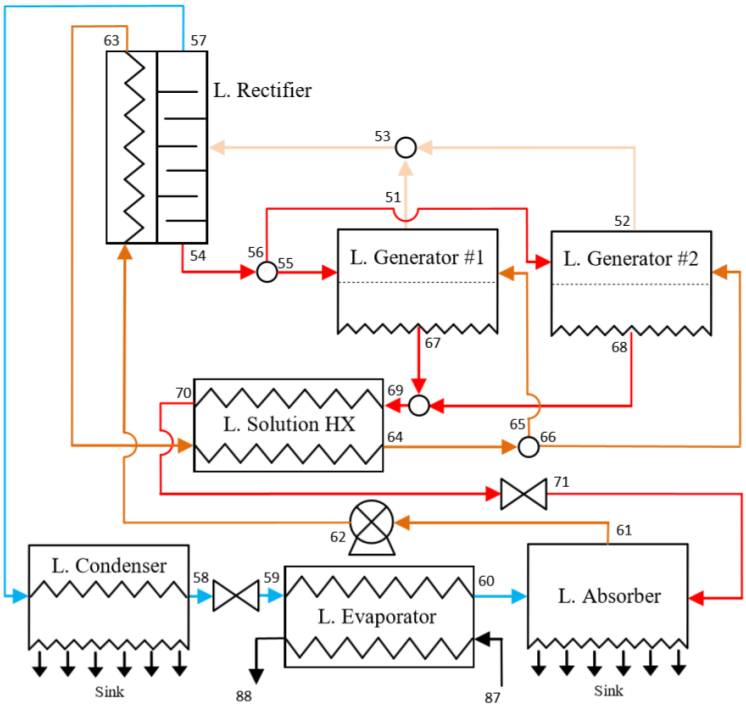

(b) Lower Cycle

Figure 3.4: 2 - stage / 3 - effect H_2O - NH_3 V.2 absorption heat pump cycle process flow diagram

efficiency in the lower cycle remains constant.

In V.1, the evaporator in the upper cycle produces 30.7 % of the total chilling effect, whilst in V.2 the evaporator produces 28.4 % of the total cooling effect;

State Point	h (kJ/kg)	P (bar)	m (kg/s)	T (°C)	s (kJ/kgK)	x (kg/kg)
1	1738	35.37	0.403	163.7	4.960	0.8440
2	547	35.37	0.091	163.7	2.019	0.3189
3	1274	35.37	0.309	74.5	3.828	0.9995
4	360	35.37	0.309	72.6	1.161	0.9995
5	360	4.97	0.309	4.0	1.307	0.9995
6	1280	4.97	0.309	9.6	4.610	0.9995
7	117	4.97	2.411	72.6	0.929	0.3189
8	124	35.37	2.411	73.8	0.939	0.3189
9	229	35.37	2.411	97.3	1.231	0.3189
10	580	35.37	2.411	165.8	2.096	0.3189
11	693	35.37	2.102	187.4	2.286	0.2189
12	290	35.37	2.102	101.3	1.319	0.2189
13	290	4.97	2.102	96.6	1.329	0.2189
14	1402	13.12	0.650	68.6	4.571	0.9924
15	74	13.12	0.010	68.6	0.838	0.5377
16	1298	13.12	0.640	40.9	4.254	0.9995
17	161	13.12	0.640	34.0	0.564	0.9995
18	161	4.97	0.640	4.0	0.592	0.9995
19	1280	4.97	0.640	9.6	4.610	0.9995
20	-85	4.97	3.594	34.0	0.350	0.5377
21	-83	13.12	3.594	34.4	0.353	0.5377
22	-61	13.12	3.594	39.2	0.425	0.5377
23	98	13.12	3.594	69.7	0.909	0.5377
24	152	13.12	2.955	86.1	1.067	0.4377
25	-42	13.12	2.955	43.2	0.492	0.4377
26	-42	4.97	2.955	43.3	0.495	0.4377

Table 3.4: State properties - 2 - Stage / 3 - Effect H_2O - NH_3 V.2 cycle

the lower evaporators produce 69.3 % and 71.6 %, respectively. This difference in cooling effect contributions between V.1 and V.2 is contrary to the difference in generation efficiency. The mass flow rates of refrigerant, sorbent and refrigerant / sorbent solution in the upper cycle are between 20 and 30 % higher in V.1, relative to V.2. The mass flow rates in the lower cycle in both V.1 and V.2 are very similar. The higher generation efficiency and reduced chilling effect in V.2 are likely the reason for the reduced mass flow rates.

The values for Φ for V.1 are 0.786 and 0.433 in the upper and lower cycles, respectively. The same values for V.2 are 0.609 and 0.390. The difference in Φ between V.1 and V.2 is apparent due to the reduction in exergetic efficiency resulting from the ordering of the rectifier and solution HX in the heat recuperation process. The difference between the temperature of the strong solution entering the generator and the generation temperature ($T_{11} - T_{10}$ and $T_{24} - T_{23}$ in Table

3.3 and 3.4), is considerably less in V.1 than V.2 in both the upper and lower cycles. This also occurs as a direct result of the reduction in exergetic efficiency, the result of which is a requirement for more externally supplied thermal energy (observed by a decrease in Φ); this reduces the COP.

Overall, the 'Double - Stage / Triple - Effect' V.1 cycle achieves a significantly higher COP_c than V.2, with a 24 % increase resulting from the change in the positions of the solution HX and rectifier.

Triple - Stage / Quintuple - Effect

The triple - stage / quintuple - effect absorption heat pump V.1 and V.2 are depected in Figures 3.5 and 3.6, respectively. These cycles are an evolution of the double - stage / triple - effect absorption heat pumps V.1 and V.2 described previously. An additional H_2O - NH_3 absorption heat pump cycle loop is added around the 'outside' of the previous upper loop; such that the upper loop becomes the middle loop.

Now, the upper loop activates the middle loop by passing thermal energy from the upper condenser and upper absorber to the middle generator. The middle loop activates the lower loop by passing thermal energy from the middle condenser and middle absorber to the lower generator.

The addition of a outer loop to the single - stage / single - effect H_2O - NH_3 absorption chiller increased the COP_c by between 0.8 and 1.0 to 1.422 and 1.765 for V.2 and V.1, respectively. It could therefore be expected that the addition of a further outer loop would yield another significant boost in performance. The double double - stage / triple - effect V.1 cycle has an upper generator temperature of 224 °C, whilst the V.2. cycle has an upper generator temperature of 187 °C; this is already quite high for an ammonia mixture. Neither simulation models of the triple - stage / quintuple - effect heat pumps depicted in Figures 3.5 and 3.6 produce a solution; the thermodynamic properties of the non-azeotropic water and ammonia mixture is outside of solvable range in the upper generator. Low-

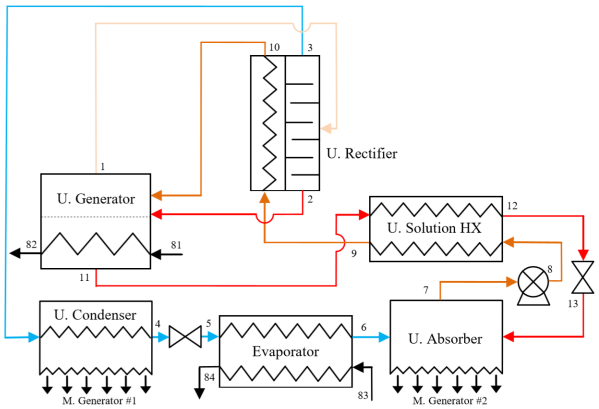

(a) Upper Cycle

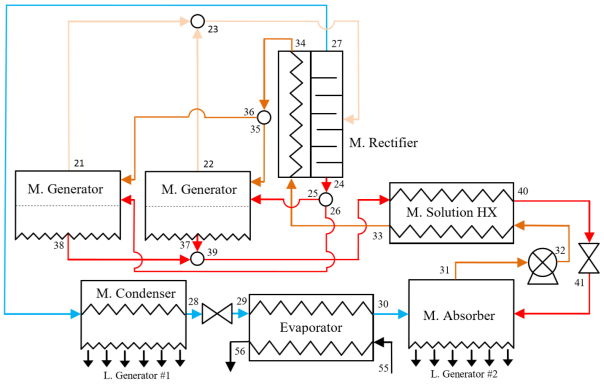

(b) Lower Cycle

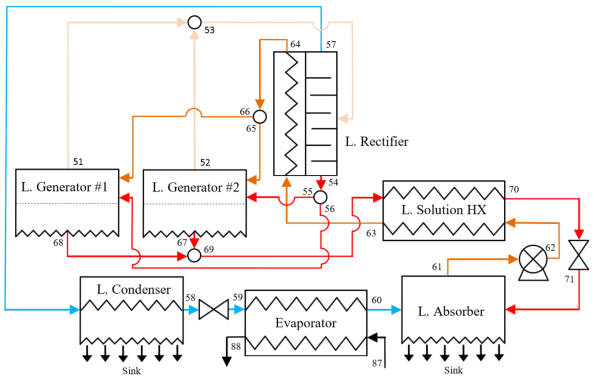

(c) Lower Cycle

Figure 3.5: 3 - stage / 5 - effect H_2O - NH_3 V.1 absorption heat pump cycle process flow diagram

ering the upper generator temperature by 'compressing' the temperature range across the loops (i.e. reducing pinch temperatures, altering pressures, isentropic efficiencies) does not yield a solution. Therefore, the triple - stage / quintuple - effect H_2O - NH_3 'Kangaroo' absorption heat pump is not a worthy candidate for further investigation.

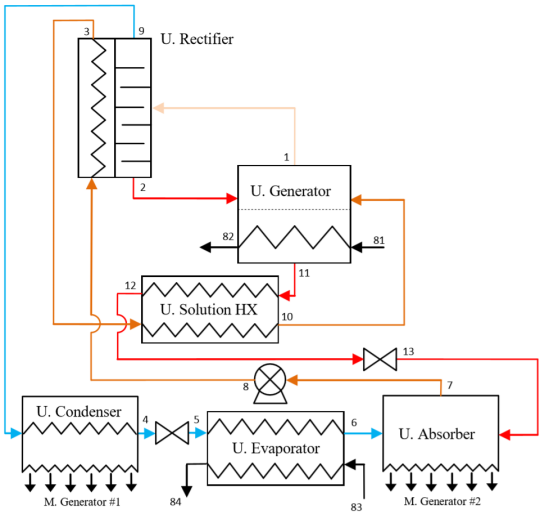

(a) Upper Cycle

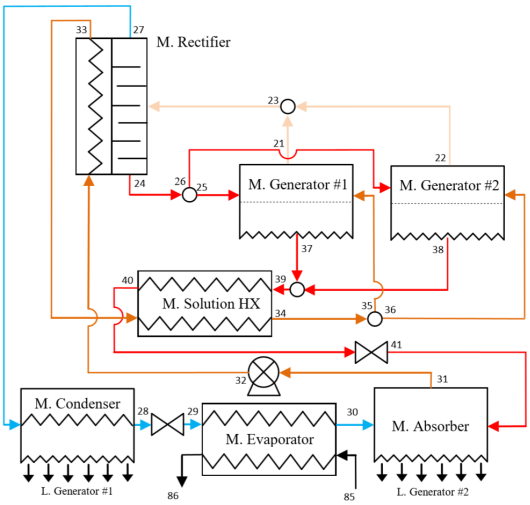

(b) Lower Cycle

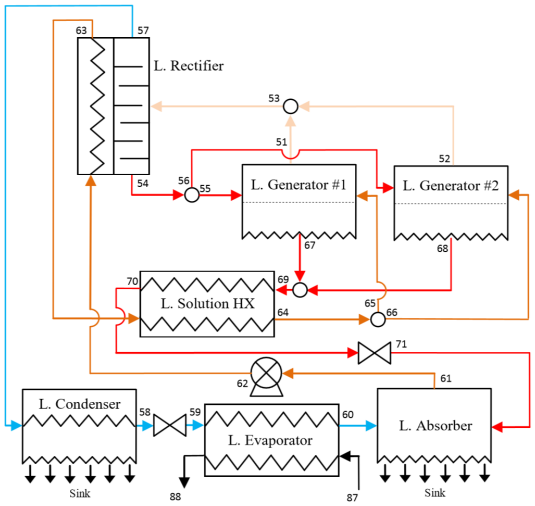

(c) Lower Cycle

Figure 3.6: 3 - stage / 5 - effect H_2O - NH_3 V.2 absorption heat pump cycle process flow diagram

3.1.3 LiBr - H_2O Compression - Absorption Cycle

The LiBr - H_2O compression / absorption heat pump cycle is a variant of the conventional LiBr - H_2O absorption heat pump cycle, and features a low pressure steam compressor. The compression / absorption heat pump cycle is a hybrid heat pump cycle; both thermal and mechanical energy inputs are required. The proportion of energy input which is thermal and mechanical has a profound effect on the performance characteristics of the cycle. The addition of a compressor into the cycle can produce a range enhancements over the standard absorption cycle, including:

- Decreasing the generation temperature
- Decreasing the evaporator temperature
- Increasing the absorber pressure
- Increasing the COP

In general, only one of these enhancements can be realised through the addition of the compressor; this is dependent upon the location of the compressor in the cycle and the pressures selected at the relevant points. It is possible to produce a blend of two of these enhancements, but this is not typically desirable. A brief introduction to each enhancement is given below, which this is followed by an analysis of compression - absorption heat pump cycles and a discussion of their technical feasibility.

Decreasing the generation temperature Lowering the generation temperature is achieved by lowering the fluid pressure within the generator. This may be desirable if the primary heat source is low temperature or has an efficiency which increases at lower temperatures. Consequently, the refrigerant vapour exiting the generator and entering the condenser is at a lower temperature, and the condenser may be unable to reject heat to atmosphere; i.e condenser exergy is reduced to

zero. The knock - on effect through the rest of the cycle is a drastic lowering of COP. However, by slightly re-pressurising the refrigerant vapour exiting the generator prior to it entering the condenser, the potential for heat rejection in the condenser can be maintained; thus the COP can remain constant. As will be shown later, the mechanical work required to re-pressurise the refrigerant vapour is relatively small.

Decreasing the evaporator temperature Lowering the evaporation pressure will reduce the evaporation temperature, thus enabling the cycle to produce chilled water at a lower temperature (n.b. this may be for process chilled water, rather than building space cooling chilled water). Ordinarily, lowering the evaporation pressure, and thus absorber pressure, would decrease the COP_c of the cycle. However, if the water vapour exiting the evaporator can be re-compressed to a higher pressure, the absorber can operate at a higher pressure, thus enabling the COP_c of the cycle to remain at consistent at lower chilled water temperatures.

Increasing the absorber pressure Raising the absorber pressure can be desirable for a number of reasons:

- *To increase the absorption temperature.* In general the waste heat from the absorber is of a temperature unusable for processes and hot water. Increasing the pressure in the absorber allows a higher operating temperature to be achieved, whilst maintaining a similar operating characteristics. Raising the operating temperature in the absorber can enable it to produce Very Low Temperature Hot Water (VLTHW) for space heating and Domestic Hot Water (DHW) in buildings, as well as low temperature industrial processes. This also reduces the requirement for, and possibly eliminates, the need for a cooling tower; dry air coolers may be sufficient for cooling the condenser.

- *To decrease the size of the absorber* A higher pressure within the absorber results in a more efficient absorption process; the rate of refrigerant absorption by the sorbent is a function of pressure and temperature, and increases at higher pressures and lower temperatures. As one of the largest components of an absorption chiller, reducing the size of the absorber may results in a more compact system.

Increasing the COP If a compressor is added at any point in the cycle, and neither of the previous three enhancements are realised, it is possible to increase the cycle COP. The increase in COP is dependant upon a number of factors, which will be discussed in the analysis.

When discussing the COP of a compression - absorption heat pump cycle, it is necessary to distinguish between the COP relative to the thermal energy input (COP_{th}), and the COP relative to the mechanical energy input (COP_{m}), such that:

$$COP_{th} = \frac{Q_{heating/cooling,out}}{Q_{generator}} \tag{3.10}$$

$$COP_{m} = \frac{Q_{heating/cooling,out}}{W_{compressor}} \tag{3.11}$$

Single - Stage / Single - Effect

A single stage compression - absorption LiBr - H_2O heat pump with the steam compressor located at the evaporator outlet is shown in Figure 3.7. As with previous analyses, Engineering Equation Solver has been used to simulate this cycle under a range of performance criteria.

The cycle is analysed using the same ambient criteria as used in the H_2O - NH_3 Kangaroo cycle detailed in the previous Section.

The effect of the compressor pressure ratio (r_p) on the $\mathrm{COP}_{c,th}$ (i.e. coefficient of performance relative to the heating work in) at four different generator

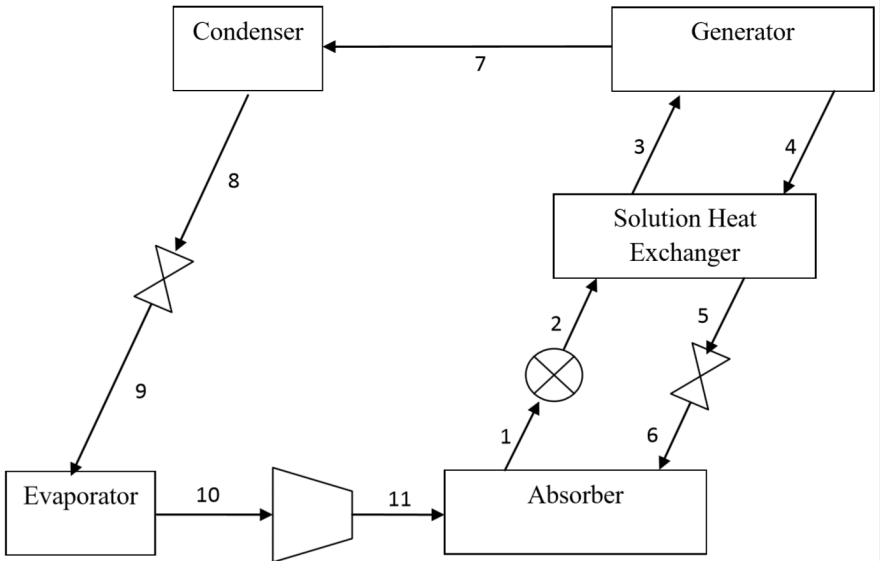

Figure 3.7: 1 - Stage / 1 - Effect LiBr - H_2O compression - absorption heat pump cycle process flow diagram

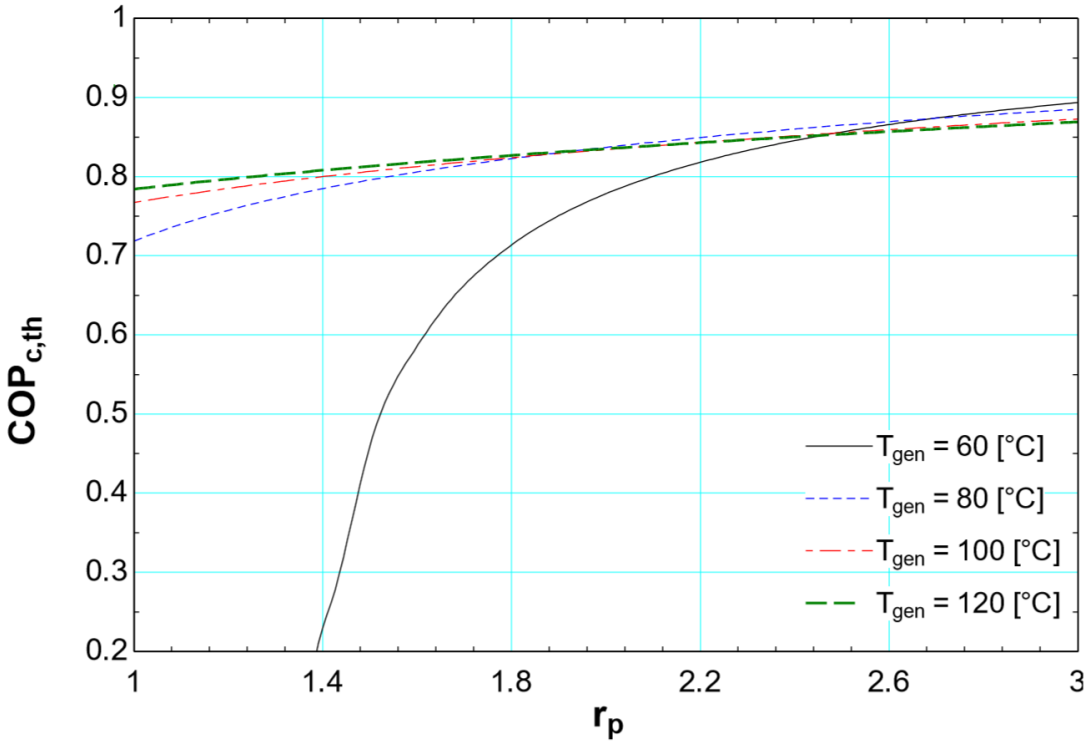

Figure 3.8: 1 - Stage / 1 - Effect LiBr - H_2O compression - absorption heat pump cycle: $\mathrm{COP}_{c,th}$ vs. r_p

temperatures is shown in Figure 3.8. It can be observed that when the compression ratio is increased, the $\mathrm{COP}_{c,th}$ increases, and this effect becomes far more profound at lower generation temperatures. With a generation temperature of 80 °C, the $\mathrm{COP}_{c,th}$ decreases sharply when the compression ratio is below 2.0,

and tends towards zero when the compression ratio is around 1.2. As generation temperature increases, the relationship between $\text{COP}_{c,th}$ and compression ratio tends to a linear relationship. Indeed, with a generation temperature of 90 °C, a near linear relationship is observed. Of further note is that at higher generation temperatures, the gradient of the line reduces (i.e. increasing compression ratio has less of an effect on $\text{COP}_{c,th}$).

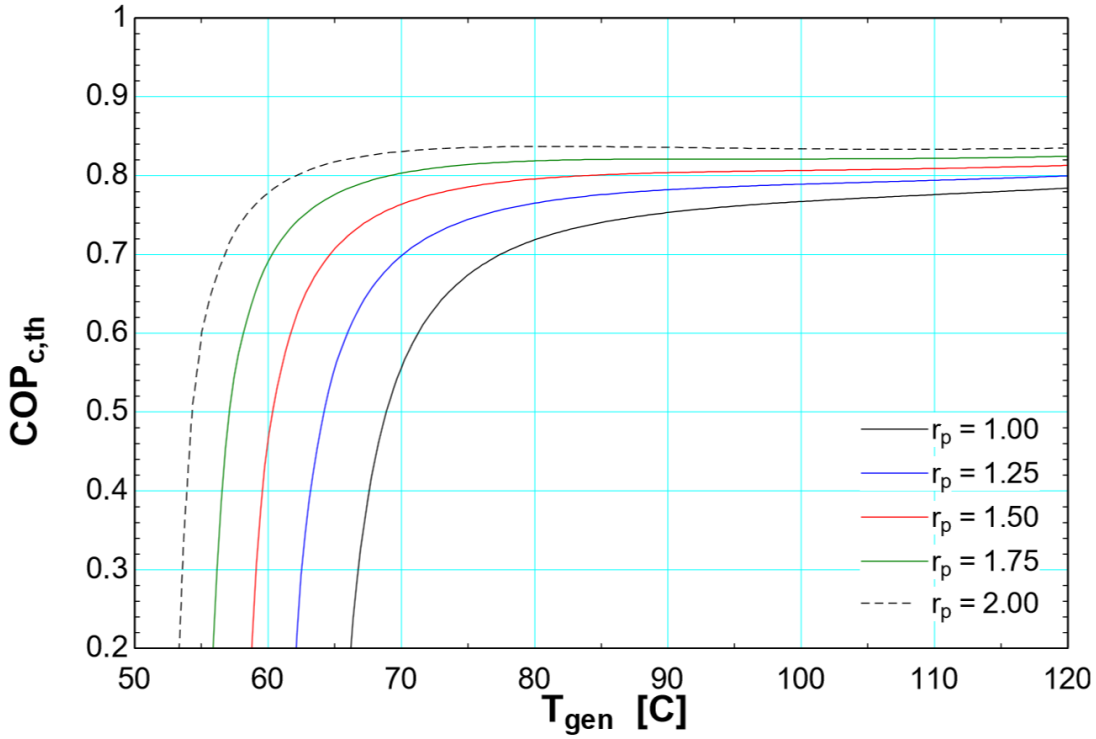

Figure 3.9: 1 - Stage / 1 - Effect LiBr - H_2O compression - absorption heat pump cycle: $\text{COP}_{c,th}$ vs. T_{gen}

A similar graph comparing $\text{COP}_{c,th}$ to generation temperature is shown in Figure 3.9. The five curves denote five compression ratios under consideration, the compression ratio of 1.00 indicating a conventional absorption chiller cycle. As the compression ratio is increased, the curves appear to shift to the left and up; implying that the minimum generation temperature at which the cycle works decreases, and the $\text{COP}_{c,th}$ increases for a given generation temperature. This is essentially the same effect observed and noted from Figure 3.8.

A graph of the cooling output relative to the mechanical work input,$\text{COP}_{c,m}$, is given in Figure 3.10. The relationship between $\text{COP}_{c,m}$ and r_p is such that

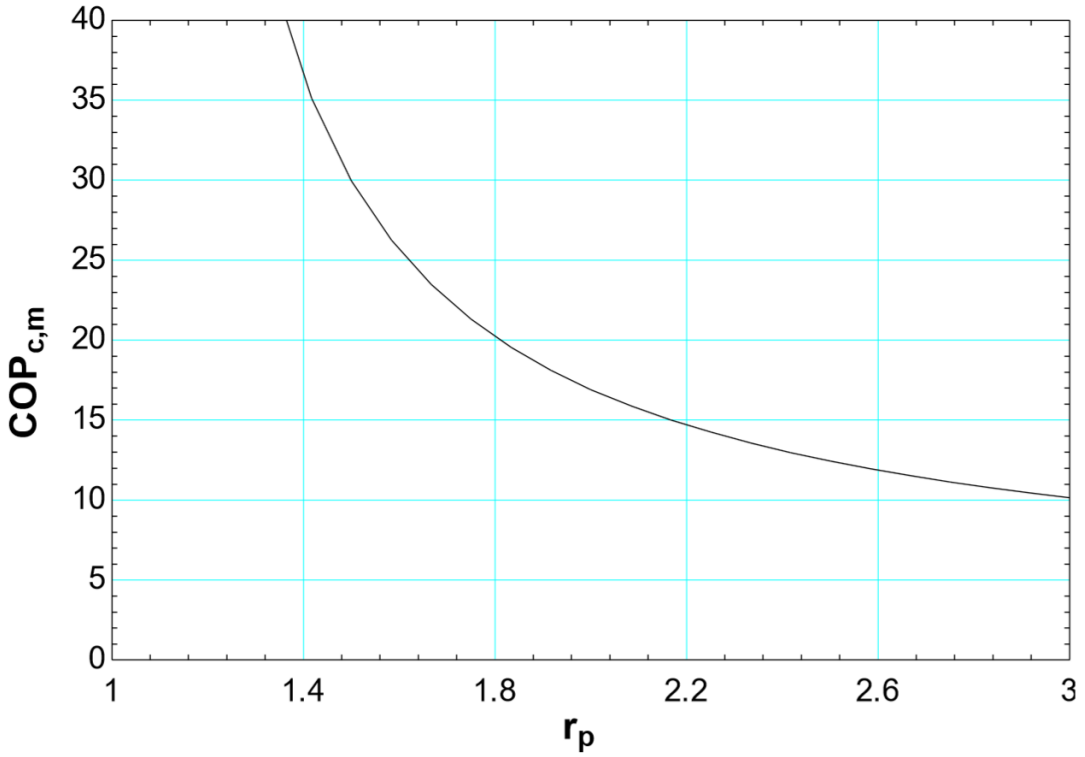

Figure 3.10: 1 - Stage / 1 - Effect LiBr - H_2O compression - absorption heat pump cycle: $COP_{c,m}$ vs. r_p

$COP_{c,m}$ tends towards a very high value when r_p is below 1.4. The minimum value for $COP_{c,m}$ under the specified r_p range is approximately 10. The $COP_{c,m}$ for a MVC is typically around 5, whilst the $COP_{c,m}$ for a conventional absorption chiller (i.e. the pump) may be around 100.

Double - Stage / Double - Effect

A double stage double effect compression - absorption LiBr - H_2O heat pump with the steam compressor located at the evaporator outlet is shown in Figure 3.11. In this cycle, heat is passed from the upper condenser directly to the lower generator via condensation of the refrigerant vapour (state point 17) within the lower generator; indicated by the dotted line. Besides the the addition of the compressor, this cycle is the same as a conventional double stage absorption chiller, used prevalently in commercial and industrial chilling processes.

The effect of r_p on the $COP_{c,th}$ at four different generator temperatures is shown in Figure 3.12. The generation temperatures simulated range between

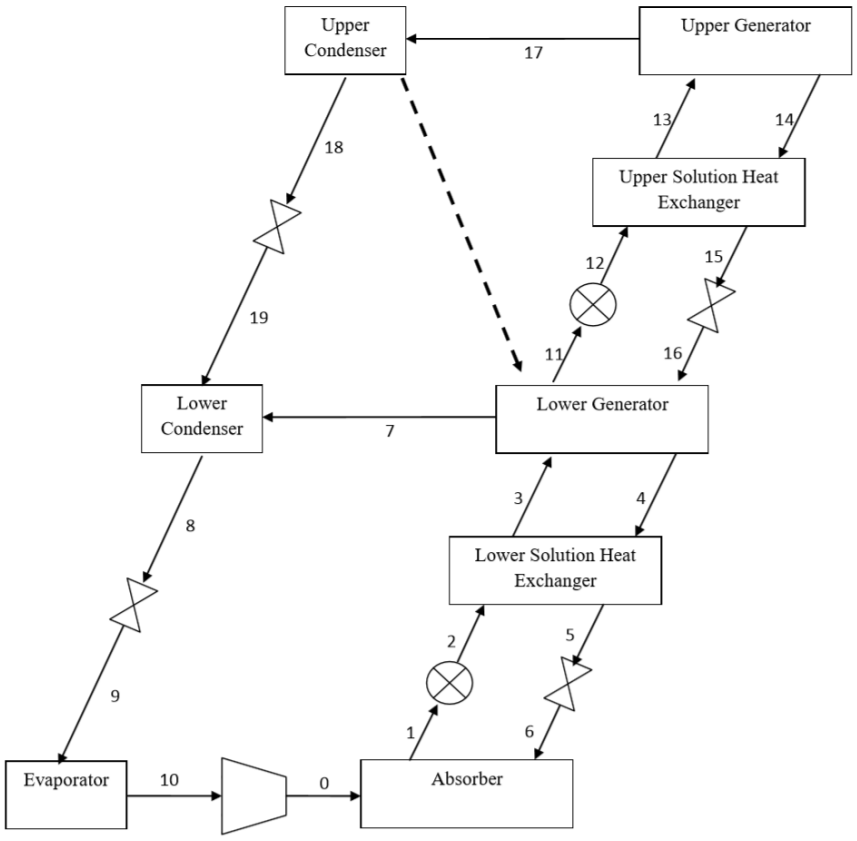

Figure 3.11: 2 - Stage / 2 - Effect LiBr - H_2O compression - absorption heat pump cycle process flow diagram

100 °C and 160 °C (20 - 50 °C greater than the previous single stage cycle). In general, it can be observed that when the r_p is increased, the $COP_{c,th}$ increases, and this effect becomes far more profound at lower generation temperatures (i.e. this characteristic is as observed in the single stage compression - absorption cycle). The relationship between $COP_{c,th}$ and r_p becomes less profound at higher generation temperatures. Further, it can be noted that this relationship tends to become more linear at higher generation temperatures, whilst at lower generation temperatures the effect is more parabolic.

It is evident from Figure 3.12 that when r_p is between 1.0 and 1.2 the highest $COP_{c,th}$ is achieved with a generation temperature of 160 °C. When r_p is between 1.2 and 1.5, the highest $COP_{c,th}$ is achieved with a generation temperature of 140 °C. When r_p is between 1.5 and 2.1, the highest $COP_{c,th}$ is achieved with a generation temperature of 120 °C . When r_p is between 2.1 and 3.0, the highest $COP_{c,th}$ is achieved with a generation temperature of 100 °C. This effect is con-

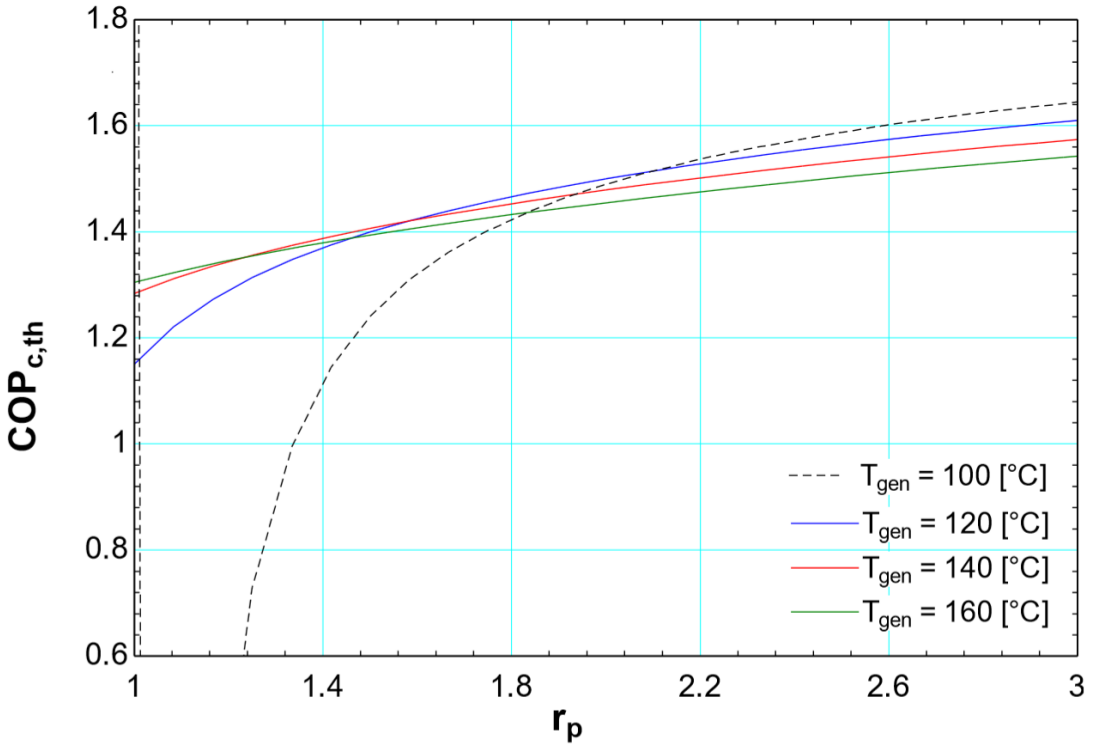

Figure 3.12: 2 - Stage / 2 - Effect LiBr - H_2O compression - absorption heat pump cycle: $\text{COP}_{c,th}$ vs. r_p

trary to that experienced with conventional absorption chiller cycles (Chapter 2).

It is believed that this effect is due to a 'compacting' of the different stages with increasing r_p. In other words, the generation temperature required in the upper cycle necessary to produce sufficient exergy in the upper condenser relative to the lower generator diminishes with greater absorber pressures. This effect will be analysed and discussed further with the 3 - stage / 3 - effect compression absorption cycle. The effect of r_p upon the generation temperature crossover point between the number of stages (N_{stage}) relative to conventional absorption cycles will also be discussed.

A graph indicating the relationship between $\text{COP}_{c,th}$ and T_{gen} at different r_p is shown in Figure 3.13. The five different curves indicate the five values of r_p simulated (n.b. when $r_p = 0$, this implies a conventional absorption chiller cycle). The shape and alignment of the curves is very similar to that discussed for the single - stage cycle in Figure 3.9.

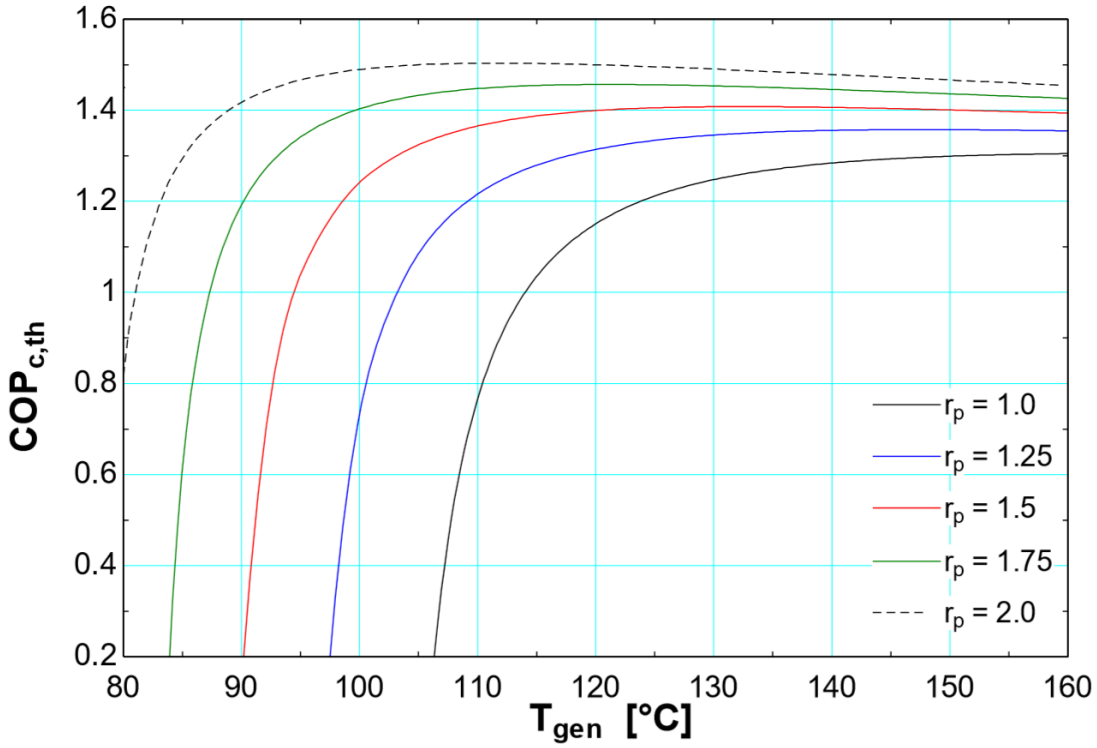

Figure 3.13: 2 - Stage / 2 - Effect LiBr - H_2O compression - absorption heat pump cycle: $COP_{c,th}$ vs. T_{gen}

There is however a noticeable difference between in the graphs; the curves are more compact in the single - stage cycle than in the double - stage cycle. In the single - stage cycle, assuming that the target $COP_{c,th}$ is 0.7 and the compression ratio can float between 1.0 and 2.0, the generation temperature must be between 56 °C and 77 °C; a ΔT_{gen} of 21 °C. In the double - stage cycle, assuming that the target $COP_{c,th}$ is 1.2 and the compression ratio can float between 1.0 and 2.0, the generation temperature must be between 83 °C and 124 °C; a ΔT_{gen} of 41 °C. This represents an almost doubling in the possible range of T_{gen} required to sustain the target COP_c for a conventional absorption chiller cycle.

This is particularly important because reducing the generation temperature from over 120 °C to below 90 °C means that a far wider range of heat sources and low grade waste heat sources can be utilised. For example, Low Temperature Hot Water (LTHW) recovered from the cooling jacket of a CHP gas - fired engine, and first and / or second stage intercooler(s). Ordinarily, only Medium Temperature Hot Water (MTHW) or steam have the required temperatures necessary to drive a

double - stage absorption chiller cycle. By using a small amount of mechanical (i.e. electrical) work it is possible to utilise a much greater range of low temperature heat sources.

Triple - Stage / Triple - Effect

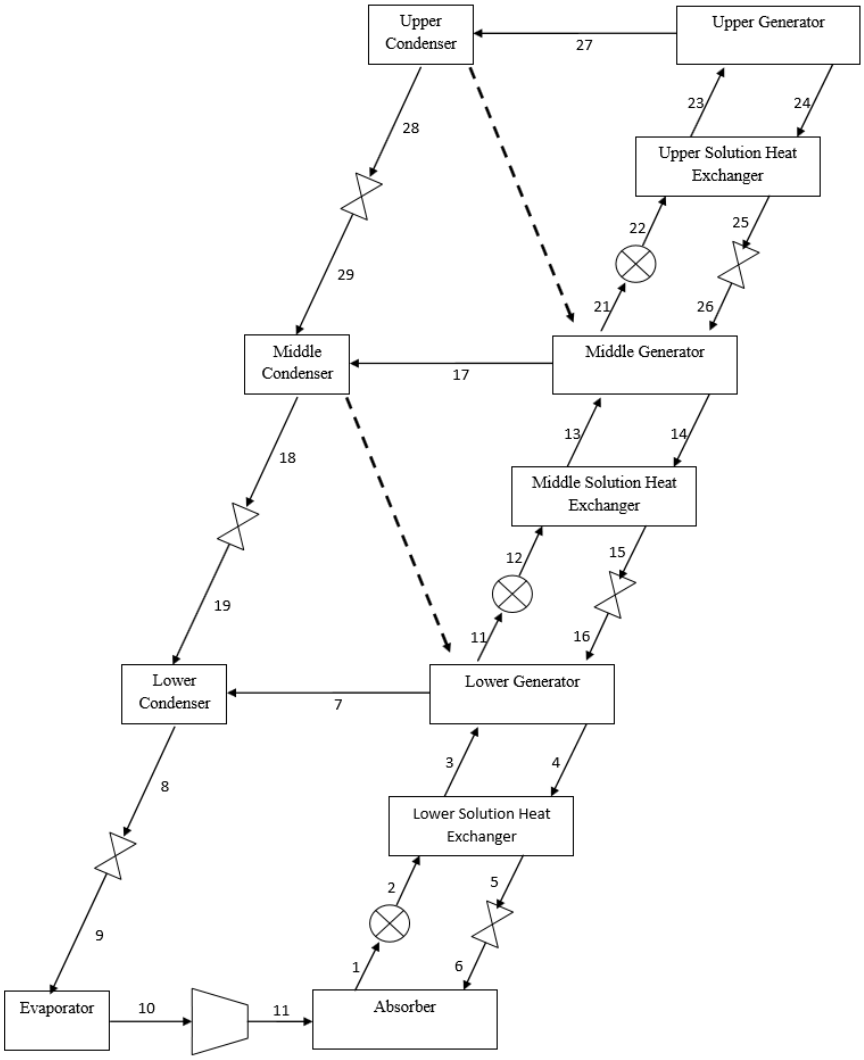

Figure 3.14: 3 - Stage / 3 - Effect LiBr - H_2O compression - absorption heat pump cycle process flow diagram

A triple - stage triple - effect compression absorption LiBr - H_2O heat pump cycle with steam compressor located at the evaporator outlet is shown in Figure 3.14. This cycle is similar to the double - stage double - effect cycle; heat is passed from the upper and middle condensers (state points 27 and 17) directly to the middle and lower generators respectively. Besides the addition of the compressor,

this cycle is the same as a conventional triple stage absorption chiller.

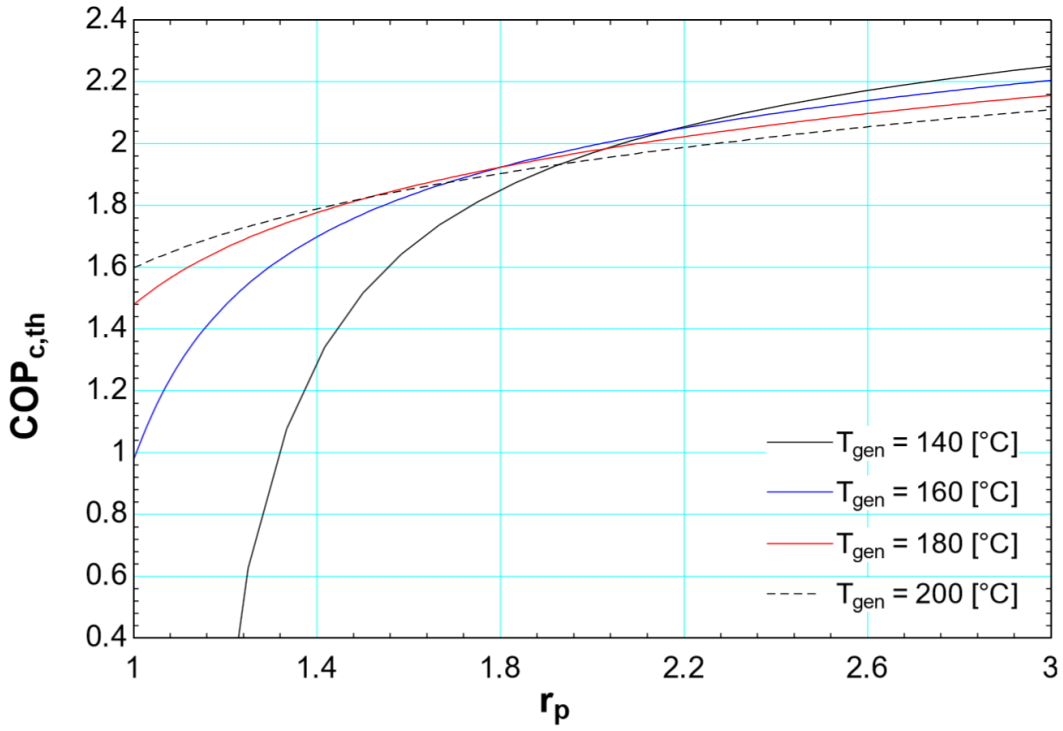

Figure 3.15: 3 - Stage / 3 - Effect LiBr - H_2O compression - absorption heat pump cycle: $\text{COP}_{c,th}$ vs. r_p

The effect of r_p on the $\text{COP}_{c,th}$ at four different generation temperatures is shown in Figure 3.15. The generation temperatures simulated range between 140 °C and 200 °C (40 °C greater than the previous double - stage cycle, but with a 20 °C temperature overlap to enable a comparison to be made).

In general, the relationship between r_p and $\text{COP}_{c,th}$ is very similar to that observed in the single - stage and double - stage compression - absorption cycles. Although there were notable differences in the shape of the curves and hence nature of the relationship between the single - effect and the double - effect cycles, the differences between the double - effect and triple - effect cycles appear to be in magnitude only. The addition of the extra stage and a corresponding increase in upper generation temperature of approximately 40 °C tends to produce an increase in $\text{COP}_{c,th}$ of between 20 and 30 % over the double - stage cycle.

A graph indicating the relationship between $\text{COP}_{c,th}$ and T_{gen} at different r_p is shown in Figure 3.16. The shape and alignment of the curves is quite different

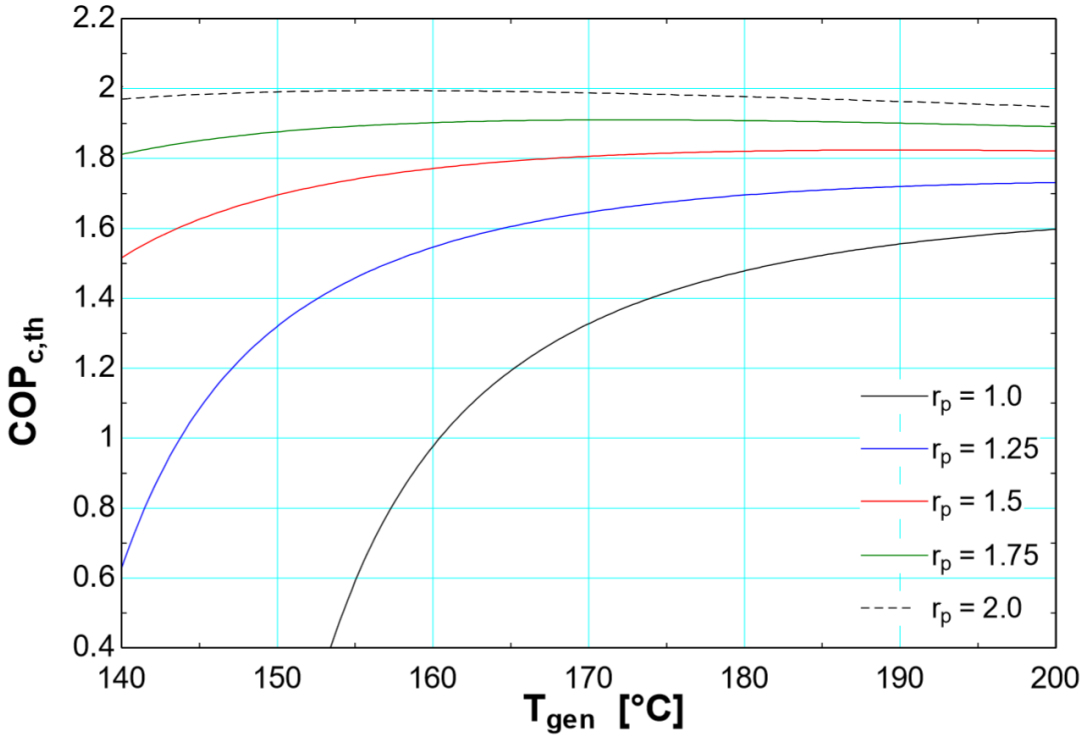

Figure 3.16: 3 - Stage / 3 - Effect LiBr - H_2O compression - absorption heat pump cycle: $\text{COP}_{c,th}$ vs. T_{gen}

to that observed for the single - stage and double - stage cycles in Figures 3.9 and 3.13.

In the single - stage and double - stage cycles, the $\text{COP}_{c,th}$ increases initially very rapidly as T_{gen} increases, and then appears to reach an asymptote. At higher r_p, changes in the magnitude of T_{gen} becomes almost like an on / off switch for the cycle; below a certain T_{gen} the $\text{COP}_{c,th}$ is almost zero, and above the appropriate T_{gen} the $\text{COP}_{c,th}$ is almost constant. There is also a very even spacing between the curves at different r_p, which suggests that $\text{COP}_{c,th}$ exhibits an almost linear system response to an increase in r_p.

However, in the triple - stage cycle both of these effects are no longer observed. The relationship between $\text{COP}_{c,th}$ and T_{gen} is highly dependent upon r_p. When r_p is 1.25, $\text{COP}_{c,th}$ changes dramatically with different values of T_{gen}, and increases steadily before reaching an asymptote of around 1.7 when $T_{gen} > 200\,°\text{C}$; the effect of increasing T_{gen} is less profound on $\text{COP}_{c,th}$ in the triple stage cycle than the single or double stage cycles. When r_p is 2.0, $\text{COP}_{c,th}$ is almost constant (at

approximately 2.0) through the range of T_{gen} simulated.

Interestingly, $\text{COP}_{c,th}$ appears to reduce very slightly from 2.0 to 1.95 when $T_{gen} > 170\,°\text{C}$. This is due to a decrease in exergetic efficiencies of the internal heat recuperation process (from condenser to generator). This reduction in cycle exergetic efficiency (COP) implies that an extra stage is likely to be required. In other words, at generation temperatures above 160 °C (i.e. driving temperatures over ∼170 °C) and with $r_p > 2.0$, a fourth stage may be required.

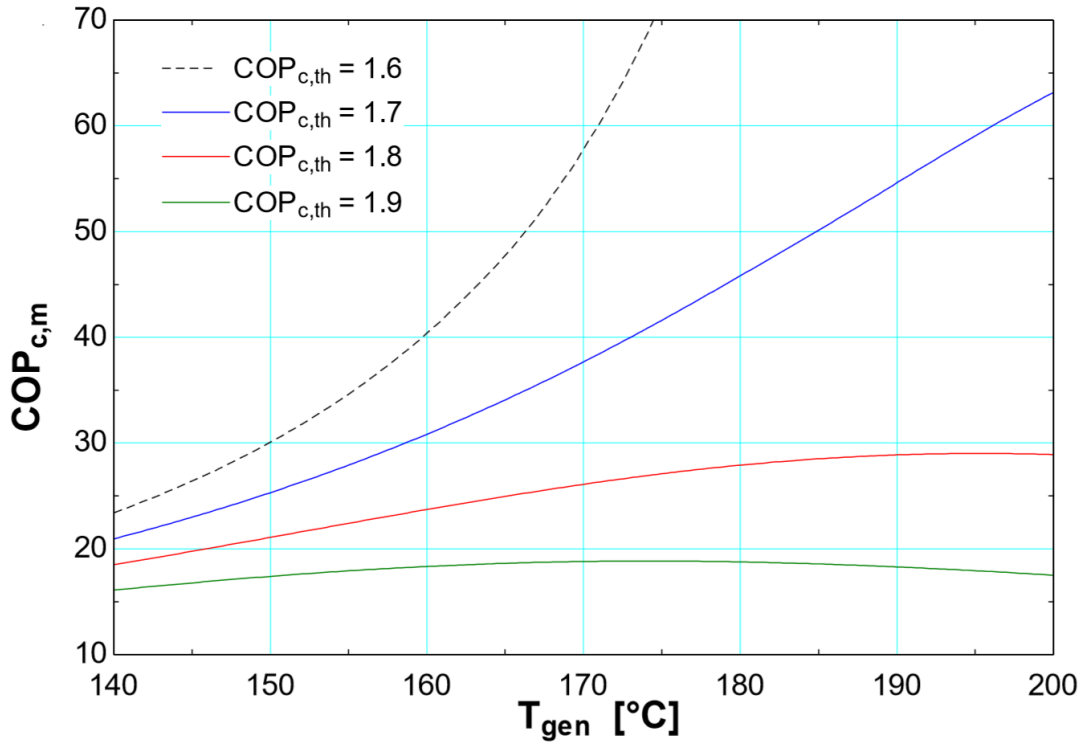

Figure 3.17: 3 - Stage / 3 - Effect LiBr - H_2O compression - absorption heat pump cycle: $\text{COP}_{c,m}$ vs. T_{gen}

Figure 3.17 shows the relationship between $\text{COP}_{c,m}$ and T_{gen} for four different values of $\text{COP}_{c,th}$. When $\text{COP}_{c,th}$ is 1.9, $\text{COP}_{c,m}$ ranges between 12 and 18, reaching a maximum when T_{gen} is 175 °C. This suggest that in order to achieve a $\text{COP}_{c,th}$ of 1.9, the optimum generation temperature to minimise mechanical work input (i.e. maximise $\text{COP}_{c,m}$) is 175 °C.

Conversely, when $\text{COP}_{c,th}$ is 1.6, $\text{COP}_{c,m}$ ranges from 24 to >70. Given that a standard triple - stage LiBr - H_2O absorption chiller will produce a COP_c of around 1.6 given a generation temperature of around 200 °C, it therefore follows that the

$COP_{c,m}$ for the triple - stage compression - absorption should tend towards infinity when $T_{gen} = 200\,°C$ and $COP_{c,m}$=1.6, as approximately observed in Figure 3.17.

Whilst the 3 - stage / 3 - effect LiBr - H_2O compression - absorption heat pump cycle has a significantly better performance that a 3 - stage / 3 - effect LiBr - H_2O absorption heat pump cycle, there is a major technical hurdle which may prevent it from becoming a viable product. The very low pressure ($\sim 10\,mbar$) and very low density ($0.03745\,kg/m^3$) of the steam exiting the evaporator, means that the steam compressor must be unfeasibly large. For a specified coolth output of 100 kW, the volumetric flowrate at the compressor inlet is $6.1\,m^3/s$. This would be beyond the flow rate capabilities of a centrifugal compressor, and the pressure ratio (~ 5) would mean a very large and complex axial compressor will multiple stages. Therefore, unfortunately the LiBr - H_2O compression - absorption heat pump cycle is not considered to be a practicable solution.

3.1.4 Conclusions

Two types of thermally activated heat pumps have been explored in this Chapter: multi - effect / multi - stage H_2O - NH_3 absorption heat pumps and multi - effect / multi - stage LiBr - H_2O compression - absorption heat pumps. It has been demonstrated that the double - stage / triple - effect H_2O - NH_3 absorption heat pump cycle can achieve a COP_c equivalent to a triple - stage / triple - effect LiBr - H_2O absorption heat pump, but with one fewer stage.

The sequence of internal heat recuperation devices within the cycle has been shown to be vital to the performance. The strong solution which exits the absorber should pass through the solution HX first and then through the rectifier in order to achieve the highest COP_c. The double - stage / triple - effect H_2O - NH_3 absorption heat pump cycle was able to achieve a theoretical COP_c of 1.765. A triple - stage / quintuple - effect cycle was conceptualised, but temperature required in the upper generator was too high for the thermophysical properties of the ammonia and water mixture to be resolved.

Whilst the double - stage / triple - effect H_2O - NH_3 absorption heat pump cycle appears to be promising, a number of patents for similar concepts already exist or have existed [52, 53]. Therefore this cycle is not considered suitable for further research and development.

Singe - stage / single - effect, double - stage / double - effect and triple - stage / triple - effect LiBr - H_2O compression - absorption heat pump cycles have been demonstrated to achieve a significant improvement in COP_c over their conventional absorption heat pump cycle counterparts. The triple - stage / triple - effect LiBr - H_2O compression - absorption heat pump has been shown to achieve a $COP_{c,th}$ of 2.0, when the steam compressor has a pressure ratio of 2.0. The net effect of the addition of the compressor to the evaporator outlet is not only an increase in $COP_{c,th}$, but also a reduction in generation temperature. The corresponding $COP_{c,th}$ has been demonstrated to be over 16.0 in all scenarios analysed.

Whilst the triple - stage / triple - effect LiBr - H_2O absorption - compression heat pump cycle appears to be a promising area for future research, the extremely low pressure and density of the steam exiting the evaporator means that the very high volumetric flowrate through the compressor would result in it being almost impracticably large. ($6.1\,m^3/s$ for $100\,kW$ of cooling output). Therefore the absorption - compression cycle is not recommended as a topic of further research.

Chapter 4

R744 Heat Pump Cycle Concepts

4.1 Introduction

The very high pressure of the R744 and presence of three phases (liquid, vapour, supercritical fluid) presents a number of challenges in the design of the cycle processes and in the design of specific components. Processes in which the operating fluid passes close to the critical point are to be avoided wherever possible, due to the severe changes in thermophysical properties which occur in this region.

A range of heat pump / chiller cycle concepts are conceptualised, developed and analysed in this Chapter. Potential applications of theses cycles include:

- **Desalination** - low temperature evaporative desalination, such as multi-effect evaporation or freeze desalination. Typically, such processes would require a heat source of over $\sim$70 °C or a coolth source of below $\sim$5 °C
- **District heating and cooling** - district heating and cooling systems provide heat or coolth (hot or chilled water) to a network at a temperature which is appropriate for building space temperature control; typically at $>$70 °C flow for heat and $<$12 °C for cooling
- **Low temperature processes** - required by many processess, in particular the food production industry.
- **Solar driven cooling** - using solar concentrating collectors to provide high temperatures to a cycle which produces chilled water for cooling in buildings located in arid and semiarid climates

The cycles which follow are thermally assisted transcritical MVC and thermally activated heat pump cycles. They combine the principles of both the reverse Rankine cycle and Brayton cycles: isothermal heat input and isobaric heat rejection, and; isobaric heat input and heat rejection, respectively. The cycles use a naturally occurring refrigerant (R744), rather than the currently commonly used synthetic HFC refrigerants. They are capable of accommodating a range of mechanical and thermal energy inputs. Thermal inputs with temperatures between

150 °C and 500 °C are researched; based on an understanding of thermodynamic principles, a higher input temperature can result in a lower mechanical energy input requirement.

A thermally and mechanically activated R744 heat pump has been conceptulaised and analysed by Deng et al. [97]. This cycle utilises a solar - thermal activated absorption chiller to assist a R744 MVC heat pump cycle to 'super - cool' the refrigerant exiting the gas cooler. This lowers the vapour fraction, x, of the refrigerant as it enters the evaporator, thereby increasing the COP. With an evaporator outlet temperature of 7 °C and a gas cooler outlet temperature of 38 °C, the cycle achieved a $COP_{c,m}$ of 3.8. The cycles presented below differ from the cycle proposed by Deng et al. in that they do not use an absorption chiller.

A considerable number of alternative cycles have been conceptualised, modelled and analysed, but are not presented within this Thesis. These are variants of Cycle 1, Cycle 2 and Cycle 3 presented below which were either unsuccessful or were part of the conceptualisation and development process.

4.2 Methodology

The cycles presented below are modelled and analysed for a 'standard case'. In these cases, the exergy of the coolth output of the cycle remains constant at 1 MW. The maximum available temperature is assumed to be 350 °C; this is a conservative estimate based upon known exhaust gas temperatures of commercially available small to medium scale gas turbines (5 MW to 20 MW) of between 450 °C and 550 °C.

The minimum heat rejection temperature was based either upon the ambient dry bulb temperature (if dry cooling is used) or the ambient wet bulb temperature (if adiabatic cooling or a cooling tower is used). This temperature is assumed to be 30 °C.

Engineering Equation Solver (EES) is used to model and simulate the cycles. EES is a commercially available equation solving programme which is capable

of numerically solving coupled non-linear algebraic and differential equations, conducting optimisation and sensitivity analyses. It uses an updated variation of the Peng-Robinson equation of state model [98] to generate thermodynamic and transport properties of single substances and mixtures. Approximately 1,000 equations are required to accurately define and model the various processes of the cycles.

Details of the modelling and simulation tools for specific components within the cycles is given in Chapter 5. An analysis and discussion of potential preliminary design methodologies for these components is also included.

4.2.1 Assumptions

The models use rely upon a number of assumptions, which are detailed below.

- The total thermal energy input is 1 MW.
- The maximum temperature at the work - expander inlet is 215 °C.
- The minimum temperature achievable in the heat rejection unit is 35 °C.
- The minimum pinch temperature in working fluid to water heat exchangers is 2 °C.
- The minimum pinch temperature in working fluid to working fluid heat exchangers is 5 °C (n.b. this is to prevent them from being impracticably large).
- Pressure losses only occur in heat exchangers (i.e. not in pipework).
- The expansion valve - orifice plate is isenthalpic.
- All process are treated as adiabatic (unless there is an intentional transfer of heat).
- Compressor and expander devices have an isentropic efficiency of 80%.

- Ejector nozzle, mixing section and diffuser are adiabatic and have an isentropic efficiency of 80%.

A method of considering Coefficient Of Performance (COP) based upon the Primary Energy Consumption (PEC) is synthesized, such that the heat pump performance can be analysed against its environmental impact in terms of primary energy. This value is termed $\mathrm{COP}_{c/hPEC}$, and gives an indication of the true primary fuel-to-heat / coolth conversion efficiency of the cycle. In order to calculate the $\mathrm{glscop}_{c/hPEC}$, a value for the thermal-to-mechanical work conversion efficiency of electricity delivered to point of use through the grid (η_{grid}) must be assumed. For this analysis, it is assumed that η_{grid} is 30%. This value encompasses an average primary fuel-to-electrical conversion efficiency in the generation of electricity from fossil fuels (35%), an electrical grid transmission and distribution efficiency (90%), and a electrical-to-mechanical efficiency of the motor which drives the heat pump compressor. (95%) This assumes centralised electricity generation. Equation 4.1 below indicates the process for calculating $\mathrm{COP}_{c/hPEC}$, which is used in determining the performance of Cycle 3.

$$COP_{c/h,PEC} = \left(\frac{1}{COP_{c/h,t}} + \frac{1}{\eta_{grid} \times COP_{c/h,m}} \right)^{-1} \tag{4.1}$$

4.3 Cycle 1

4.3.1 Description

In Cycle 1, a low quality heat source with input temperature of approximately 220 °C (selected as a comparison to the maximum driving temperature used in LiBr-H_2O absorption heat pumps) is required to provide the thermal input to the Brayton portion of the cycle. The components which enable the processes of the cycle to occur are: a transcritical superheated vapour compressor, a supercritical fluid compressor, one supercritical turbine and a further supercritical turbine, a recuperating heat exchanger, two gas/supercritical fluid coolers, an evaporator

and an expansion valve. The processes associated with this cycle are described below:

- 1 - 2: internal heat recuperation (hot side)
- 2 - 3: supercritical fluid cooler (providing heat for external use)
- 3 - 4: second stage expansion turbine
- 4 - 5: thermal expansion valve
- 5 - 6: evaporator (providing coolth for external use)
- 6 - 7: first stage compressor
- 7 - 8: supercritical fluid intercooler (providing heat for external use)
- 8 - 9: second stage compressor
- 9 - 10: internal heat recuperation (cold side)
- 10 - 11: heat addition (from external source)
- 11 - 1: first stage expension turbine

The working fluid operates at four pressure levels as it passes through the cycle. The minimum pressure is 43 bar, which occurs in the evaporator and is results in an evaporation temperature of 8.3 °C. The maximum pressure is tentatively set at approximately 250 bar, and occurs in the cold side of the supercritical fluid intercooler and the heat addition heat exchanger. Whereas the minimum pressure is dictated by the desired chilled water temperature, the maximum pressure is a specified design parameter which affects the performance characteristics of the cycle.

The cycle produces a chilled water at 10 °C, which is suitable for a chilled water flow and return temperature in modern air conditioning systems of 10 °C and 15 °C, respectively (older systems typically operate with a flow and return of 6 °C and 12 °C).

A temperature - entropy plot of the cycle is given in Figure 4.1. A single line progress flow diagram of the cycle is shown in Figure 4.2.

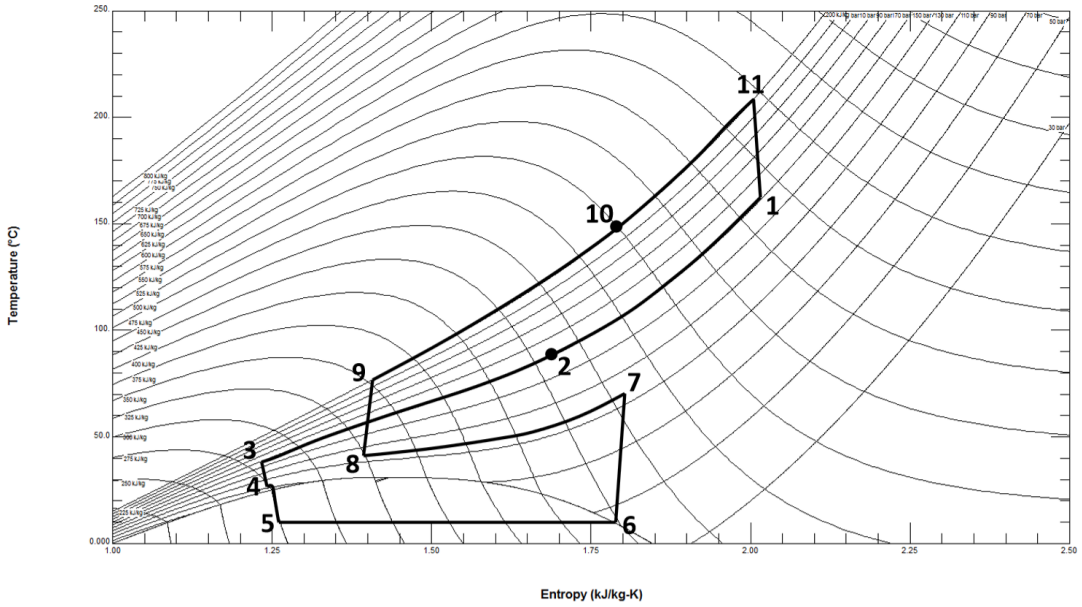

Figure 4.1: Temperature - Entropy plot of R744 heat pump cycle 1

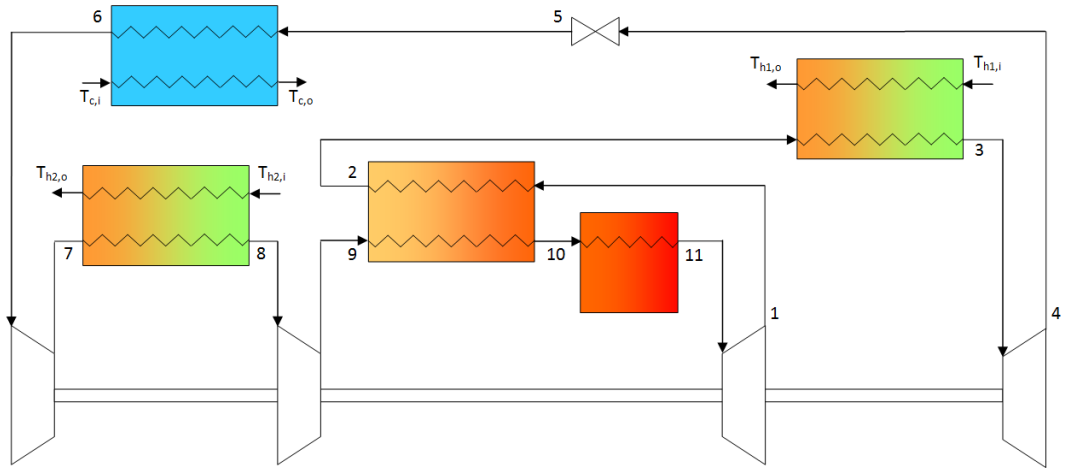

Figure 4.2: Process flow diagram of R744 heat pump cycle 1

4.3.2 Internal Heat Recuperation Heat Exchanger

An accurate pinch analysis of the internal heat recuperation heat exchanger is crucial in determining how much exergy can be contained and re-used within the cycle. Due to the characteristics of R744 and the close proximity to the critical point in the hot side of the recuperator, the thermophysical properties of the fluid

are highly variable depending upon small changes in temperature and pressure. A temperature pinch occurs due to the difference in C_p between the hot and cold flows (implied by the 'flattening' of isobars close to the critical point on a Temperature - Entropy plot.

A one-dimensional analysis heat transfer characteristics of the internal heat recuperator is presented in Chapter 5.

4.3.3 Intercooling Pressure

Optimising the intercooling pressure minimises compression work, thereby increasing the COP relative to mechanical work input. In order to determine the optimum intercooling pressure (i.e. pressure at the first - stage compressor outlet), a parametric analysis is conducted. However, optimising the first - stage compressor outlet pressure may lower the intercooling temperature, which could reduce the amount of useful heat available in the intercooler. The analysis takes account of this by to ensuring that the intercooler inlet temperature (state point 7) is closely matched to the gas cooler inlet temperature (state point 2).

Figure 4.3 shows the relationship between compression work and the intercooler pressure. The optimum intercooler pressure, as defined by the minimum compression work required, is identified as 97 bar.

4.3.4 Results and Discussion

The fluid properties at each state point are given in Table 4.1. For the maximum at the work - expander inlet of 215 °C, the cycle is operating under the joint thermally and mechanically activated regime.

For the mechanical work input, the cycle achieves a $\mathrm{COP}_{c,m}$ of 7.0 and a $\mathrm{COP}_{h,m}$ of 12.4. For the thermal work input, the cycle achieves a $\mathrm{COP}_{c,th}$ of 1.6 and a $\mathrm{COP}_{h,th}$ of 2.8.

The COP values for mechanical work input conversion to coolth and heating are on par with, if not marginally higher than the best R744 based MVC heat

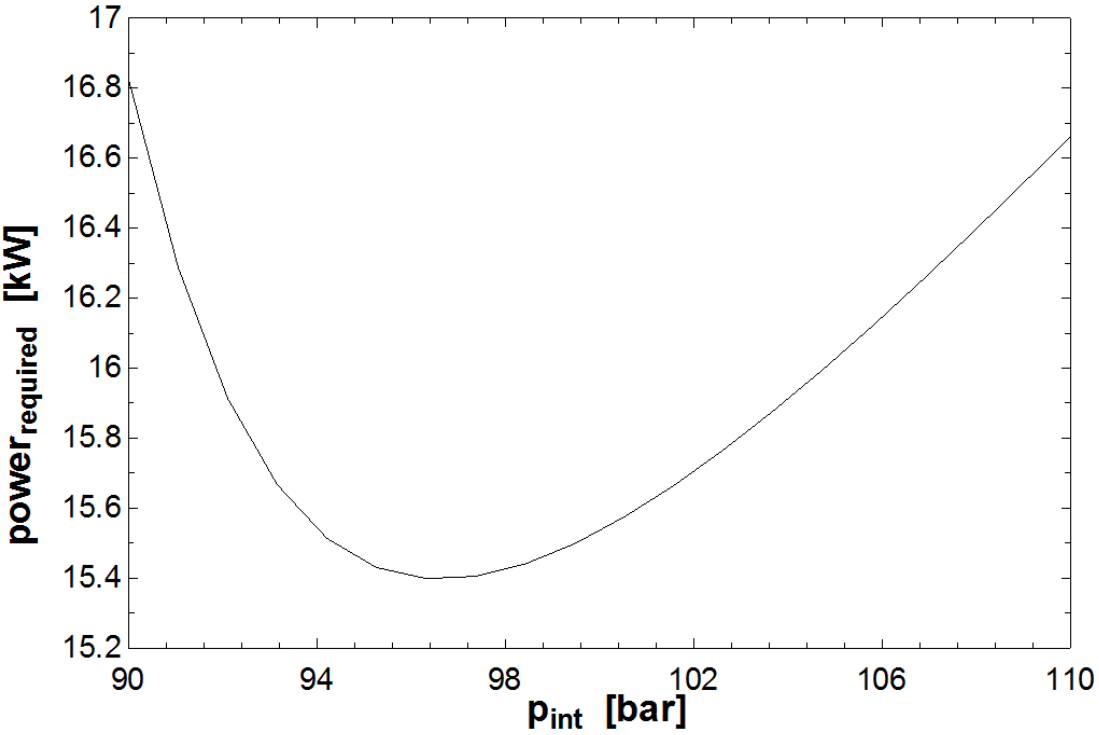

Figure 4.3: Parametric analysis of the optimum intercooling pressure

pumps in the literature [99] and indeed commercially available HFC based MVC heat pumps.

The COP values for thermal input conversion to coolth and heating are equal to a modern triple - effect LiBr - H_2O absorption chiller. Neither MVC heat pumps, nor absorption heat pumps are capable of providing simultaneous heating and cooling at the temperatures achieved by this cycle.

State Point	T (°C)	P (bar)	h (kJ/kg)	s (kJ/kgK)	x (-)	ρ (kg/m^3)
1	168.9	150	573.3	2.039	-	214.1
2	81.0	150	41.6	1.636	-	420.7
3	40	150	285.5	1.246	-	780.2
4	28.8	80	277.9	1.252	-	724.9
5	8.4	43.3	277.9	1.274	0.278	-
6	8.4	43.3	424.6	1.795	1.000	-
7	73.0	97	461.0	1.814	-	227.1
8	40.0	97	318.0	1.374	-	603.9
9	73.8	250	345.6	1.388	-	717.7
10	150.0	250	503.3	1.801	-	415.5
11	215.0	250	604.5	2.024	-	308.1

Table 4.1: Cycle 1 fluid properties at each state point

The minimum heat rejection temperature (state points 3 and 8) has a strong effect on the COP. Figure 4.4 shows the relationship between $\text{COP}_{c/h,th/m}$ and

the ambient temperature.

As the ambient temperature increases, COP_c reduces, both in terms of the mechanical and thermal work input. This is due to the increased enthalpy at state point 3 and consequent vapour mass fraction, x, entering the evaporator at state point 5; this is a known performance characteristic of a heat pump. However, the close proximity of the fluid to the critical point through both the gas cooler and intercooler means that changes in ambient temperature become more influential on the cycle performance.

Upon observing Figure 4.1, it can be seen that isobars 'flatten' close to the critical point. Therefore, a small increase in temperature results in a large shift to the right on a Temperature - Entropy plot, resulting in a large increase in both entropy and vapour mass fraction (assuming that the fluid is to consequently be isenthalpically throttled). In the same manner, a small decrease in temperature results in a large shift to the left on the Temperature - Entropy plot, resulting in a large decrease in entropy and vapour mass fraction. The former results in a decrease in COP_c, whilst the latter results in an increase in COP_c, as observed in Figure 4.4a.

It is evident from Figure 4.4a that the changes in ambient temperature affect the $COP_{c,m}$ considerably more than the $COP_{c,th}$. Throughout the range of ambient temperatures considered, $COP_{c,th}$ changes by 30%, whilst $COP_{c,m}$ changes by 57%. The $COP_{c,m}$ is more dependent upon ambient temperature due to the dependency of the intercooler on the ambient temperature and consequent changes the second stage compression work.

The relationship between ambient temperature and COP_h, shown in Figure 4.4b, is very similar to that between the ambient temperature and COP_h. The changes in ambient temperature affect the $COP_{h,m}$ considerably more than the $COP_{h,th}$. Throughout the range of ambient temperatures considered, $COP_{h,th}$ changes by 13%, whilst $COP_{h,m}$ changes by 46%.

The change in COP_h is less than that shown by COP_c. An increase in ambi-

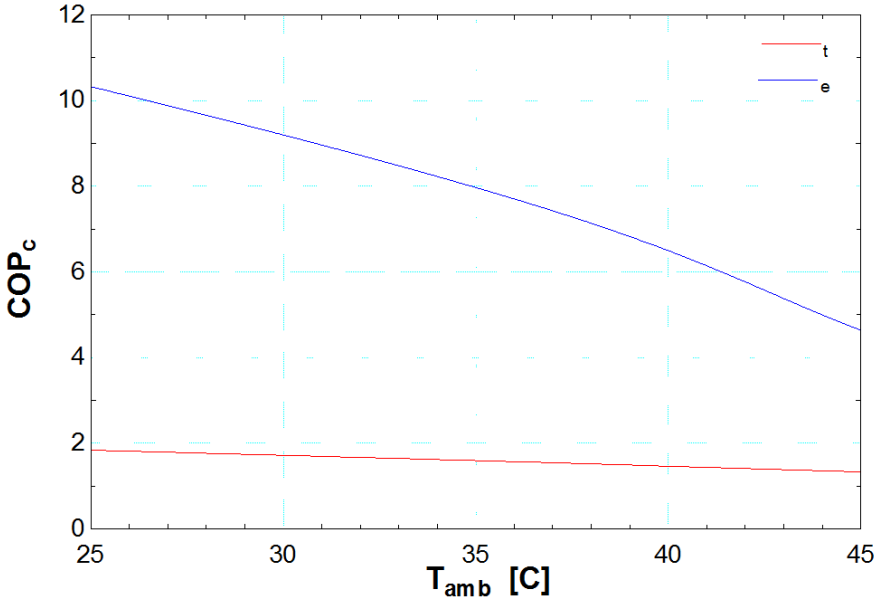

(a) COP_c

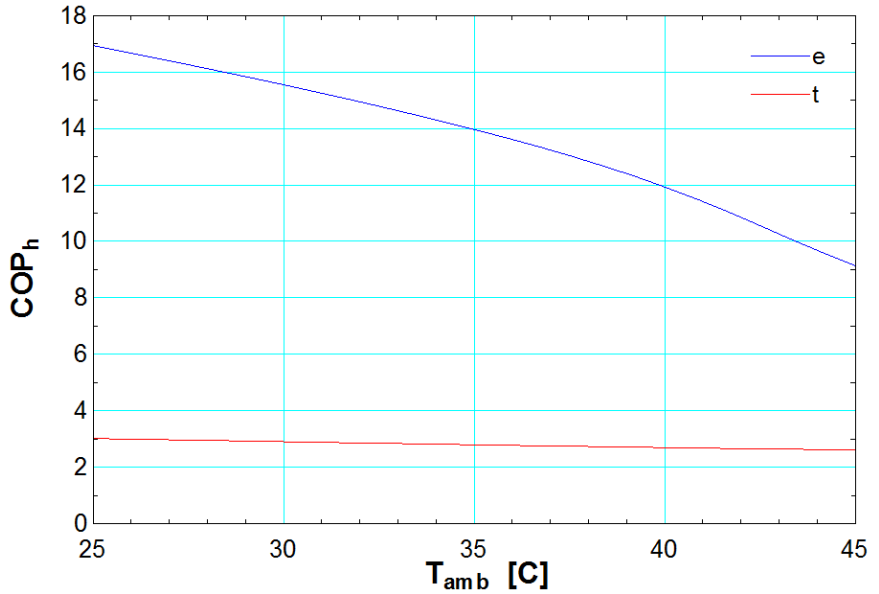

(b) COP_h

Figure 4.4: Plots of COP against ambient temperature for thermal and mechanical inputs for Cycle 1

ent temperature primarily affects the evaporator inlet conditions and intercooler outlet conditions. Intercooler pressure affects the compression work, and therefore both $\mathrm{COP}_{c,m}$ and $\mathrm{COP}_{h,m}$ show high dependency upon ambient temperature (57% and 48%). The evaporator inlet conditions affect the COP_c but not does not affect COP_h, and this explains why $\mathrm{COP}_{c,th}$ is much more dependent upon ambient temperature than $\mathrm{COP}_{h,m}$ (30% vs 13%).

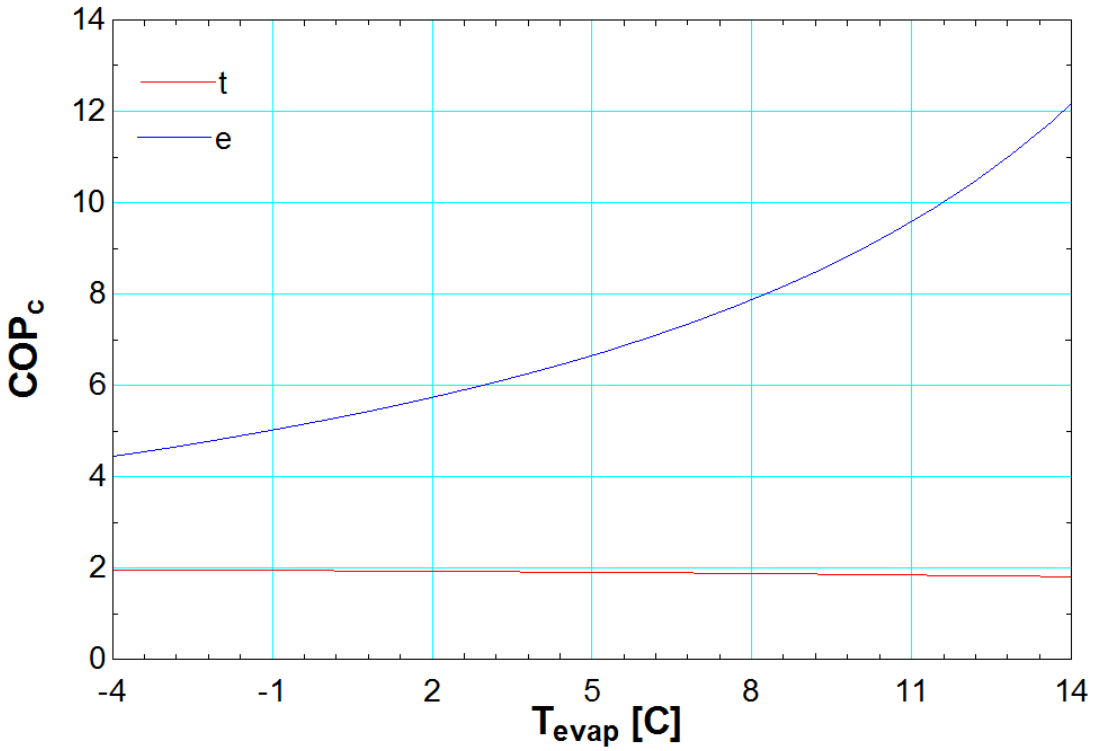

Figure 4.5: A plot of COP_c against evaporation temperature for Cycle 1

Figure 4.5 shows the relationship between the evaporation temperature (i.e. pressure), and $COP_{c,m}$ and $COP_{c,th}$. The $COP_{c,m}$ decreases sharply with a reduction in evaporator temperature, dropping from 12.2 at an evaporator temperature of 14 °C down to 4.5 at an evaporation temperature of -4 °C. Conversely, the $COP_{c,th}$ increases very marginally with a reduction in evaporation temperature, increasing from 1.7 at an evaporator temperature of 14 °C to 1.9 at an evaporation temperature of -4 °C.

When the evaporation temperature is reduced (i.e. evaporation pressure is reduced), the first stage compressor pressure ratio increases, which results in an increase in mechanical work input. This causes a decrease in the $COP_{c,m}$. However, because R744 is a wet fluid, as the evaporation pressure is reduced the enthalpy of evaporation increases; therefore the coolth produced by the evaporator increases. This slows down the decrease in $COP_{c,m}$ as the evaporation temperature is reduced.

The increase in the enthalpy of evaporation at lower pressures explains the marginal increase in $COP_{c,th}$ when the evaporation temperature is reduced. There

is no further relationship between evaporation temperature and thermal input.

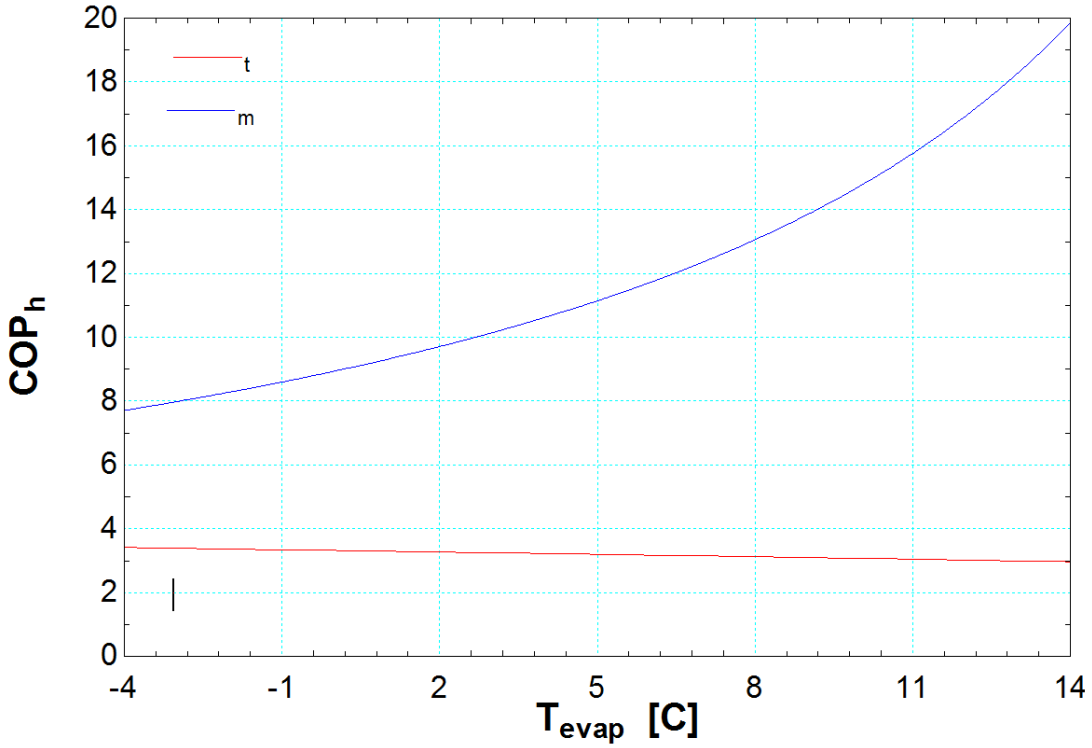

Figure 4.6: A plot of COP_h against evaporation temperature for Cycle 1

Figure 4.6 shows the relationship between the evaporation temperature and $\text{COP}_{h,m}$ and $\text{COP}_{h,th}$. The relationship shows an almost identical trend to that shown in 4.5 between evaporation temperature and COP_c. When evaporation temperature is reduced, $\text{COP}_{h,m}$ decreases; this is due to the same reasons as $\text{COP}_{c,m}$. However, the small increase in $\text{COP}_{h,th}$ that occurs when evaporation temperature is reduced is due purely to the increase in enthalpy of evaporation (which increases enthalpy at state point 6). The thermophysical properties of R744 (i.e. the curvature of isobars and isenthalps on a Temperature - Entropy plot) are such that when the pressure of dry saturated vapour (or, in reality, slightly superheated vapour) entering the first stage compressor is reduced, the compressor outlet conditions (state point 7) are at a much higher temperature and enthalpy. This not only increases the useful heat available (i.e. COP_h), but also the maximum temperature for external use.

Figure 4.7 shows the relationship between the temperature at the first stage compressor outlet (state point 7) and the evaporation temperature. The internal

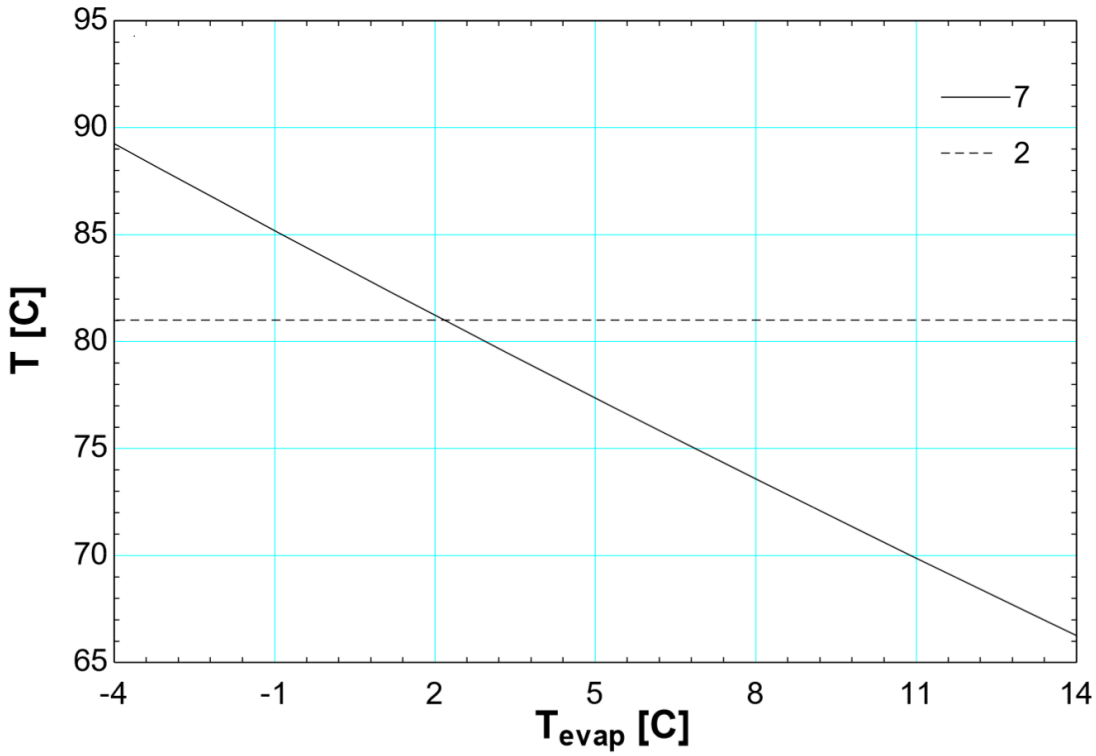

Figure 4.7: A plot of T_7 and T_2 against evaporation temperature for Cycle 1

heat recuperator hot side outlet (state point 2) is also plotted for reference. In order to simplify the hot water circuit, it is desirable to match the upper temperatures of the two hot streams (T_2 and T_3). With this in mind, the ideal evaporation temperature is between 2 and 3 °C. The target evaporator temperature of approximately 8 °C results in a temperature difference between T_2 and T_3 of 7 °C.

4.4 Cycle 2

4.4.1 Description

Cycle 2 represents a minor modification of the Cycle 1 discussed previously. The primary difference is the addition of an ejector following the second stage expander. The purpose of the ejector is to decrease the compression work required by increasing the pressure of the dry saturated vapour (or, in reality, slightly superheated vapour entering the first stage compressor, whilst not altering the

evaporation temperature. The ejector also decreases the enthalpy/ vapour mass fraction of the working fluid entering the evaporator. This increases the exergy of the fluid, and therefore reduces the mass flow through the evaporator.

A review of literature and intellectual property regarding the design, integration and performance of ejectors within R744 heat pump cycles is provided in Chapter 5. A preliminary design method for a ejector for this cycle (and the subsequent Cycle 3) is also provided, along with a discussion of the expected performance characteristics.

As a result of the inclusion of an ejector, it is necessary to have a vapour - liquid separator to split the two - phase flow at the outlet of the ejector expansion diffuser. The saturated liquid is goes into the evaporator, whilst the dry saturated vapour goes into the first stage compressor. This is discussed in more detail in Chapter 5.

The addition of the ejector allows the reverse Rankine aspect of the cycle to be powered purely from the Brayton aspect of the cycle, such that the only energy stream required to activate the cycle is a mid - grade temperature source. As before, the cycle can provide simultaneous heating and cooling effects. As an evolution of the analysis of Cycle 1, the performance characteristics of the supercritical fluid cooler has been conducted. This includes and optimisation of the hot water circuit configuration, volume flow rate and flow and return temperatures.

The cycle is designed to operate in a trigeneration system, where the prime mover is a gas turbine. It produces hot water at both 65 °C and 40 °C, and chilled water at 10 °C. Therefore the maximum expander inlet temperature is specified such that the heat input can be provided exhaust gases of the gas turbine but a recuperator. The amount and quality of thermal energy available for recuperation (i.e. exergy) bears significance upon the cycle performance, specifically COP, as will be demonstrated.

A single line progress flow diagram of Cycle 2 is shown in Figure 4.8, and a

temperature - entropy plot of the cycle is given in Figure 4.9.

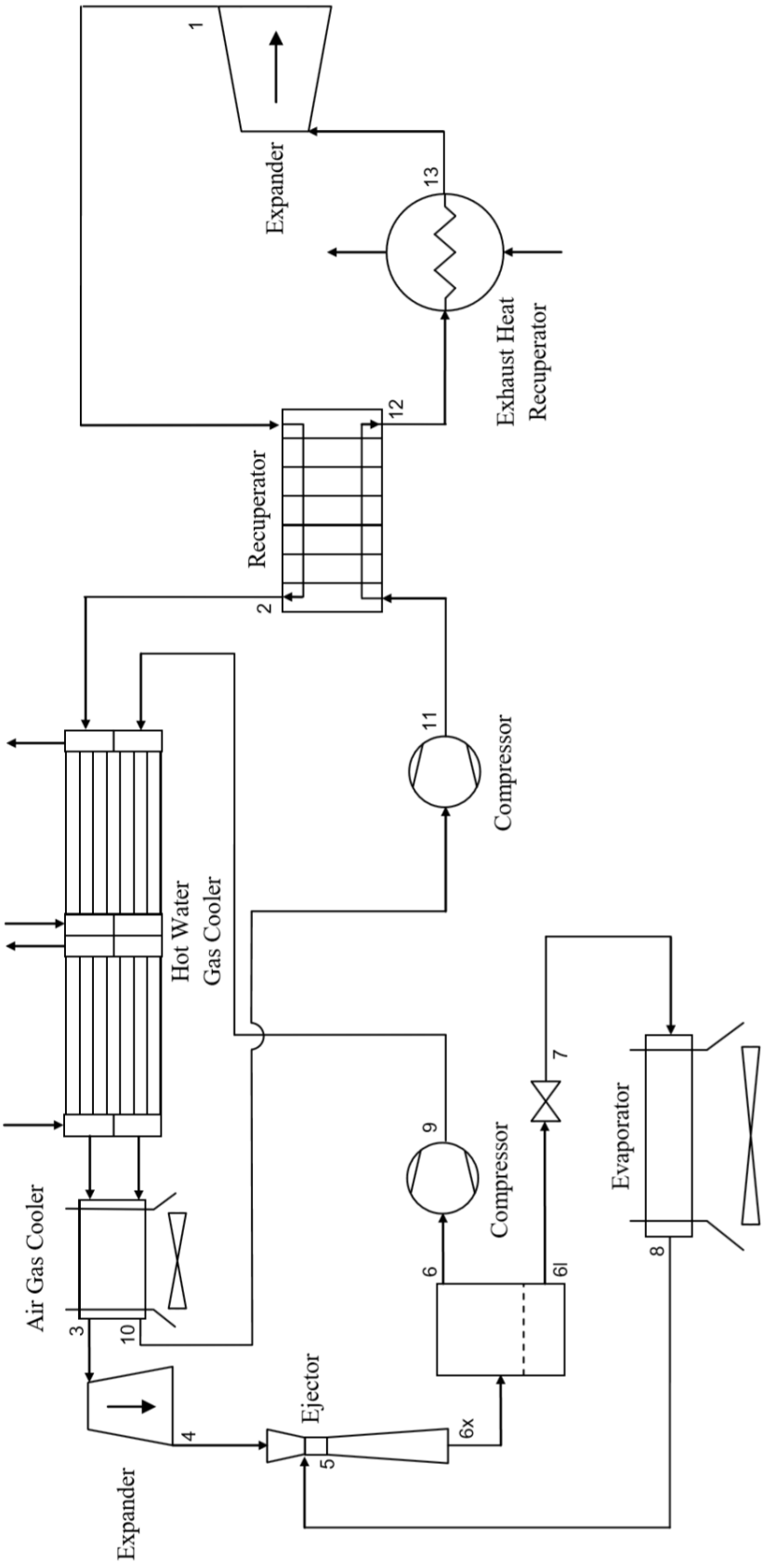

Figure 4.8: Process flow diagram of R744 heat pump Cycle 2

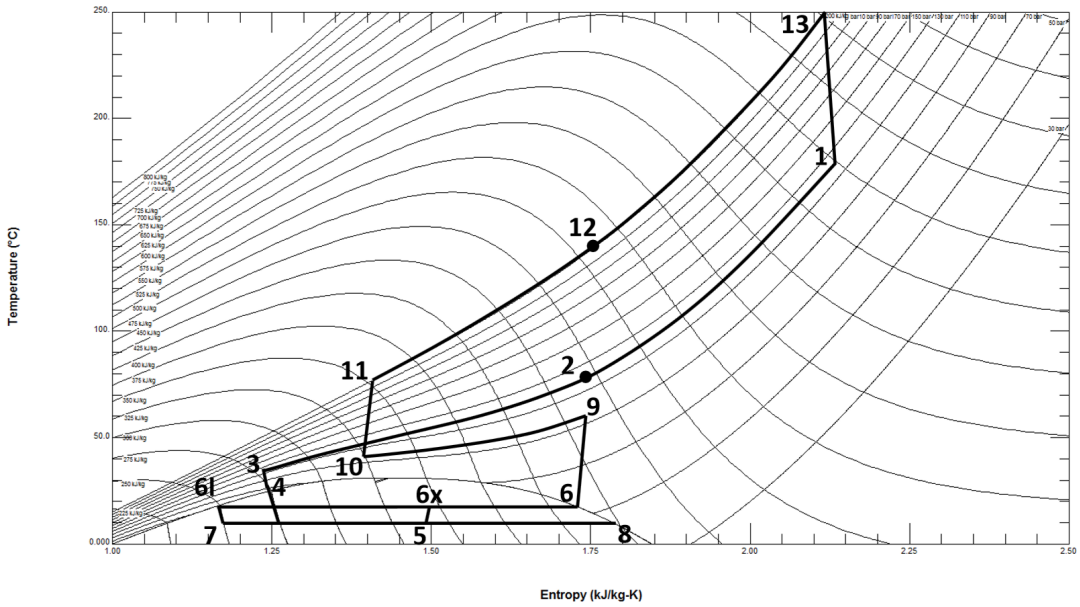

Figure 4.9: Temperature - entropy plot of R744 heat pump Cycle 2

The processes associated with this cycle are described below:

- 1 - 2: internal heat recuperation (hot side)
- 2 - 3: supercritical fluid cooler (providing heat for external use) air cooler
- 3 - 4: second stage expander
- 4 - 5: nozzle stage of ejector (pressure reduction of ejector motive flow)
- 5 - 6x: mixing and diffuser stage of ejector
- 6x - 6l: separation of two - phase flow into dry saturated vapour
- 6l - 7: thermal expansion valve
- 7 - 8: evaporator (providing coolth for external use)
- 8 - 5: nozzle stage of ejector (entrained flow pulled in to negatively pressurised motive flow)
- 6x - 6: separation of two - phase flow into saturated liquid
- 6 - 9: first stage compressor

- 9 - 10: supercritical fluid intercooler (providing heat for external use) and air cooler
- 10 - 11: second stage compressor
- 11 - 12: internal heat recuperation (cold side)
- 12 - 13: heat addition (from external source)
- 13 - 1: first stage expander

The maximum working fluid pressure, which occurs at the outlet of the second compressor, cold side of the internal heat recuperator and at the expander inlet, is 250 bar. The minimum working fluid pressure is 43 bar, which occurs in the refrigerant side of the evaporator heat exchanger. There are four intermediate pressure which the working fluid operates at.

The pressure at first stage compressor outlet and intercooler hot side has been previously optimised to 97 bar. The pressure at first stage expander outlet varies depending upon the first expander inlet temperature; if the inlet temperature increases, the mechanical work output increases for a constant pressure ratio and isentropic efficiency.

In order to ensure that the net mechanical work output of the expanders to the compressors of zero, the first stage expander pressure ratio must decrease as the inlet temperature increases. Decreasing the first stage expander pressure ratio increases the pressure in the hot side of the internal heat recuperator, and consequently increases the exergy at state point 2. This subsequently reduces the enthalpy at state point 3 (inlet to the second stage expander), which in turn reduces the vapour fraction of the working fluid in the mixing section and diffuser section of the ejector (state points 5 and 6x, respectively). The overall result in an increase in the liquid refrigerant produced in the vapour - liquid separator, and therefore an increase in the COP_c. The nature of this relationship will be discussed in the results section.

The second expander outlet pressure (state point 4) is a fixed parameter, specified above the critical pressure at 80 bar to ensure that there is no mixed phase flow within the expander. The ejector outlet pressure is a calculated parameter, which is dependent upon the motive and entrained fluid inlet pressure and the isentropic efficiency of the nozzle, mixing and diffuser sections (this is discussed in more detail in Chapter 5).

4.4.2 Results and Discussion

Cycle 2 has been simulated simulated across a range of maximum first stage expander inlet temperatures. A first stage expander inlet temperature of 350 °C is denoted as the 'base case'.

The fluid properties at each state point for the 'base case' are given in Table 4.2. Under base case conditions, the cycle achieves a $COP_{c,th}$ of 1.58, which is directly comparable to a triple - stage LiBr - H_2O absorption chiller [54] [47] [48]. The corresponding $COP_{h,th}$ is 2.41, which is achievable in a double - stage or triple - stage LiBr - H_2O absorption heat pump, provided that the heat source (evaporation temperature) is sufficiently high. Both $COP_{c,m}$ and $COP_{h,m}$ are zero.

State Point	T (°C)	P (bar)	h (kJ/kg)	s (kJ/kgK)	x (-)	ρ (kg/m^3)
1	305.1	160	736.6	2.361	-	151.5
2	67.6	160	364.1	1.482	-	569.5
3	33.0	160	258.8	1.156	-	857.1
4	21.4	80	251.0	1.161	-	815.3
5	5.3	40	328.7	1.461	0.539	193.2
6x	11.6	46.8	332.0	1.461	0.533	233.1
6l	11.6	46.8	230.1	1.103	0	849.2
6	11.6	46.8	421.1	1.774	1.000	142.6
7	8.4	43.3	230.1	1.105	0.042	700.7
8	8.4	43.3	424.5	1.795	1.000	128.3
9	68.3	97	454.5	1.791	-	26.0
10	30.0	97	273.1	1.229	-	761.9
11	51.3	250	296.6	1.242	-	827.5
12	266	250	674.1	2.159	-	261.6
13	350	250	781.9	2.345	-	213.6

Table 4.2: Cycle 2 fluid properties at each state point

As per Cycle 1, Cycle 2 provides coolth at approximately 8 °C, which implies

that chilled water can be produced at approximately 10 °C. State points 2 and 9 indicate the maximum temperature available at the hot side of the heat pump (in the intercooler and supercritical fluid cooler, respectively), which can be recovered for use in the production of hot water. The overall temperature lift is 60 °C, and herein lies the significant advantage of Cycle 2 over multi - stage absorption chiller; the ability to provide chilled water and hot water simultaneously.

The relationship between $COP_{c,th}$ and $COP_{h,th}$ and the first stage expander inlet temperature (state point 13) is shown in Figure 4.10. It is evident that as the inlet temperature is reduced, both $COP_{c,th}$ and $COP_{h,th}$ decrease, and that this effect is non - linear. The lowest temperature considered in this analysis of 200 °C produces a $COP_{c,th}$ of 0.78 and a $COP_{h,th}$ of 1.62. The highest temperature analysed is 450 °C and produces a $COP_{c,th}$ of 1.86 and a $COP_{h,th}$ of 2.80.

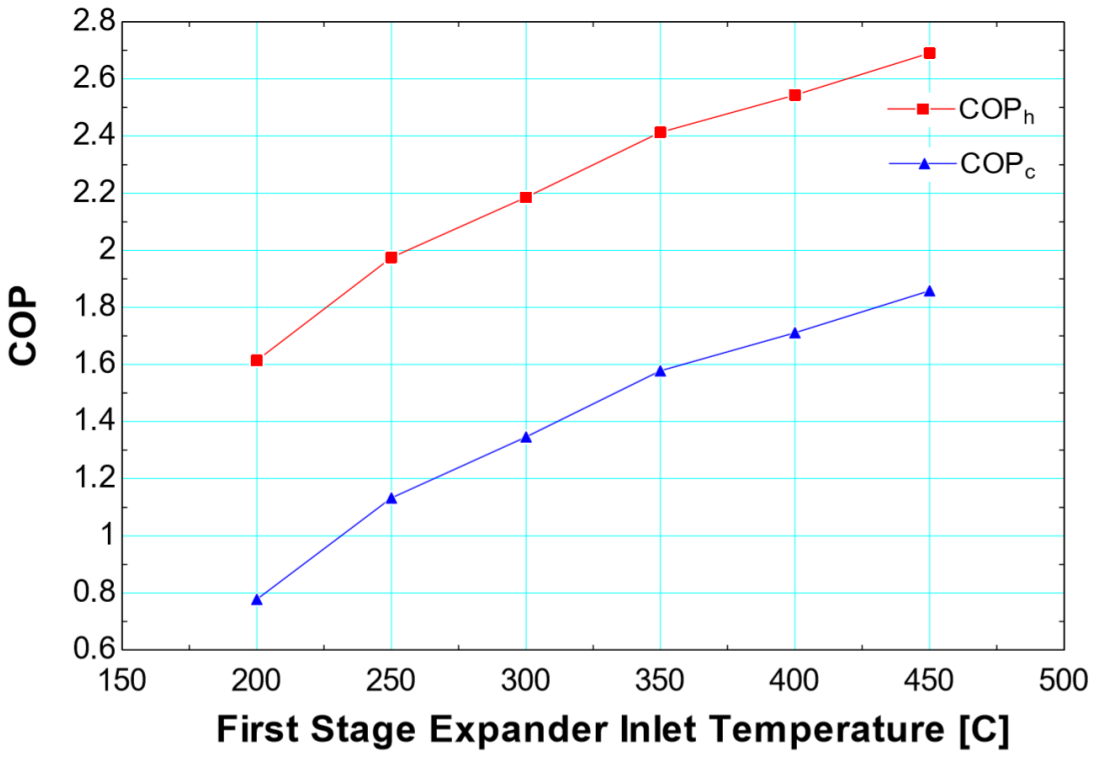

Figure 4.10: A plot of COP_C and COP_h against first stage expander inlet temperature for Cycle 2

As the first stage expander inlet temperature is reduced, the first stage expander pressure ratio must increase to ensure the same mechanical work output. Figure 4.11 shows the relationship between the inlet temperature and outlet pres-

sure for the first stage expander (n.b. expander inlet pressure is a fixed parameter, therefore changes in outlet pressure are as a direct result of changes in pressure ratio). This correlation is very similar in shape to the relationship to that observed in Figure 4.10. This can be said to imply that the first stage expander bears significant influence upon both $\mathrm{COP}_{c,th}$ and $\mathrm{COP}_{h,th}$.

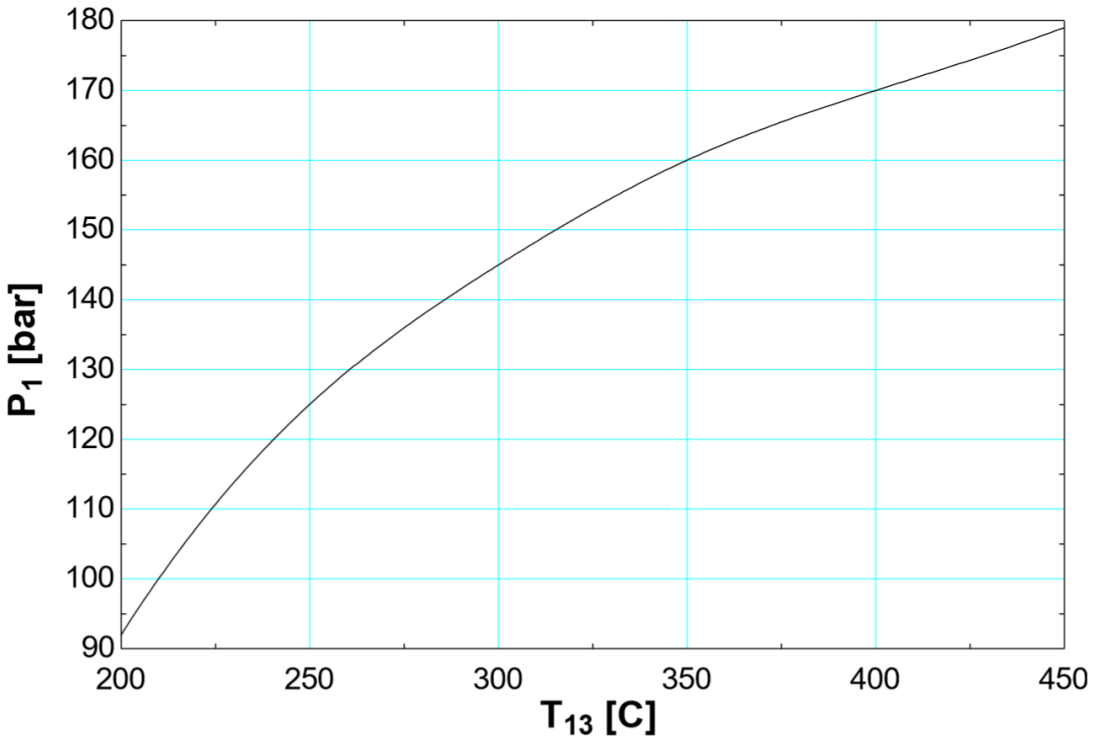

Figure 4.11: A plot of fluid pressure at state point 1 (first stage expander outlet) against temperature at state point 13 (first stage expander inlet temperature) for Cycle 2

At expander inlet temperatures below 200 °C the COP drops sharply, and the model indicates that with a temperature below approximately 190 °C the cycle becomes unfeasible; that is to say the expanders do not produce enough mechanical work to drive the compressors, and the cycle requires a net mechanical work input. This can be explained in conjunction with Figure 4.11, which shows that at an expander inlet temperature of 200 °C, the fluid pressure in the supercritical fluid cooler is 90 bar. In order to prevent condensation in the supercritical fluid cooler, the fluid pressure must be above the critical pressure (73.8 bar). As the expander inlet temperature drops below approximately 190 °C, the fluid pressure in the supercritical fluid cooler drops to below the critical pressure.

4.5 Cycle 3

4.5.1 Description

Cycle 3 is an evolution of Cycle 2, and includes a modification which could potentially allow for the continuous variation of mechanical and thermal energy inputs to the cycle. The second - stage compressor has a split - flow arrangement, with two outlets at different pressures. The lower pressure outlet is at the same pressure as the second stage expander inlet, whilst the second stage outlet is the first stage expander inlet pressure.

A single line progress flow diagram of Cycle 3 is shown in Figure 4.12, and a temperature - entropy plot of the cycle is given in Figure 4.13.

The processes associated with this cycle are described below:

- 1 - 2: internal heat recuperation (hot side)
- 2 - 3: supercritical fluid cooler (providing heat for external use) air cooler
- 3 - 4: second stage expander
- 15 - 4: second stage expander
- 4 - 5: nozzle stage of ejector (pressure reduction of ejector motive flow)
- 5 - 6x: mixing and diffuser stage of ejector
- 6x - 6l: separation of two - phase flow into dry saturated vapour
- 6l - 7: thermal expansion valve
- 7 - 8: evaporator (providing coolth for external use)
- 8 - 5: nozzle stage of ejector (entrained flow pulled in to negatively pressurised motive flow)
- 6x - 6: separation of two - phase flow into saturated liquid
- 6 - 9: first stage compressor

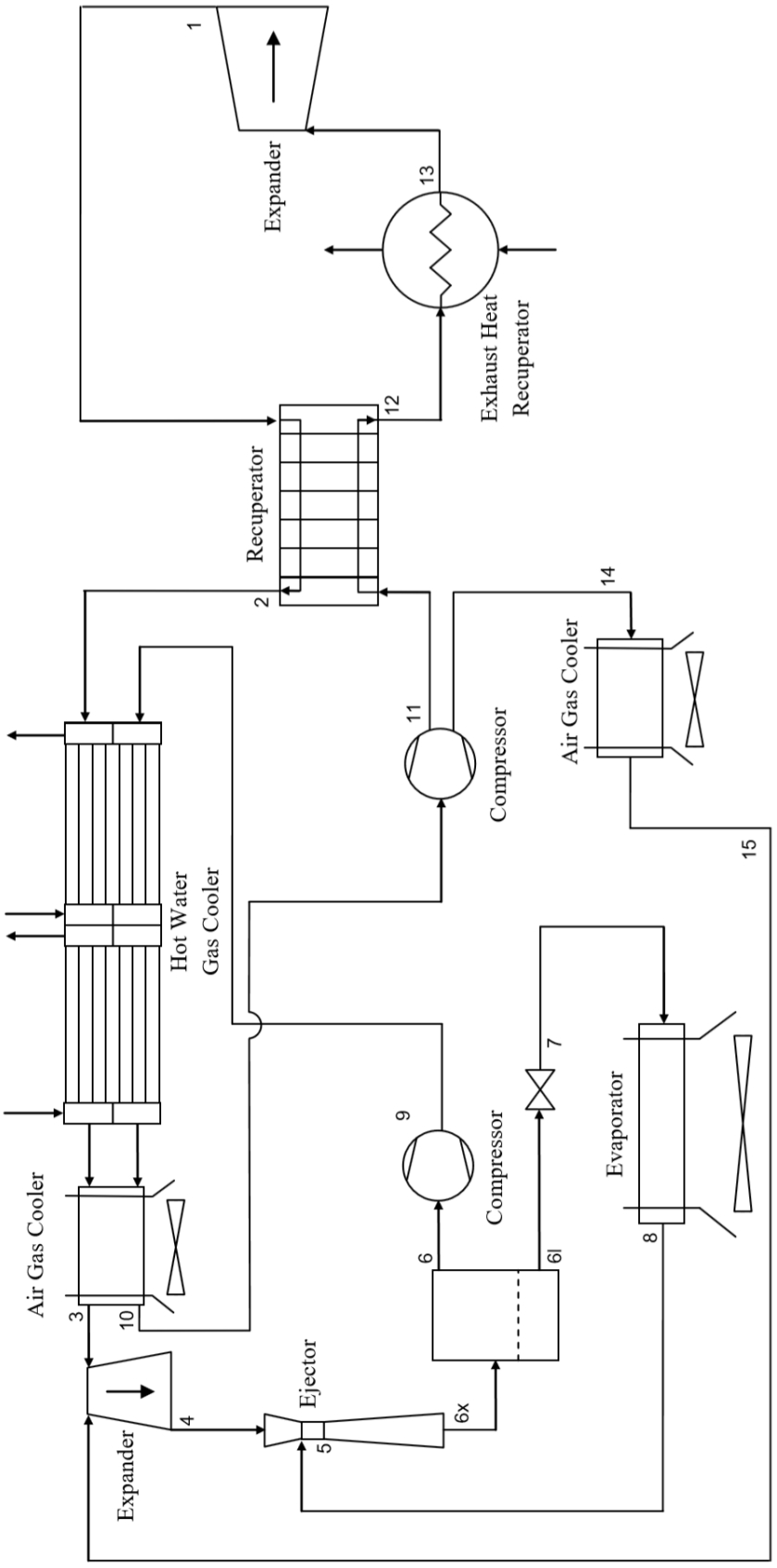

Figure 4.12: Process flow diagram of R744 heat pump Cycle 3

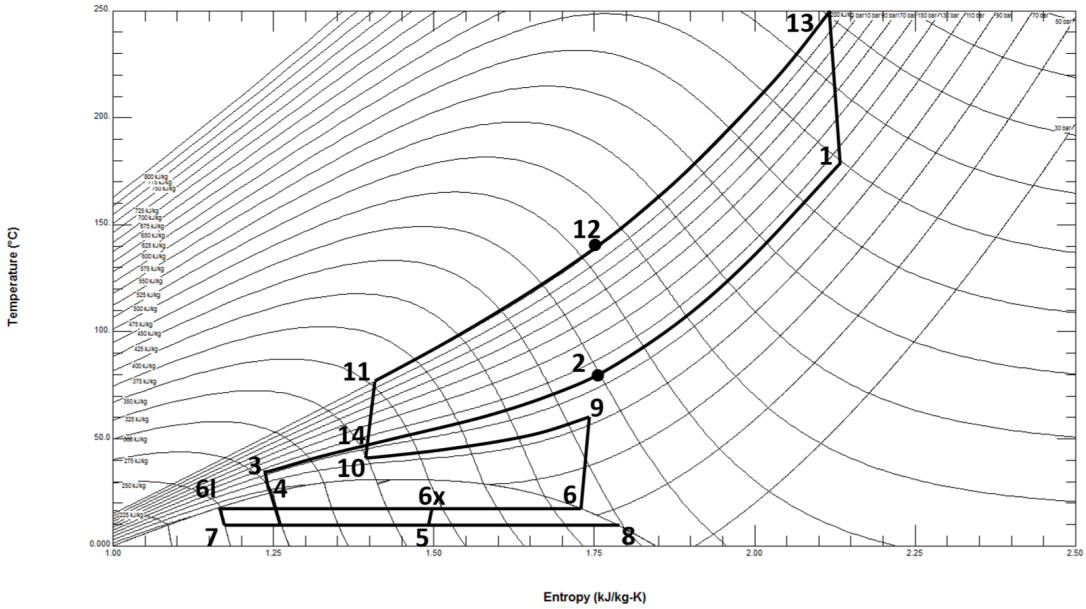

Figure 4.13: Temperature - entropy plot of R744 heat pump Cycle 3

- 9 - 10: supercritical fluid intercooler (providing heat for external use) and air cooler
- 10 - 14: second stage compressor (first split)
- 10 - 11: second stage compressor (second split)
- 11 - 12: internal heat recuperation (cold side)
- 12 - 13: heat addition (from external source)
- 13 - 1: first stage expander
- 14 - 15: external heat rejection

By increasing the mass flow leaving the split in the second stage compressor (state point 14), it is possible to increase the mechanical work input and decrease the thermal work input whilst maintaining a constant cooling work output. Therefore, depending upon the availability of thermal energy (if recuperated exhaust heat) and / or the price of electricity, the mix can be adjusted accordingly. This is, in principle, a fully hybrid heat pump cycle.

Although in theory, this appears to be an extremely advantageous feature over the previous Cycle 2, in reality there would be significant control complexities and design challenges to be overcome. Firstly is the design of a split flow supercritical R744 compressor with an inlet pressure of ∼95 bar, and intermediate pressure of ∼115 bar, and a final pressure of ∼250bar, with a variable mass flow ratio at the two outlets. Secondly, is the control of the second stage expander inlet conditions for the two streams (state point 3 and state point 15). Thirdly, the design of the heat addition and heat recuperation heat exchangers, such that they are able to operate with a variable mass flow rate of working fluid, whilst maintaining the desired inlet and outlet conditions. It is also necessary to include an air cooled heat exchanger to reject heat from the flow exiting the split flow compressor at an intermediate pressure (state point 14).

The split ratio, γ, is defined as the mass flow ratio of working fluid at state point 11 relative to the mass flow of working fluid at state point 10 ($\gamma = \frac{\dot{m}_{11}}{\dot{m}_{10}}$). In pure thermal work input $\gamma = 1$, whilst in pure mechanical work input $\gamma = 0$.

4.5.2 Results and Discussion

When operating in a pure thermal work input mode, Cycle 3 achieves the same values for $\text{COP}_{c,th}$ and $\text{COP}_{h,th}$ as Cycle 2 (1.58 and 2.41, respectively). When operating in a pure mechanical work input, Cycle 3 achieves a $\text{COP}_{c,m}$ of 5.12 and a $\text{COP}_{h,m}$ of 5.80. These values are are higher than many conventional MVC R744 heat pumps [76] [100], although a patent was filled in 2010 for a R744 heat pump cycle which can achieve a COP_c of 7.47 under the ideal operating conditions [99].

Figure 4.14 demonstrates the relationship between $\text{COP}_{c,PEC}$ and $\text{COP}_{h,PEC}$ and the split ratio, γ. The data presented in figure 4.14 is based upon a first stage expander inlet temperature (state point 13) of 250 °C. It can be observed that an increase in γ produces contrasting behaviour in $\text{COP}_{c,PEC}$ to $\text{COP}_{h,PEC}$.

When the cycle is operating in pure thermal input mode ($\gamma = 1$) $\text{COP}_{c,PEC}$

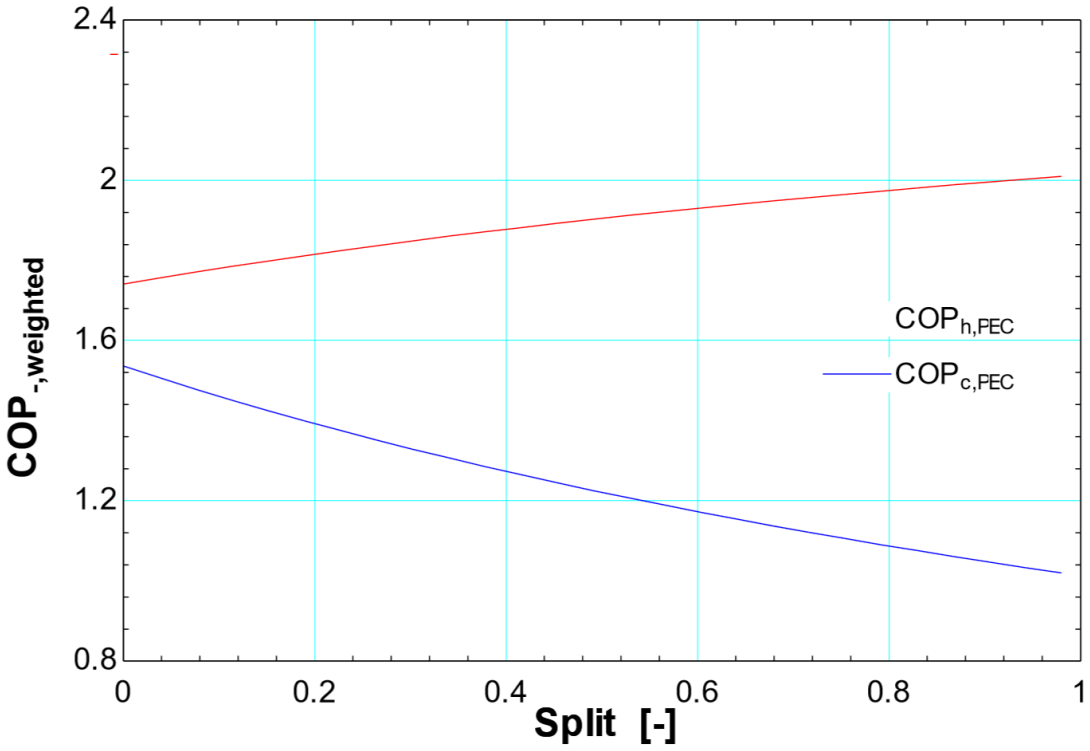

Figure 4.14: A plot of the relationship between $\text{COP}_{c,PEC}$ and $\text{COP}_{h,PEC}$ and the split ratio, γ for Cycle 3

is 1.03 and $\text{COP}_{h,PEC}$ is 2.02. As γ decreases, and the proportion of mechanical work input increases, $\text{COP}_{c,PEC}$ increases and $\text{COP}_{h,PEC}$ decreases. The increase in $\text{COP}_{c,PEC}$ is due to the difference in COP_c when operating in pure thermal work input mode (1.02) and COP_c when operating in pure mechanical input mode (5.12). The decrease in $\text{COP}_{h,PEC}$ can be explained via an understanding of the cycles process. When the γ is increased, the mass flow of working fluid passing through the Brayton portion of the cycle is reduced, and subsequently the mass flow of working fluid passing through the supercritical fluid cooler (state points 2 to 3) is reduction. Consequently, the heat production of cycle is reduced. When the cycle is operating in pure mechanical input mode the $\text{COP}_{c,PEC}$ is 1.54 and the $\text{COP}_{h,PEC}$ is 1.74.

Figure 4.15 shows the relationship between $\text{COP}_{c/h,m/th}$ across the entire range of split ratio, γ. Observation of Figures 4.15a and 4.15b shows that the coolth output from mechanical work input behaves in a manner which is the opposite to the cooling work output from the thermal work input, as γ changes.

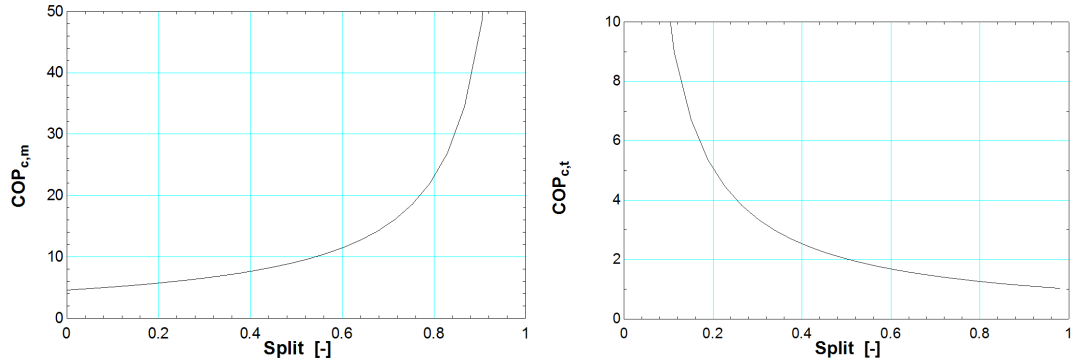

(a) $\text{COP}_{c,m}$

(b) $\text{COP}_{c,th}$

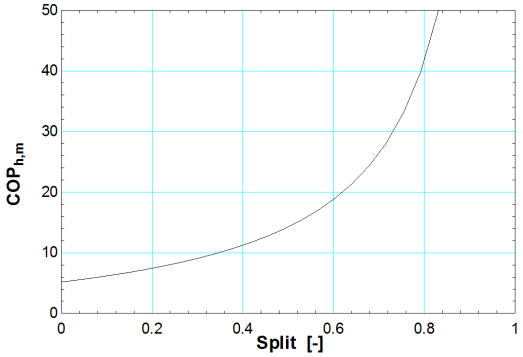

(c) $\text{COP}_{c,m}$

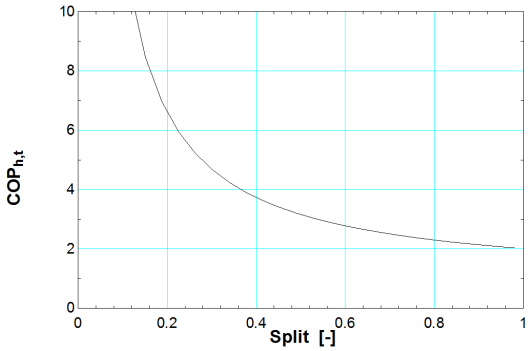

(d) $\text{COP}_{c,th}$

Figure 4.15: A plot of the relationship between $\text{COP}_{c/h,h/m}$ split ratio for Cycle

The $\text{COP}_{c,m}$ tends to infinity as γ approaches 1, and $\text{COP}_{c,th}$ tends to infinity as γ approaches 0. In reality, this implies that the mechanical and thermal work inputs are approaching 0. Exactly the same relationship is observed in Figures 4.15c and 4.15d for $\text{COP}_{h,m}$ and $\text{COP}_{h,m}$.

4.6 Cycle Selection and Discussion

Three cycles have been presented and discussed, although many more were conceptualised, modelled and analysed; a basic block schematic of other cycles is given in the Appendix.

Cycle 1 is an earlier concept, which was not capable of operating on thermal work input alone at the temperatures discussed. The input of both mechanical and thermal work provides an interesting range of possible operating modes for hybridised trigeneration systems with gas - fired reciprocating engines or gas turbine. Conventional thermal load or electrical load following control algorithms

are unlikely to be appropriate. A hybrid control algorithm which considers both supply and demand factors would be required; the complex performance characteristics of the heat pump, particularly with regard to ambient temperature and evaporator pressure, mean that this is necessary.

In order for Cycle 1 to operate under a pure thermal regime, it is necessary to have an expander inlet temperature of approximately 400 °C. However, the COP achieved is relatively low when compared to Cycle 2. Therefore, due to potential control issues and poor performance, Cycle 1 is not considered to be a viable option for further consideration.

Cycle 2 is a evolution of Cycle 1, which aimed to overcome the potential control complexities resulting from two types of work inputs, as well as poor performance. The principal desire was to increase the COP to be equivalent to a triple - stage LiBr - H_2O absorption chiller, but enabling the simultaneous production of heat and coolth and with significantly fewer processes (heat exchangers, vessels, pumps, etc.). The addition of a transcritical ejector to the cycle enable this to be possible; a $COP_{c,th}$ of 1.58 and a $COP_{h,th}$ of 2.41 have been demonstrated to be theoretically possible with a first stage expander inlet temperature of 350 °C to the cycle. As with Cycle 1, the performance of Cycle 2 is highly dependent upon the first stage expander inlet temperature and the evaporator temperature. However, the cycle is able to function at first stage expander inlet temperatures at low as 190 °C; although $COP_{c,th}$ is only marginally better than a single - stage LiBr - H_2O absorption chiller. The maximum $COP_{c,th}$ of 1.86 and $COP_{h,th}$ of 2.691 (at first - stage expander inlet temperatures of 450 °C) mean that Cycle 2 has potential for further investigation.

Cycle 3 is an evolution of Cycle 2, which incorporates the potential for a hybrid mix of continuously variable thermal and mechanical work inputs. The performance of Cycle 3 under pure thermal work input is identical to Cycle 2. However, increasing the mix of mechanical work input increases the COP_c in terms of Primary Energy Consumption (PEC), but decreases the COP_h in terms

of Primary Energy Consumption (PEC). This cycle has great potential in a hybrid trigeneration scheme, due to the flexibility of the work inputs and the opportunity this affords to alter the mix of energy flows to best match demands. However, the complexity of the split flow compressor means that this cycle will be considered no further.

Therefore Cycle 2 is believed to be the best candidate for further research and development.

4.7 Sensitivity Analysis

The COP of Cycle 2 is particularly a function of the isentropic efficiencies of the two compressors and the two expansion turbines. A sensitivity analysis has been conducted using the EES software, to determine the effect of the isentropic efficiencies on the COP_c and COP_h of Cycle 2.

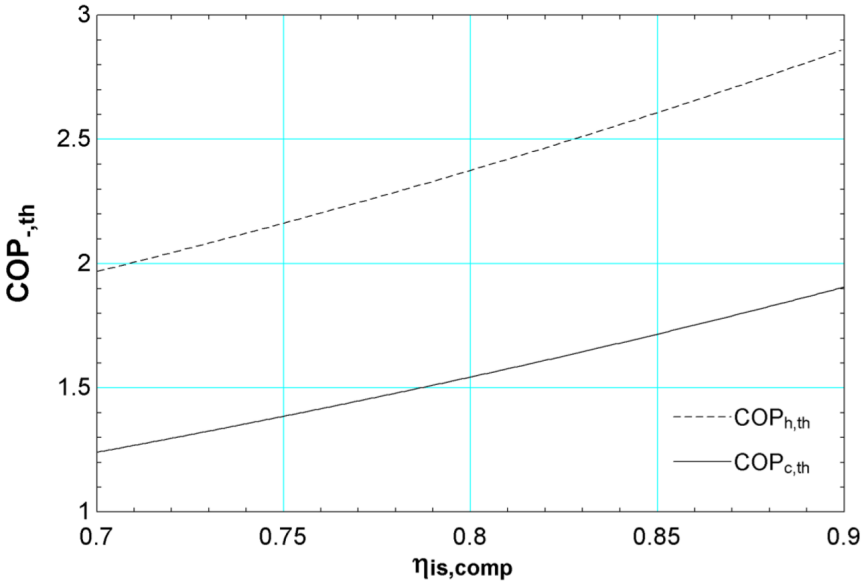

Figure 4.16: Sensitivity analysis of the COP_c and COP_h of Cycle 2 to the isentropic efficiency of the compressors

Figure 4.16 highlights the relationship between the isentropic efficiency of the compressors and the COP. The relationship demonstrates that the COP reduces as the compressor isentropic efficiencies are reduced, in an approximately linear fashion. The gradient of the curve for COP_h is marginally greater than for COP_c,

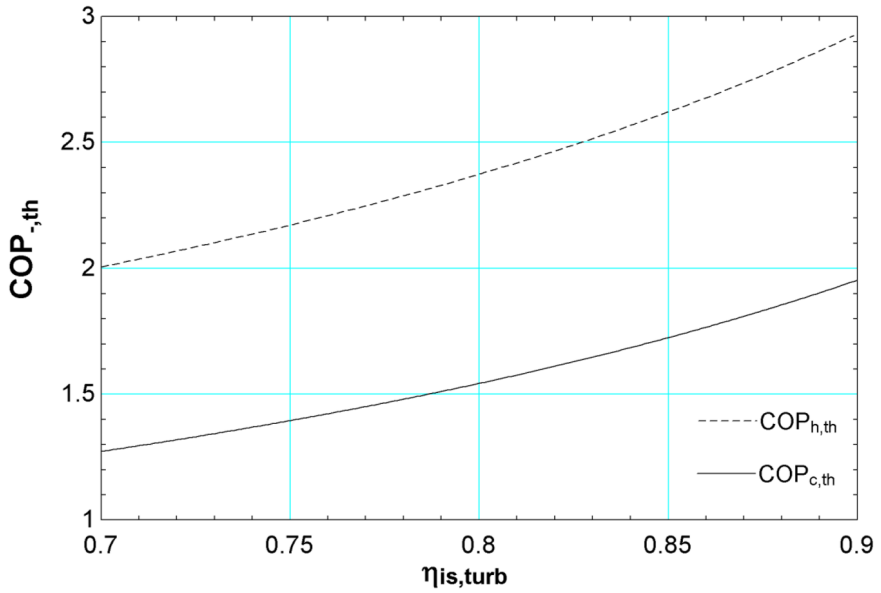

Figure 4.17: Sensitivity analysis of the COP_c and COP_h of Cycle 2 to the isentropic efficiency of the expanders

indicated that the isentropic efficiency of the compressors has a bigger effect on COP_h.

Figure 4.17 highlights the relationship between the isentropic efficiency of the expanders and the COP. The relationship demonstrates that the COP reduces as expander isentropic efficiencies are reduced. The gradient of the curves increases at higher isentropic efficiencies and reduces at lower isentropic efficiencies. As with the relationship observed in Figure 4.16, the COP_h appears to vary marginally more over the range of expander isentropic efficiencies considered.

Figure 4.18 shows the effect of varying the isentropic efficiencies of both the two compressors and the two expanders on the COP. This demonstrates that there is a very non linear relationship between the isentropic efficiencies and the COP. A COP_c of 2 and COP_h of 3 is achieved with isentropic efficiencies of approximately 87 %. If the isentropic efficiencies reduce to 77 % the COP_c reduces to approximately 1.3 and the COP_c reduces to approximately 2.1, a 35 % and 30 % reduction, respectively.

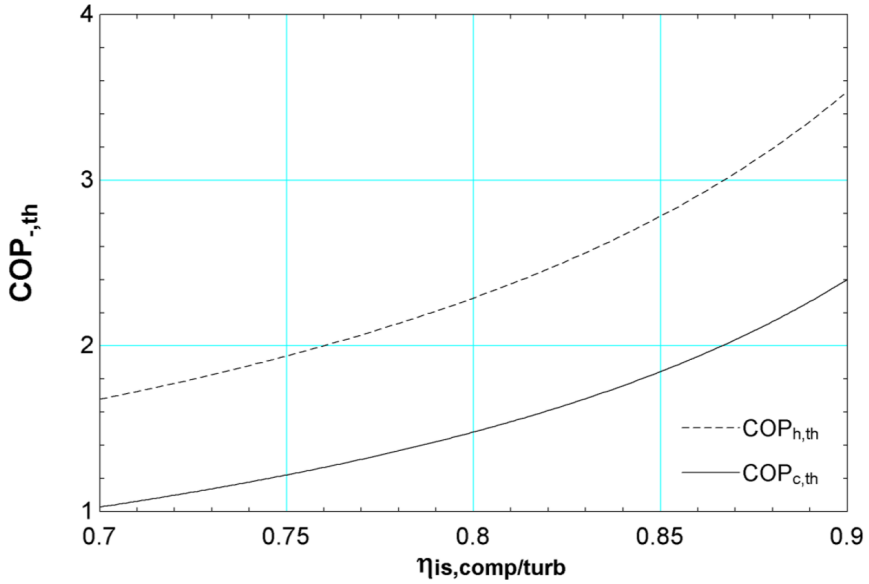

Figure 4.18: Sensitivity analysis of the COP_c and COP_h of Cycle 2 to the isentropic efficiency the compressors and expanders

4.8 Comparison to a 'Separate Cycle System'

It must be demonstrated that Cycle 2 gives a significant performance benefit over a 'separates' system in order to justify its complexity. Therefore, the performance of Cycle 2 is analysed relative to a low temperature recuperated exhaust heat supercritical CO_2 Brayton cycle, linked to a basic transcritical R744 MVC heat pump.

The R744 heat pump cycle generates hot water using a supercritical fluid cooler, which generates hot water at 40 °C and 60 °C. In order to reduce the temperature of the working fluid as close as possible to ambient, the supercritical fluid cooler is followed by an air cooler.

The thermal to mechanical work conversion efficiency of the Brayton cycle is dependent upon the expander inlet and outlet conditions, in particular temperature and pressure. Figure 4.21 shows the relationship between expander inlet pressure and outlet pressure, assuming an expander inlet temperature of 250 °C.

The maximum thermal to mechanical conversion efficiency the cycle can achieve is 19.24%. The data in Figure 4.21 shows that cycle efficiency is greater at lower expander outlet pressures (P_{min}) and higher inlet pressures (P_{max}), as would typ-

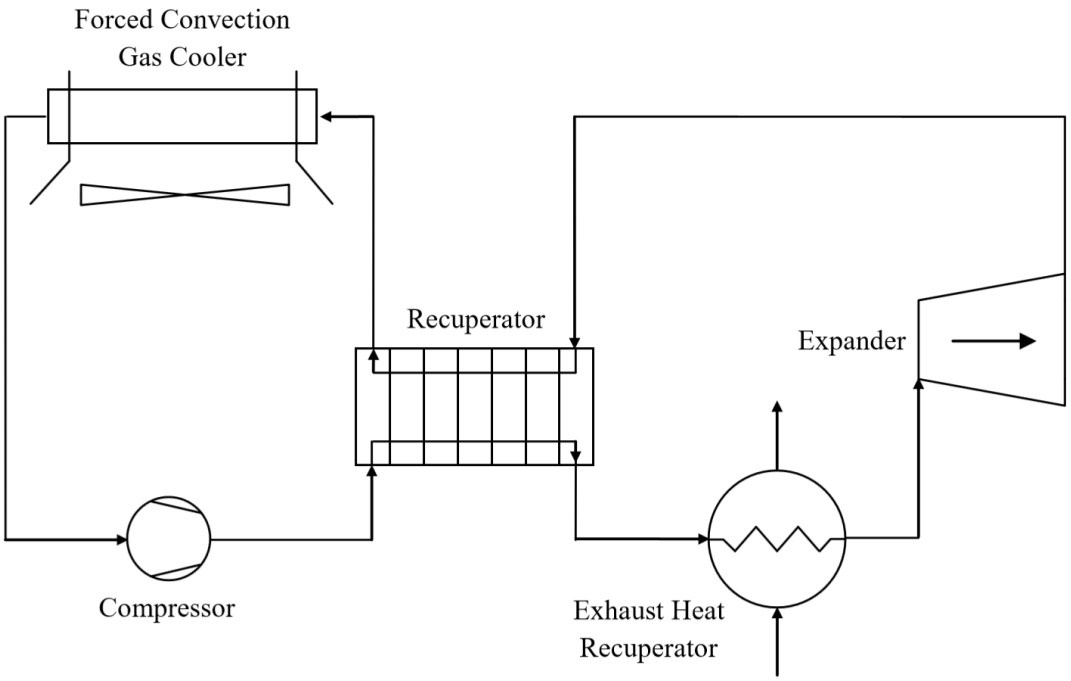

Figure 4.19: Supercritical CO_2 Brayton cycle process flow diagram

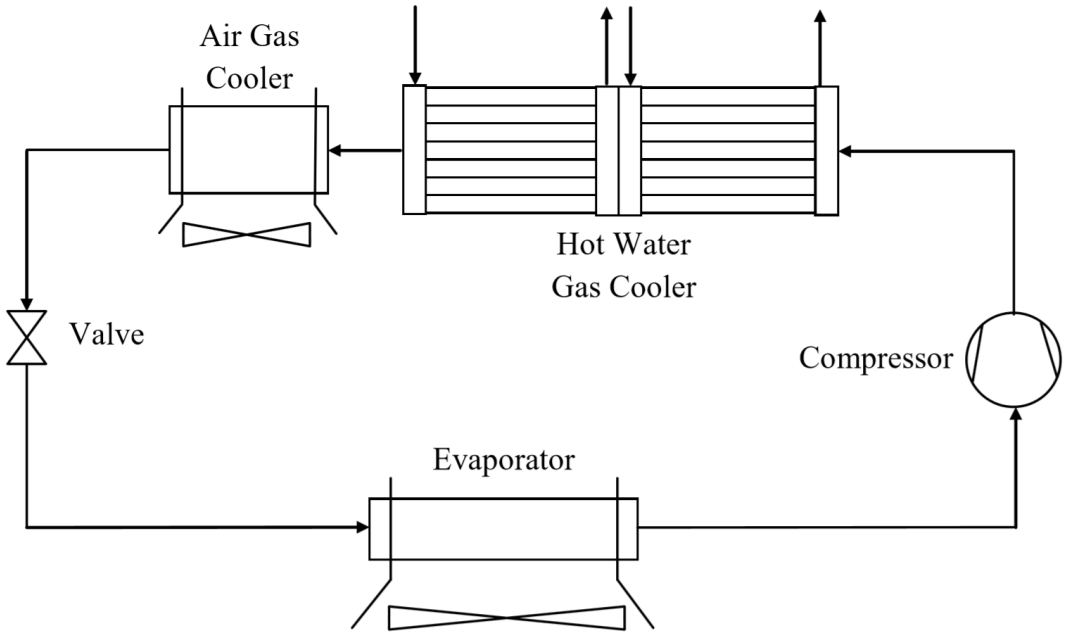

Figure 4.20: Basic transcritical R744 MVC cycle process flow diagram

ically be expected of a Brayton cycle. Increasing the pressure ratio across the expander is desirable from an efficiency perspective, but high pressure ratios can lead to reduced isentropic efficiencies across compression and expander devices (this analysis assumes the same isentropic efficiency for all pressure ratios). A further comment of caution with a high pressure ratio is the decrease in effectiveness

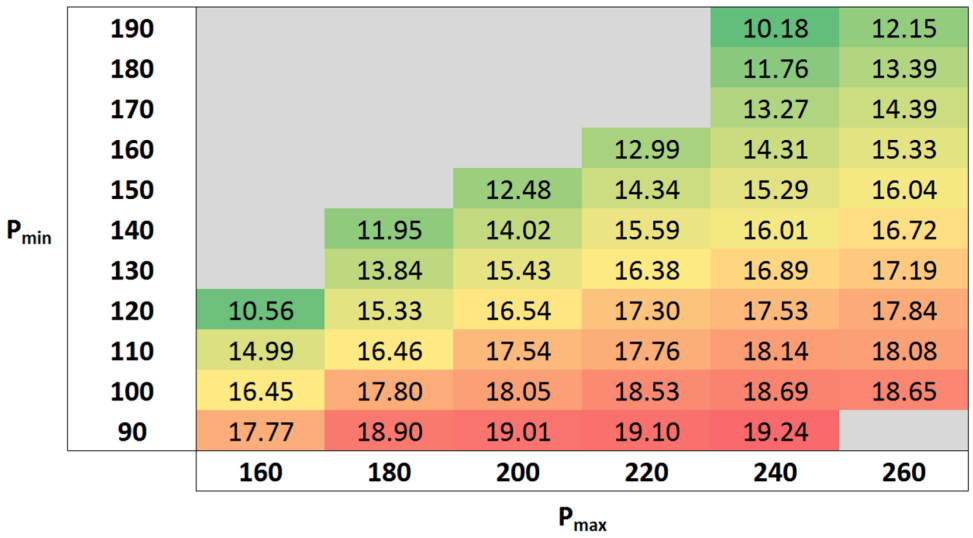

Figure 4.21: Supercritical CO_2 Brayton cycle thermal to mechanical conversion efficiencies for a range of inlet and outlet pressures.

of the internal heat recuperator (for a given heat exchanger surface area), due to the difference in C_p between the high pressure cold side and low pressure hot side; this problem becomes much worse when the expander outlet temperature is close to the critical pressure. The decrease in recuperator effectiveness occurs as a result of temperature pinch towards the cold end of the heat exchanger.

The R744 MVC heat pump cycle achieves a simultaneous COP_c and COP_h of 3.52 and 4.12, respectively. Coupling the two cycles, and not accounting for mechanical to electrical losses, if any, the implied $\text{COP}_{c,th}$ and $\text{COP}_{h,th}$ are defined by Equation 4.2.

$$COP_{c/h,th} = \eta_{Brayton} \times COP_{c/h} \tag{4.2}$$

Therefore, $\text{COP}_{c,th}$ is 0.68 and $\text{COP}_{c,th}$ is 0.80. The corresponding values $\text{COP}_{c,th}$ and $\text{COP}_{h,th}$ achieved by Cycle 2 with an first stage expander inlet temperature of 250 °C are 1.12 and 1.96, respectively - this is a 65% and 145% increase in COP. This is a significant improvement in performance which makes a very strong argument for the integration of a CO_2 mechanical work cycle and a heat pump cycle into a single loop. The thermodynamic benefit derived from the sharing of compression work, the internal recuperated of exergy, the thermo-

physical properties of R744 and the two - phase ejector yields this performance gain.

The ejector increases the inlet pressure of first stage compressor, which reduces the work required to compress the gas, which subsequently allows the first stage expander pressure ratio to be reduced which consequently increases the cooling work potential of the evaporator. The advantage gained by sharing compression work is best understood with reference to the overlap in pressures of the two parts of the cycle: the Brayton cycle and the reverse Rankine cycle. This can be observed on Figure 4.8 by the difference in pressure between P_3 and P_9, and the fact that $P_3 > P_9$.

4.9 Integration into a Trigeneration System

To assess the suitability of Cycle 2 for integration within a trigeneration system which has a gas turbine as the PGU, a high level assessment of the total efficiency of the system is required. In order to do this, the exergetic efficiency of the exhaust heat recuperation process must be ascertained. This is dependent upon the conditions of the exhaust gases after they exit the gas turbine, the conditions of the exhaust gases after the recuperator and the ambient conditions. The conditions of the exhaust gases is fixed parameters and are dependent upon the specific performance of the gas turbine, which are a commonly available performance parameter from suppliers and manufacturers. For the sake of this high level analysis, it is assumed that the exhaust gases can be treated as air at 500 °C and 0.5 barg. Assuming that the heat recovery process is fully reversible, the exergetic efficiency (η_{ex}) of the exhaust heat recuperation process can simply defined by Equation 4.3.

$$\eta_{ex} = \frac{\Delta h_{recuperator}}{B_{G.T.exhaust}} \tag{4.3}$$

$B_{G.T.exhaust}$ represents the exergy in the exhaust stream of the gas turbine.

Thus, assuming that C_p is constant with temperature, Equation 4.3 can be expressed as shown in Equation 4.4.

$$\eta_{ex} = \frac{T_{G.T.exhaust} - T_{12}}{T_{G.Texhaust} - T_{amb}} \tag{4.4}$$

Figure 4.22 shows the relationship between T_{12} and T_{13} (i.e. the internal heat recuperator code side outlet temperature and first stage work expander inlet / exhaust heat recuperator working fluid side outlet temperatures, respectively). The relationship between T_{12} and T_{13} is almost linear, and it can be observed that $T_{13} - T_{12} \approx 100°C$. This implies that the c_p of the two fluid streams (air and R744) are approximately constant, and therefore the enthalpy transfer in the exhaust heat recuperator is linear..

Using Equation 4.4, Figure 4.22 can be converted to demonstrate the relationship between the exergetic efficiency of the exhaust heat recuperation process and the first stage expander inlet temperature, T_{13}. This relationship is shown in Figure 4.23. It is assumed that the ambient temperature is 30 °C.

The exergetic efficiency is a direct measure of the enthalpy of the gas turbine exhaust which can be recovered by Cycle 2, enabling it to ultimately produce chilled water and hot water for building and process consumption. Ascertaining the optimum first stage expander temperature (T_{13}) to maximise the overall production of chilled water and hot water is vital in optimising the performance for the trigeneration system. The COP of Cycle 2 when integrated within a trigeneration system is defined in Equation 4.5.

$$COP_{c,trigen.system} = COP_{c,th} \times \eta_{ex} \tag{4.5}$$

Figure 4.24 shows the relationship between $COP_{c,trigen.system}$ and T_{13}. This indicates the optimum first stage work expander inlet temperature to maximise the coolth production potential of Cycle 2 integrated within a gas turbine trigeneration system; it is evident that this temperature is approximately 275 °.

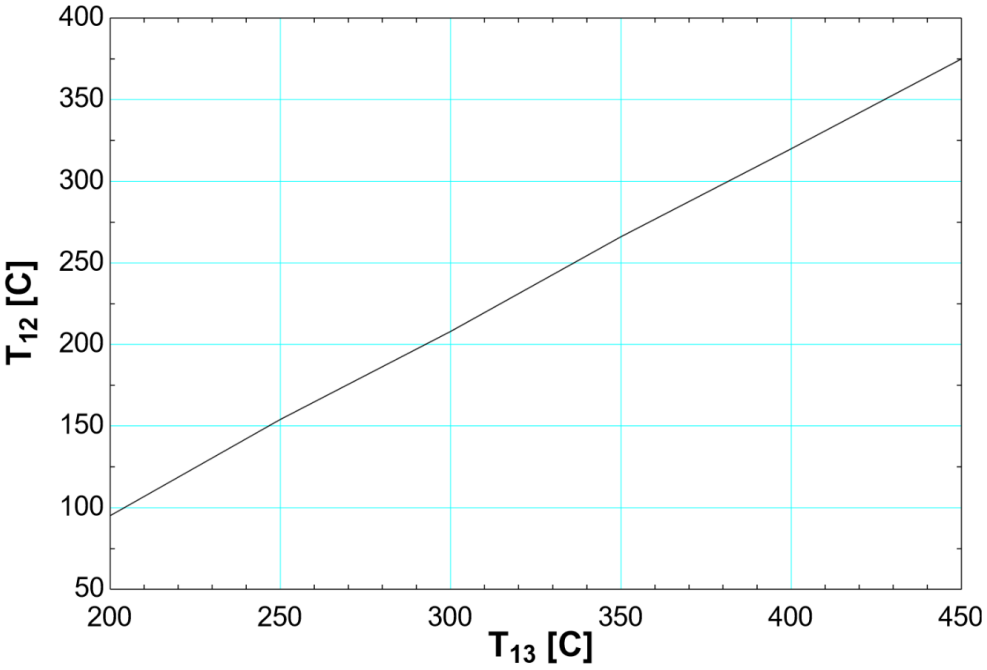

Figure 4.22: A plot of the relationship between temperature at state point 12 (internal heat recuperator inlet) against temperature at state point 13 (first stage expander inlet temperature) for Cycle 2

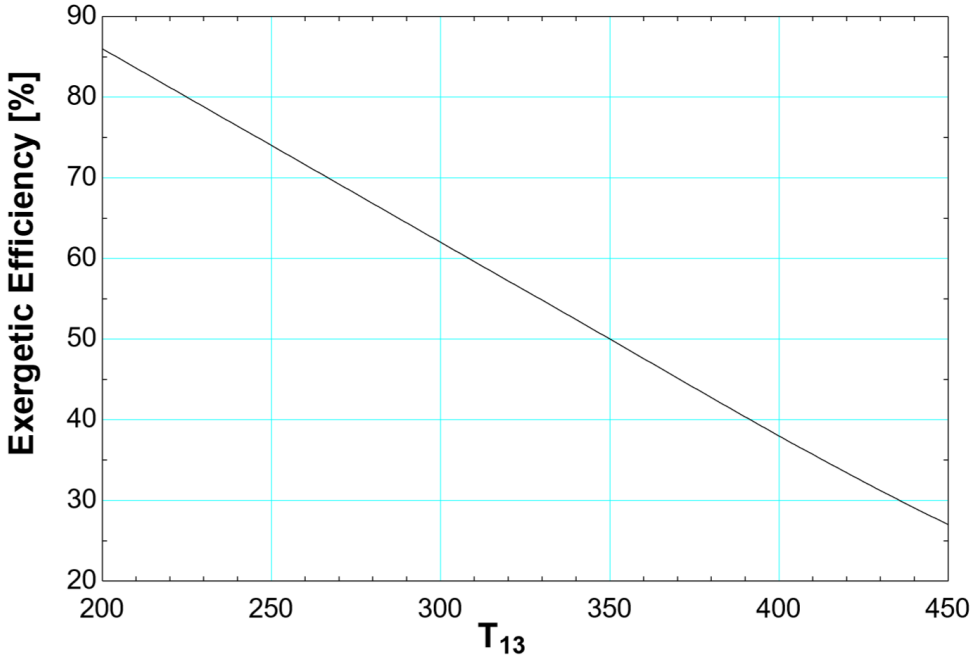

Figure 4.23: A plot of the relationship between the exergetic efficiency of the exhaust heat recuperation process and T_{13}

Whereas a higher T_13 gives a higher COP_c for the cycle alone, this is clearly not the optimum solution for the cycle when integrated within a trigeneration system.

Figure 4.24 shows the relationship between shows the relationship between

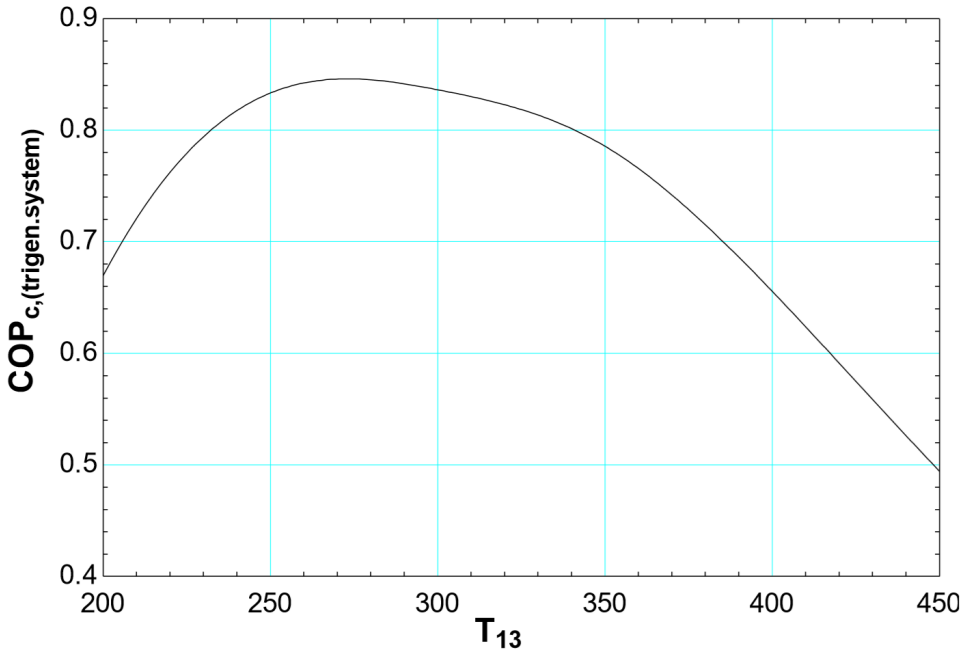

Figure 4.24: A plot of the relationship between $COP_{c,trigen.system}$ and T_{13}

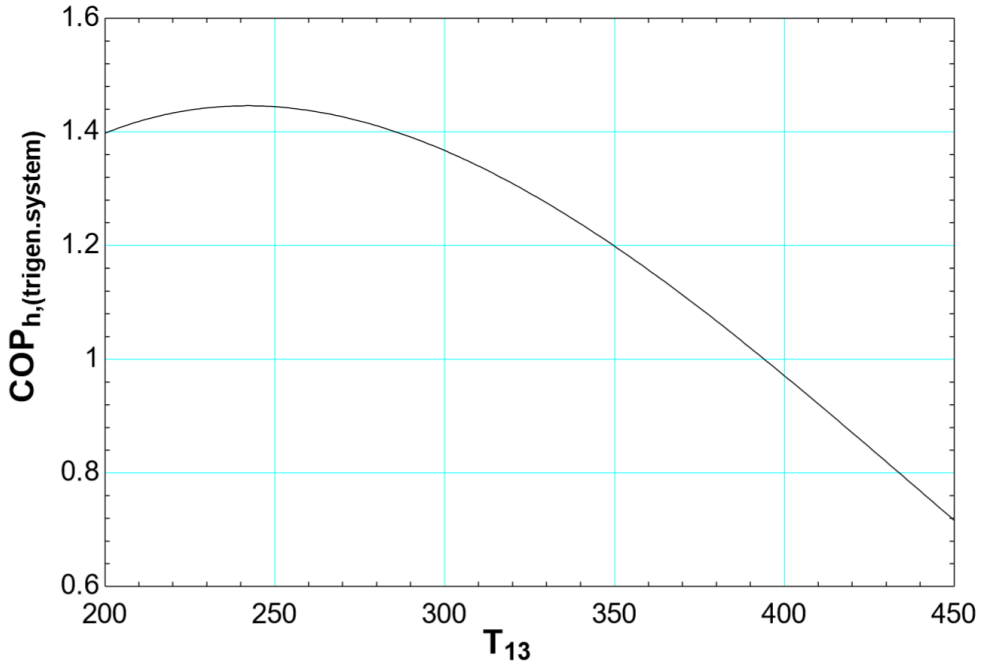

Figure 4.25: A plot of the relationship between $COP_{h,trigen.system}$ and T_{13}

$COP_{h,trigen.system}$ and T_{13}. This indicates the optimum first stage work expander inlet temperature to maximise the heat production potential of Cycle 2 integrated within a gas turbine trigeneration system; it is evident that this temperature is approximately 240 °C. This is slightly lower than the optimum T_{13} for coolth production, which could allow for system fine tuning.

An plot illustrating the potential COP_c in a 'direct firing' scenario (i.e. where natural gas is combusted to directly provide thermal energy to the cycle via the exhaust heat recuperator, or via an intermediate heat transfer fluid) is given in Figure 4.26. This is compared to the $\text{COP}_{c,th}$ for Cycle 2 itself. The difference between the two curves is an illustration of the exergetic efficiency of the heat addition process. Unlike with heat addition from exhaust, direct firing of natural gas results in a much T_{13} giving the highest performance (i.e. it gives a higher exergetic efficiency).

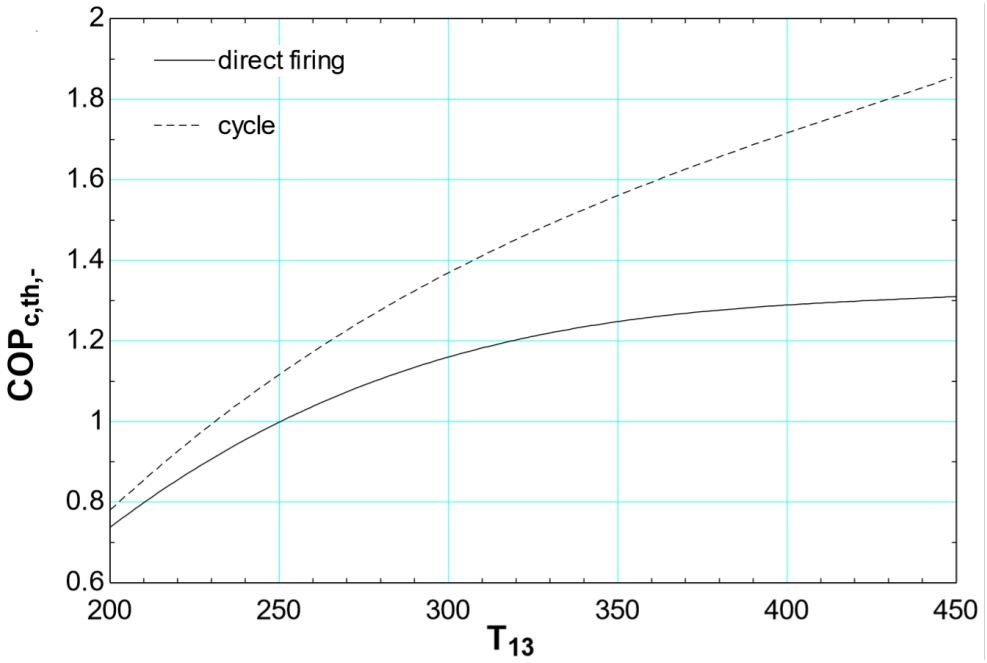

Figure 4.26: A plot to compare the relationship between $COP_{c,th,directfiring}$ and $COP_{c,th,cycle}$ against T_{13}

4.10 Conclusions

Three novel thermally and mechanically or pure thermally activated transcritical R744 heat pump cycles have been conceptualised, modelled and analysed. Each of these cycles are capable of providing simultaneous heating and cooling, and are designed to use the thermal energy in the exhaust gases from a Primary Generation Unit (PGU), in this instance a gas turbine. Cycle 2 was identifed as the preferred heat pump cycle as it provides a higher COP_c and COP_h than Cycle

1. Cycle 3 is a minor evolution of Cycle 2 and is capable of providing mechanical work output as well as producing hot water and chilled water, however the small magnitude of the mechical work output and complexity of a split flow compressor meant that Cycle 3 was not pursued further. Cycle 2 is capable of providing coolth (10 °C) at a $COP_{c,th}$ of 1.58 and hot water (65 °C) at a $COP_{h,th}$ 2.41, with a first stage expander inlet temperature of 350 °C.

These performance figures for COP_c are very similar to those theoretically achieved by triple - stage LiBr - H_2O absorption chillers, as demonstrated earlier (n.b. typically $COP_c = 1.6$). However, Cycle 2 is capable also simultaneously producing hot water at 65 °C. Cycle 2 requires half the number of processes of a triple - stage LiBr - H_2O absorption chiller and uses a single working fluid, further simplifying the system and the control. Chapter 5 provides an overview of an initial component analysis and design for key components of Cycle 2, such as: the internal heat recuperator, ejector, work expander and supercritical fluid cooler.

It was then shown that Cycle 2 performs considerably better than a 'separates system' of a supercritical CO_2 Brayton cycle linked to a R744 MVC heat pump cycle, achieving a 65% and 145% increase in $COP_{c,th}$ and $COP_{h,th}$ respectively, with an expander inlet temperature of 250 °C.

Lastly, it has been demonstrated that when integrated within a trigeneration system with a gas turbine as the PGU, the optimum first stage work expander inlet temperature is between 240°C and 275 °C. The cycle was able to achieve a maximum COP_c of 0.84, and maximum COP_c of 1.45 in this scenario (i.e. for every 1 kWh of exhaust heat, 0.84 kWh of coolth and 1.45 kWh of hot water are produced).

A considerable number of alternative cycles have been conceptualised, modelled and analysed, but are not presented within this Thesis. These are viewed as stepping stones towards the cycles that have been presented within this Chapter, and form the basis of the trial - and - error style design process.

Chapter 5

R744 Heat Pump Cycle Preliminary Component Analysis

5.1 Introduction

This Chapter provides an overview of preliminary component analysis for the novel thermally activated R744 simultaneous heating and cooling heat pump cycle 'Cycle 2' discussed in Chapter 4. Components analysed include:

- The supercritical fluid cooler / hot water generator, which cools the working fluid following the first stage compressor and the hot side of the internal heat recuperator.
- The internal heat recuperator, which preheats the supercritical fluid exiting the second stage compressor prior to the external heat addition.
- The ejector.
- Concepts for the compressor and work expander.

5.2 Heat Exchanger Modeling

Temperature pinch in heat exchangers is modeled using a discretised $\epsilon - NTU$ method. The $\epsilon - NTU$ method can be used to calculate the rate of heat transfer in heat exchanger when the Log Mean Temperature Difference method is not suitable, for example when c_p and the heat transfer coefficient, U, are not constant. The Number of Transfer Units, NTU, is defined by Equation 5.1, where A is the heat transfer area.

$$NTU = \frac{UA}{C_{p,min}} \tag{5.1}$$

The effectiveness, ϵ, is defined by Equation 5.2.

$$\epsilon = \frac{1 - e^{(-NTU(1-C_r))}}{1 - C_r e^{(-NTU(1-C_r))}} \tag{5.2}$$

Where $C_r = \frac{C_{p,max}}{C_{p,min}}$.

The heat exchanger is discretised into > 250 blocks (n number), with fluid thermophysical properties recalculated for each block.

The numbering convention used to describe the counterflow heat exchanger is shown in Figure 5.1.

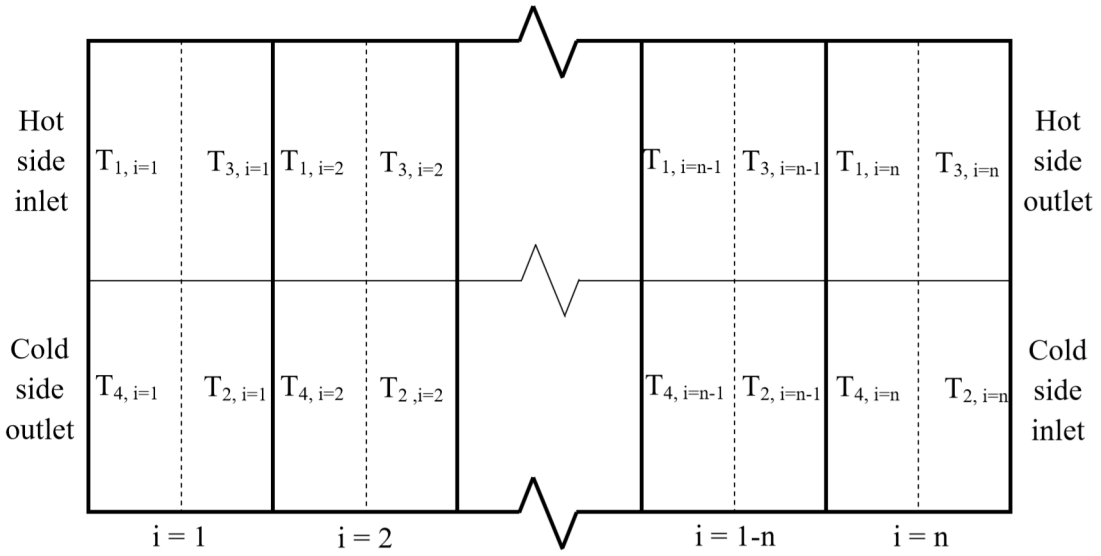

Figure 5.1: Diagram to indicate the numbering convention for counterflow heat exchanger

The $\epsilon - NTU$ method requires the hot and cold side inlet temperatures to be known for every block; this is not possible with a discretised counterflow heat exchanger. Whilst iterative finite volume techniques (such as are used in computational fluid dynamics software) would yield a solution, such software is not available and creating an custom code script would take considerable time and may require significant computational time. Therefore, a simple finite difference method is proposed, which relies on an assumption. The assumption produces an error (e), such that $\lim_{n\to\infty} e = 0$.

The temperature and thermophysical properties at the hot side outlet (i.e. expander outlet) and cold side inlet to the heat exchanger side are both known; this means that $T_{1,i=1}$ and $T_{2,i=n}$ are known. In order to resolve the thermophysical properties in, say, block $i = 1$ using the $\epsilon - NTU$ method, $T_{2,i=1}$ must be known; however this is an output of the model, not an input. If $T_{2,i=1}$ is assumed, $T_{3,i=1}$ and $T_{4,i=1}$ can be calculated using an appropriate empirical heat transfer

relationship. The calculated values for $T_{2,i=1}$ and $T_{3,i=1}$ are then assigned to $T_{4,i=2}$ and $T_{1,i=2}$, respectively. However, the same problem occurs again; $T_{2,i=2}$ but now be assumed.

Given that the hot side inlet ,$T_{1,i=1}$, is known (defined by the expander outlet conditions), a sensible estimate for the cold side outlet, $T_{4,i=1}$, can be made (with a value much less than $T_{1,i=1}$). If the temperature drop of each side across the block is very small compared to the temperature difference between the hot and colde side then $T_{4,i=1}$ can be assumed to be equal to $T_{2,i=1}$ (which is known), such that:

if

$$T_{1,i} - T_{3,i} \ll T_{1,i} - T_{4,i} \tag{5.3}$$

then

$$T_{2,i} \simeq T_{4,i} \tag{5.4}$$

Each block can now be solved linearly and the temperature profile of the two streams can be ascertained, yielding the pinch point temperature and location along the heat exchanger. The cold side outlet temperature, $T_{4,i=1}$, is then increased and the calculations re-run until. This is repeated until the desired pinch point temperature is achieved. This is a semi-iterative scheme, as demonstrated in the algorithm which follows in Figure 5.2.

The development and validation of a three - pass R744 air cooled gas cooler is discussed by Yin, Bullard and Hrnjak [101]. The model was based upon the Gnielinski empirical relationship for heat transfer in a micro - tubes, and was found to be within 2% of the results of the physical test. Therefore, in this instance the empirical Gnielinski-Petukhov relationship for turbulent flow within an annulus [102] is used to calculate the overall heat transfer coefficient, U, for each block of the shell and tube heat exchanger. The cold side is the flow within

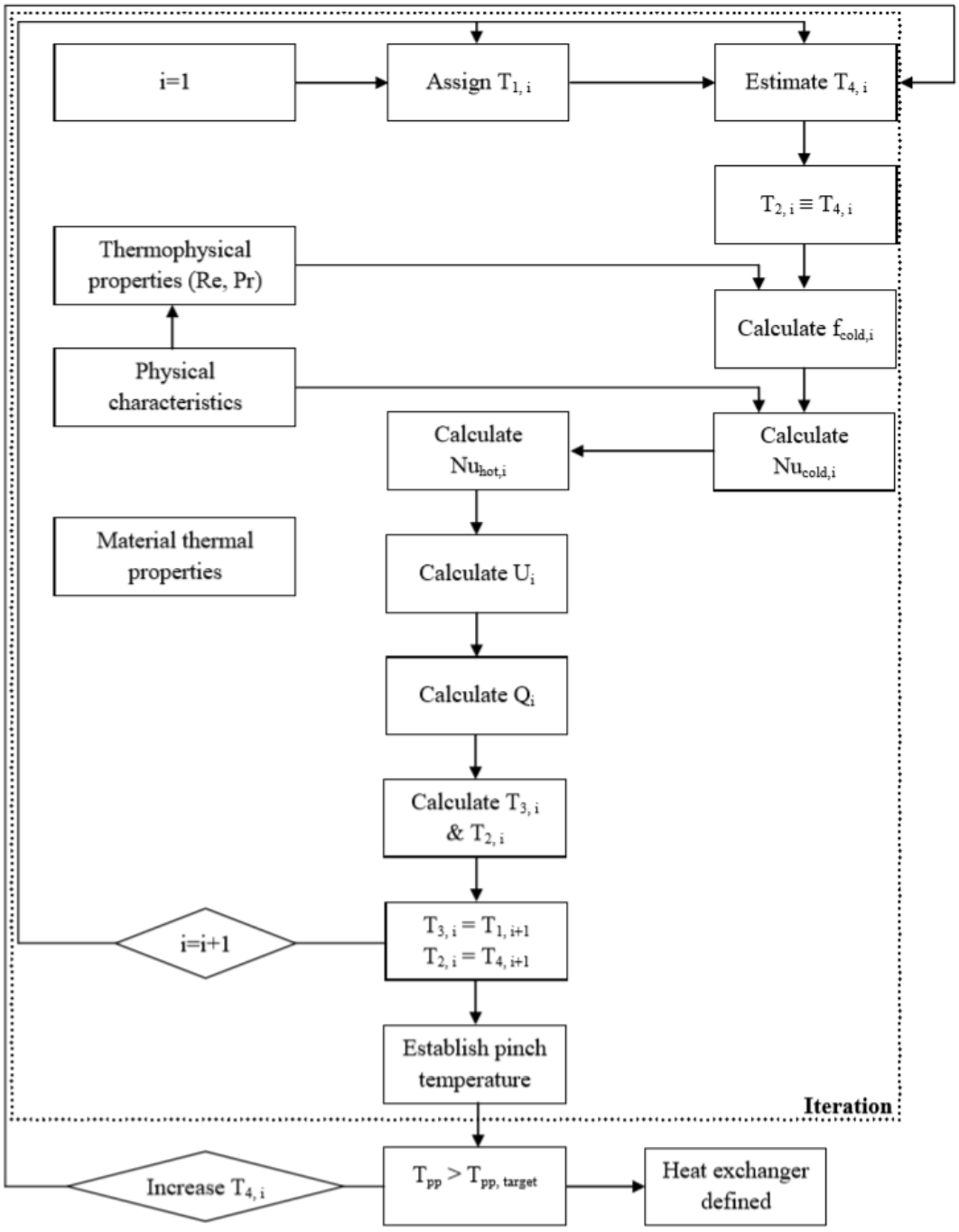

Figure 5.2: Alrogithm used to model a counterflow heat exchanger

the annulus, and the hot side is the flow around the annulus.

$$Nu_{cold,i} = \frac{\left(\left(\frac{f_{cold,i}}{8}\right) \cdot Re_{cold,i} \cdot Pr_{cold,i}\right) \cdot (1 + D_{inner}/L)^{0.666}}{1.07 + 12.7 \cdot \left(\frac{f_{cold,i}}{8}\right)^{0.5} \cdot \left(\left(Pr_{cold,i}^{0.666}\right) - 1\right)} \tag{5.5}$$

$$Nu_{hot,i} = Nu_{cold,i} \cdot \left(0.86 \cdot \left(\left(D_{outer}/D_{inner}\right)^{0.16}\right)\right) \tag{5.6}$$

The f, used in the calculations for Nu number, is calculated using the Filonenko (1954) relationship defined by Equation 5.7.

$$f_{cold,i} = \left(0.79 \cdot \ln\left(Re_{cold,i}\right) - 1.64\right)^{-2} \tag{5.7}$$

The Prandtl Number, Pr, represents the ratio of momentum diffusivity to thermal diffusivity, and the Reynolds Number, Re, represents the ratio of inertial forces to viscous forces.

By assuming that each annulus represents an individual tube of a single pass countrerflow shell and tube heat exchanger. Assuming that each tube and surrounding fluid is adiabatic (i.e. the temperature profile on the shell (hot) side is uniform in a cross sectional slice of the heat exchanger), the entire shell and tube heat exchanger can be approximated using a series of parallel annuli.

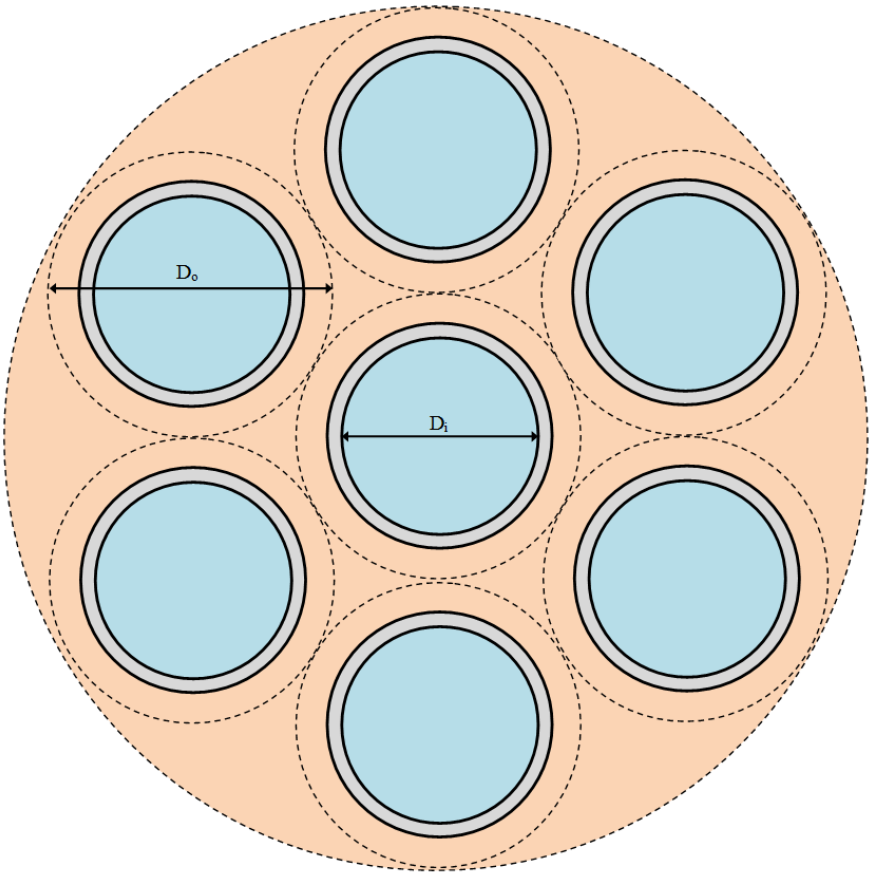

Figure 5.3: Diagrammatic representation of a cross section through the shell and tube heat exchanger

A diagrammatic representation of a cross section through the shell and tube

heat exchanger is given in Figure 5.3. The inner diameter of the annular flow, D_i, is the inner diameter of the tube. The outer diamter of the annular flow, D_o, is the distance between interference zones in the shell, which is represented by the dotted lines on Figure 5.3. The tubes are relatively thin (1.5 mm), therefore it is assumed that they have infinite heat transfer conductance (zero heat transfer resistance).

5.2.1 Hot Water Generator

Optimisation of the supercritical fluid cooler / hot water generator is vital in ensuring the maximum COP is achieved. [75]. The design and analysis of R744 hot gas coolers is well documented [76, 101, 103]. US patent #2010/0313582 A1 [99] is for a high efficiency R744 heat pump cycle, and specifically identifies the use of a internal recuperator to cool the working fluid prior to the expansion value, which is preceded by a gas cooler; this is similar in concept to Cycle 2, which has a double - stage gas cooler preceded by an internal heat recuperator.

The hot water generator is modeled as a twin - parallel, two - stage, counter - flow, single - pass shell and tube type heat exchanger. It cools the refrigerant at two points within the cycle and provides hot water for external use. The hot side flow inlets are the compressed flow exiting the first stage compressor (the 'hot - side low pressure flow') and the outlet of the hot side of the internal heat recuperator. (the 'hot - side high pressure flow'). The fluid entering at both of the cold side inlets is water at ambient temperature. A schematic of the hot water generator with approximate inlet and outlet temperatures is given in Figure 5.4.

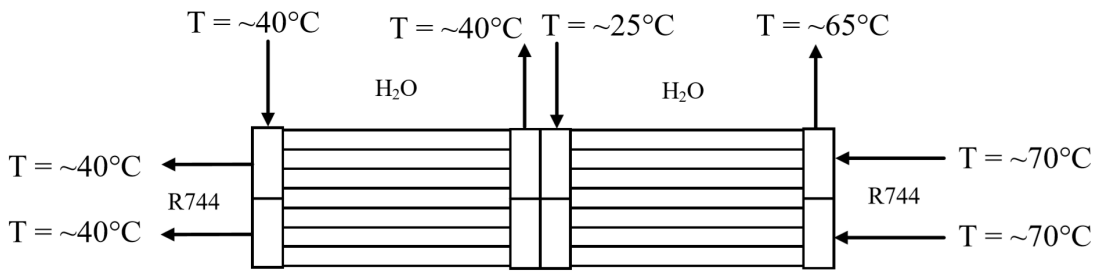

Figure 5.4: Schematic of the hot water generator

The two hot - side flows are at different pressures: 97 bar for the hot - side low pressure flow and ∼150 bar for the hot - side high pressure flow. The difference in pressures means that there thermophysical properties of the working fluid as it moves along the tubes and cools vary differently; the C_p is very non - linear in the hot - side low pressure flow. However, both flows can be made to exhibit a very similar temperature glide throughout the heat exchanger by altering the flow speeds and ratio of heat transfer area (i.e. number of tubes). Therefore, it is possibly for the two flows to be cooled within a single heat exchanger, thus simplifying the system complexity, cost and size.

The hot - side low pressure flow and hot - side high pressure flow pass through tubes of inner diameter 3 mm and outer diameter 4.5 mm (safety factor of > 3 for mild steel). In total there are 1,000 tubes; 525 on the hot - side low pressure flow and 475 on the hot - side high pressure flow. These criteria ensure that the pressure drop through the tubes is below 1 bar.

The calculated temperature profile of the hot - side low pressure flow and associated cold - side is shown in Figure 5.5. The cooling water flow is provided in two stages which both have inlet temperature of 25 °C and outlet temperatures of 60 °C and 40 °C. The mass flowrate of cooling water in the first - stage of the hot water generator is the equal to the mass flow rate of refrigerant. However, the mass flowrate of cooling water in the second - stage of the hot water generator is 230% greater than the mass flow rate of refrigerant. This large increase is due to the increase in C_p in working fluid as it passes the second - stage of the hot water generator and is close to the critical point. A slight 'bulge' in the temperature profiles can be observed in the second - stage, as the working fluid is around 40 °C. The lengths of the first - stage and second - stage are 1.34 m and 1.62 m, respectively.

The calculated temperature profile of the hot - side high pressure flow and associated hot - side is shown in Figure 5.6. As before, the cooling water flow is provided in two stages which both have inlet temperature of 25 °C and outlet

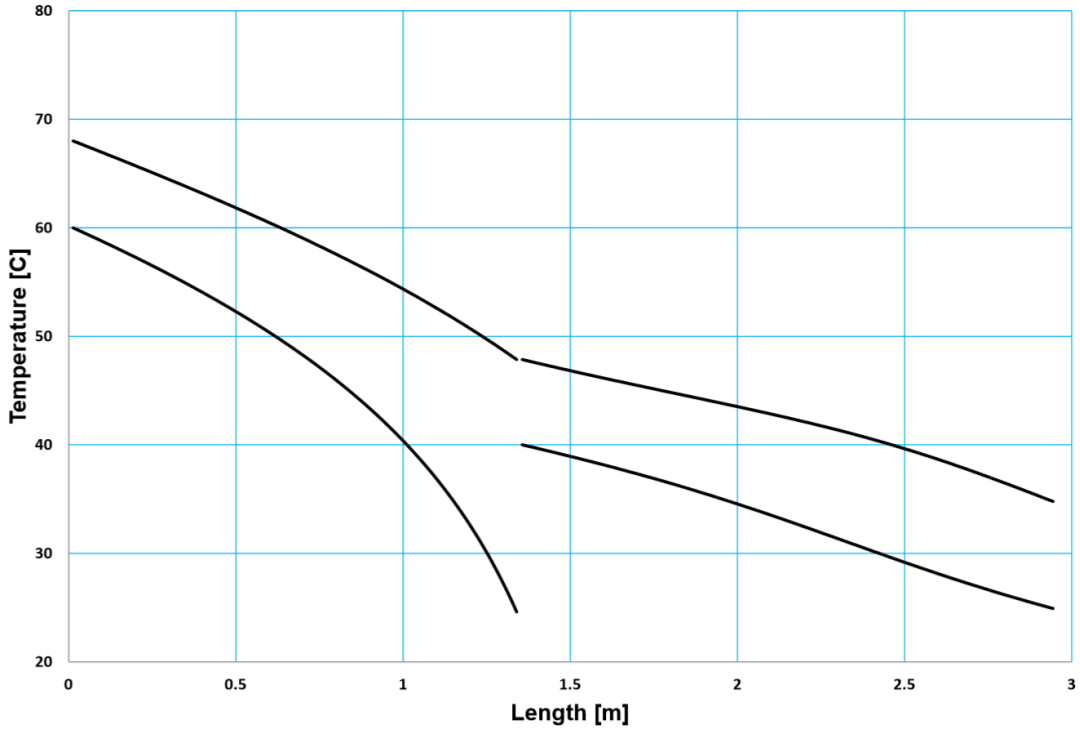

Figure 5.5: Hot water generator hot - side low pressure temperature profile

temperatures of 60 °C and 40 °C. As before, the mass flowrate of cooling water in the first - stage of the hot water generator is equal to the mass flow rate of the refrigerant. The mass flowrate of cooling water in the second - stage of the hot water generator is 33% greater than the mass flow rate of refrigerant. This is a significant reduction from the hot - side high pressure flow second - stage, which is due to the reduction in C_p. The lengths of the first - stage and second - stage are 1.19 m and 1.50 m, respectively.

This analysis demonstrates that the two parallel hot - side flows (high pressure and low pressure) exhibit very similar temperature profiles. Therefore, both flows can be integrated within a single heat exchanger, provided that number and length of tubes is selected appropriately. The approximate specification given in this analysis (for a 1 MW_c heat pump) indicate that when compared to the complexity and number the heat exchangers required in a triple - stage LiBr - H_2O absorption heat pump, the hot water generator proposed here is relatively technically simple, but requires a high number of small diameter tubes. A more detailed analysis would provide possible methods of conducting a detailed design

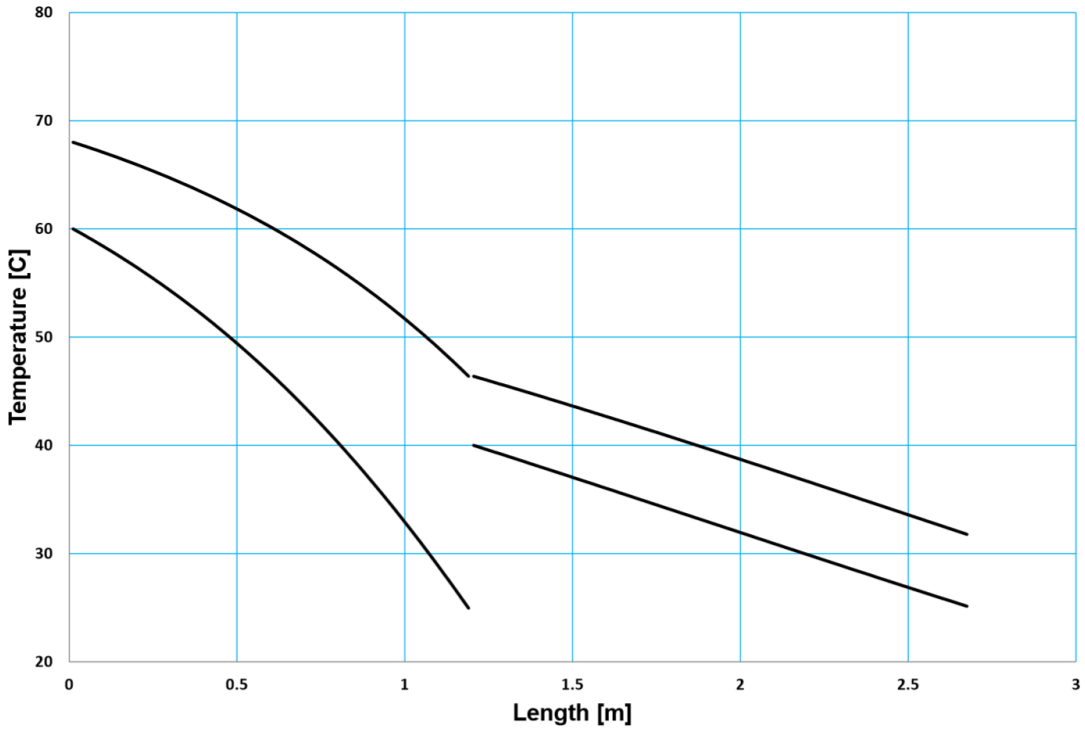

Figure 5.6: Hot water generator hot - side high pressure temperature profile

of a heat exchanger which fulfills the requirements of the hot water generator.

5.2.2 Internal Heat Recuperator

The internal heat recuperator is modeled as a single - pass shell and tube heat exchanger. It allows the cycle to re-use the relatively high grade thermal energy at the first - stage work expander outlet, and transfer it to the high pressure low leaving the second stage compressor. This increases the cycle performance by reducing the heat input requirement from external sources and increases the exergetic efficiency of the cycle.

Chapter 4 highlighted the effect of the first - stage work expander inlet temperature upon the COP, and eluded to the fact that it is partly due to an increasing 'pinch effect' in the internal heat recuperator when the inlet temperature, and consequent outlet pressure, are reduced.

The higher pressure cold side passes through the tubes, whilst the lower hot side passes through the shell. There are 3,000 mild steel tubes of inner diameter 4 mm and outer diameter 5 mm. A minimum pinch temperature of 8°C is

specified; based on simulations, this is believed to be a value which prevents the overall length of the heat exchanger becomes too large.

The temperature profile of the internal heat recuperator for the case where the first - stage work expander inlet temperature is 350°C is given in Figure 5.7.

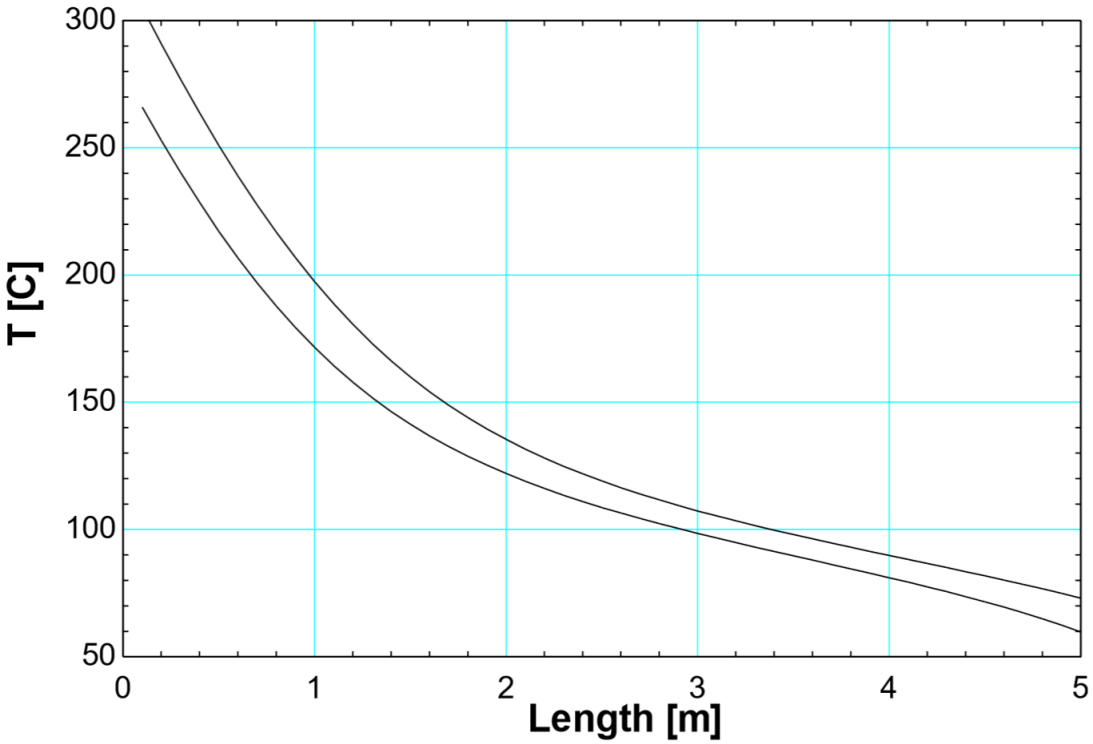

Figure 5.7: Internal heat recuperator temperature profiles (first - stage work expander inlet temperature of 350 °C

For the case shown in Figure 5.7, the overall bulk heat transfer value, U, is 586 W/m^2.K. The local heat transfer conductance varies along the heat exchanger between 552 W/m^2.K and 620 W/m^2.K. The total length of the tubes is 6.4 m, which indicates that the the internal heat recuperator will be large and may be expensive.

5.3 Ejector Modelling

5.3.1 Review of previous work

Nakagawa et al. [104] conducted a physical test to analyse the effect of internal heat exchanger (from gas cooler outlet to evaporator outlet) on the performance

of a two - phase ejector R744 refrigeration cycle. The results suggested an improvement in COP_c of upto 27% can be achieved with the addition of an ejector and maximum heat recuperation. It is suggested that a higher COP_c could be attained through the recovery of more heat, although this may cause overheating of the compressor.

The results also show that the COP_c is more sensitive to gas cooler pressure in the ejector cycle than in a basic R744 refrigeration cycle; the motive fluid inlet total pressure should be at least 100 bar in order to obtain a reasonable performance gain. It is noted that the "*ejector system without [internal heat exchanger] had lower COP than similar conventional systems in most of the conditions used, except at high* P_c" [104].

The study shows that for the four configurations of basic R744 refrigeration cycles analysed (with internal heat exchanger, without internal heat exchanger, with ejector and without ejector), an increase in gas cooler temperature decreases COP. It also shows that an increase in evaporator temperature increases COP.

Li and Groll [87] provide a further analysis of an ejector - expansion device within a transcritical R744 refrigeration cycle when used for air conditioning purposes. The effect odf the entrainment ratio and pressure drop in the receiving section of the ejector on the relative performance of the cycle was investigated using a theoretical model. It is found that the ejector provides a 7 - 18% increase in COP over the basic transcritical R744 cycle.

An experimental evaluation of a prototype R744 ejector was conducted by Elbel and Hrnjak [105], with the aim of reducing throttling losses in transcritical R744 refrigeration cycle operation. The study was based upon a full cycle simulation defined within EES, where 2,500 non - linear time - dependent equations. Experimentally obtained correlations for volumetric, compression and isentropic efficiency are used within the compressor module. Assumptions include:

- Fluid properties are uniform across the cross - sectional diameters
- Thermodynamic non - equilibrium effects are not considered

- The ejector is to be treated as adiabatic
- Inlet and outlet flow kinetic energies are to be treated as negligible
- Ejector geometries are not accounted for

A needle extending into the throat of the motive nozzle allows for the control of the high - side pressure; this represents an additional degree of freedom in the system. The study indicated that the value of mixing pressure is irrelevant, so long as it is lower than the entrained inlet pressure.

5.3.2 Ejector

The operating principle of a two - phase ejector is based upon the conversion of static pressure into kinetic energy and vice versa, as defined by Bernoulli's Principle.

The high velocity low static pressure refrigerant ('motive flow') entering the ejector is accelerated in the nozzle. The motive flow is throttled to such an extent that it has a lower static pressure that the low pressure dry saturated refrigerant vapour exiting the evaporator ('entrained flow'), but a much higher velocity. This allows the motive flow to transfer momentum to the entrained flow, this process occurs in the mixing chamber.

Following the mixing chamber, the two - phase high speed mixed flow is expanded in the diffuser, where it is slowed down and regains static pressure. The two - phase flow exiting the diffuser has a resultant pressure which is higher than the entrained flow entering the ejector. Figure 5.8 shows a basic schematic of an ejector.

Modelling

In order to model the ejector a number of state points must first be assigned, these are illustrated on Figure 5.9.

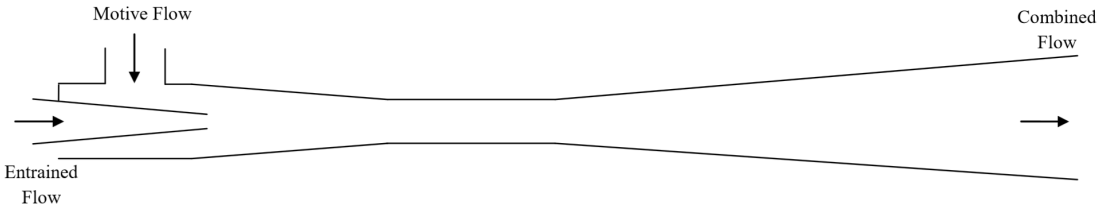

Figure 5.8: Schematic diagram to illustrate the fluid inlets and outlets of an R744 ejector

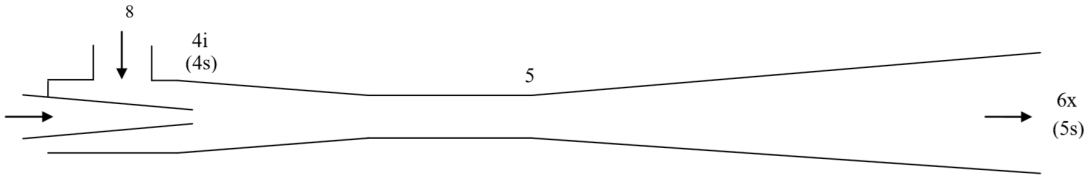

Figure 5.9: Schematic diagram to illustrate the state points in the R744 ejector

A series of simple equations enable the input and output states of the ejector to be modeled. This relies upon a number of assumptions regarding isentropic efficiencies, conservation of mass, momentum and energy.

The ratio of the entrained mass flowrate to the motive mass flowrate as the termed the entrainment ratio, μ, and is calculated using Equation 5.8:

$$\mu = \frac{\dot{m}_8}{\dot{m}_4} \tag{5.8}$$

Assuming an isentropic efficiency for the motive flow nozzle, η_{4n}, the actual value for the enthalpy at state point 4i (ie. the motive flow at the motive nozzle exit) can be calculated using Equation 5.9:

$$h_{4i} = h_4 - \frac{\eta_{4n}}{h_4 - h_{4s}} \tag{5.9}$$

By applying the conservation of momentum and energy, the velocity of the motive fluid as it exits the motive nozzle, $u_4 i$, can be calculated from Equation 5.10:

$$u_{4i} = \sqrt{2 \cdot (h_4 - h_{4i})} \tag{5.10}$$

Assuming the flow is fully mixed at the outlet of the mixing section, the velocity of the combined flow at the outlet of the mixing section can be calculated using Equation 5.11:

$$u_5 = \left[\rho_5 \cdot \left(\left(\frac{1}{\rho_{4i} u_{4i}(1+\mu)}\right) + \left(\frac{\mu}{\rho_{8i} u_{8i}(1+\mu)}\right)\right)\right]^{-1} \tag{5.11}$$

, where u_{8i} is approximated by Equation 5.12:

$$u_{8i} = \sqrt{2 \cdot (h_8 - h_{8i})} \tag{5.12}$$

, and densities are calculated from fluid thermophysical properties. The enthalpy of the entrained flow nozzle outlet,h_{8i}, is calculated using assumed isentropic efficiency for the entrained nozzle, η_{8n}, and Equation 5.13:

$$h_{8i} = h_8 - \frac{\eta_{8n}}{h_8 - h_{8s}} \tag{5.13}$$

The enthalpy of the combined flow, h_{6x}, can be defined by Equation 5.14 (assuming that the process is adiabatic):

$$h_{6x} = \left(\frac{h_4}{1+\mu}\right) + \left(h_8 \cdot \frac{\mu}{1+\mu}\right) \tag{5.14}$$

Similarly, the enthalpy of the combined flow, h_{6x}, can be also be calculated assuming an isentropic efficiency of the diffuser, η_d, using Equation 5.15:

$$h_{6x} = \frac{h_{5s} - h_5}{\eta_d} + h_5 \tag{5.15}$$

The enthalpy of the fluid at the end of the mixing section can be calculated using the conservation of energy and mass, as shown in Equation 5.16:

$$h_5 = \frac{h_4 + \mu h_8}{1+\mu} - \frac{1}{2} u_5^2 \tag{5.16}$$

The pressure of the combined flow at the outlet of the ejector can be calculated via assuming a value for the pressure at the end of the mixing section, P_5, with

an iterated procedure and Equation 5.17:

$$P_{6x} \cdot \left(\frac{1}{u_{4i} \cdot \rho_{4i} \cdot (1+\mu)} + \frac{\mu}{u_{8i} \cdot \rho_{8i} \cdot (1+\mu)} \right) + u_5 = P_5 \left(\frac{1}{u_{4i} \cdot \rho_{4i} \cdot (1+\mu)} + \frac{\mu}{u_{8i} \cdot \rho_{8i} \cdot (1+\mu)} \right) + \frac{1}{1+\mu} \cdot u_{4i} + \frac{\mu}{1+\mu} \cdot u_{8i} \quad (5.17)$$

An approximation of the motive flow nozzle shape and combined flow diffuser shape is calculated based upon a linear increase / decrease in fluid velocity, respectively. This is calculcated using a simple 1 dimensional analysis, and is expected to serve as a concept design, which will be further optimised with 2 or 3 dimensional computational fluid dynamics packages and / or physical testing.

Figure 5.10 shows the calculated profile for the motive flow nozzle and the corresponding mean bulk fluid velocity. It can be noted that the nozzle is of a particularly elongated shape; this is believed to be due to the drastic drop in bulk fluid density once the R744 drops below the saturation curve as the static pressure drops (at $\sim 60\,\text{bar}$), as illustrated in Figure 5.11. As the fluid density drops, the consequent reduction in cross - sectional area to maintain a constant increase in velocity reduces.

The length of the nozzle section is shown as dimensionless on Figure 5.10, and will require further analysis to ascertain the optimum length. If the nozzle is too long, the boundary layer friction losses will be too great and isentropic efficiency will reduce; if the nozzle is too short there will be undesirable flow characteristics and the isentropic efficiency will reduce.

Figure 5.12 shows the calculated profile for the combined flow diffuser and the corresponding mean bulk fluid velocity. As was noted with the nozzle, the diffuser is also elongated in shape; this is also due to the non-linearity of bulk fluid density as the fluid velocity reduces, as illustrated in Figure 5.13.

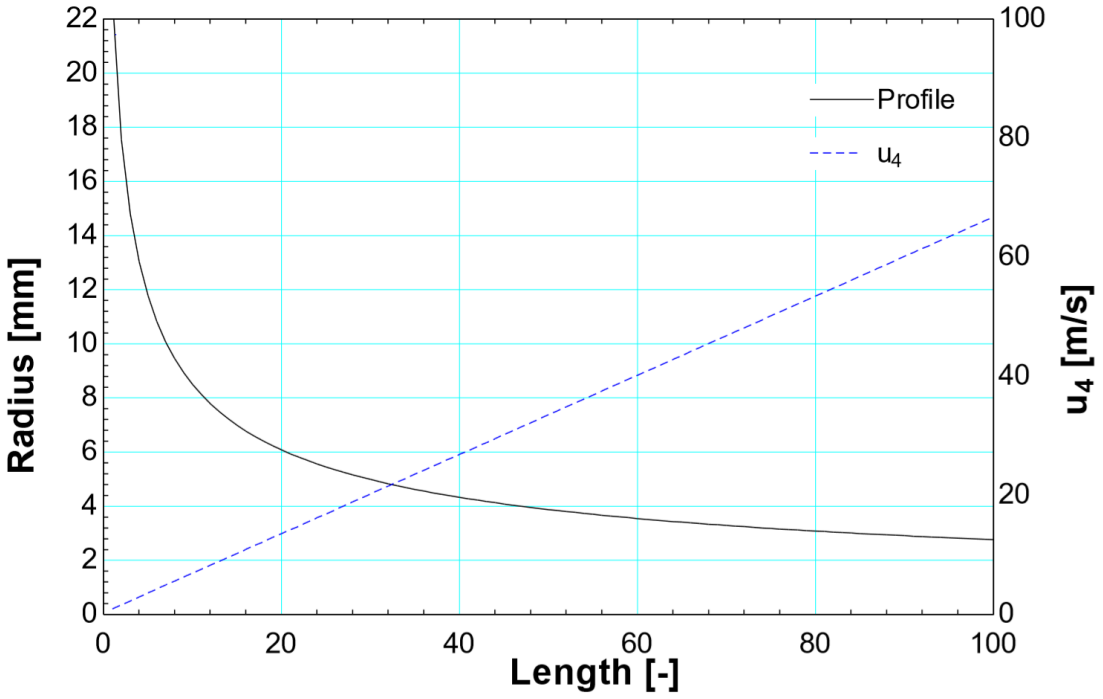

Figure 5.10: Ejector motive flow nozzle shape and mean bulk fluid velocity along the nozzle length

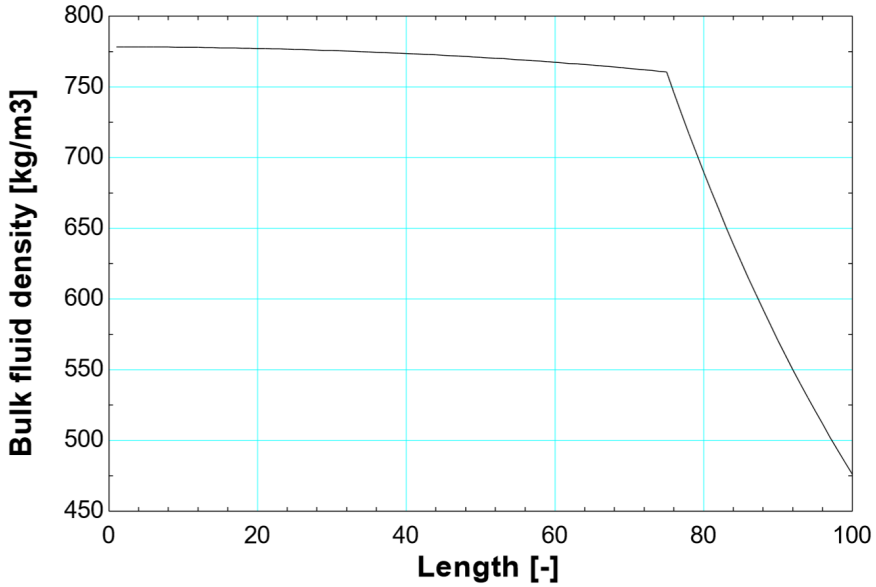

Figure 5.11: Ejector bulk fluid density along the nozzle length

5.4 Compressor / Work Expander Modeling

5.4.1 Centrifugal Compressor

Cycle 2 has two compressors, and a high level preliminary design of the blade channels is given here.

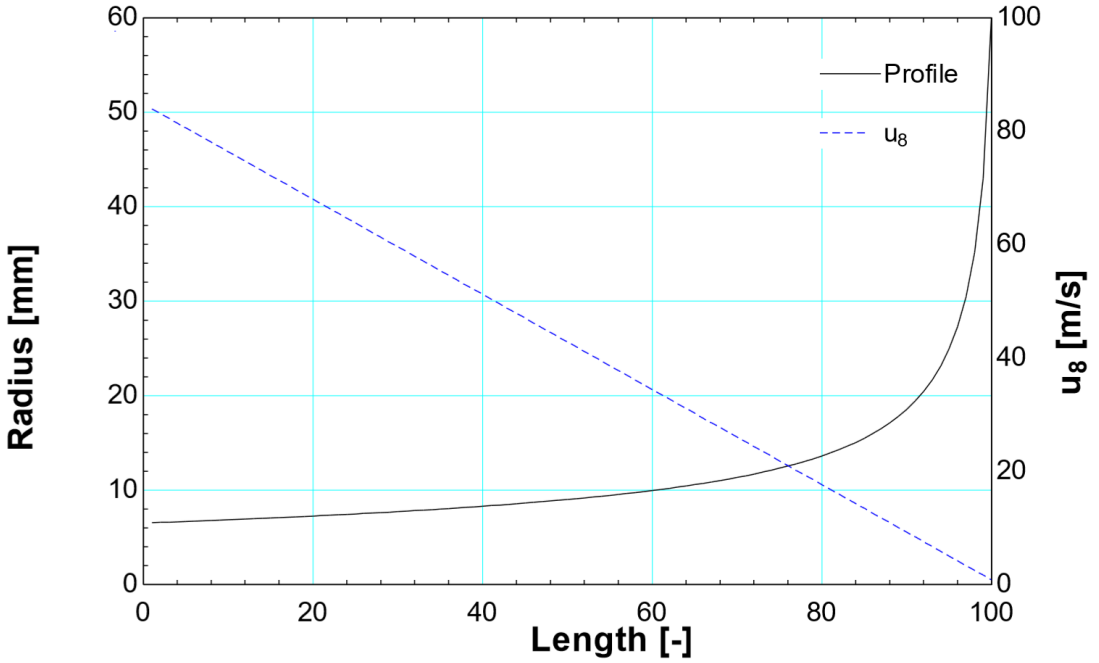

Figure 5.12: Ejector combined flow nozzle shape and mean bulk fluid velocity along the nozzle length

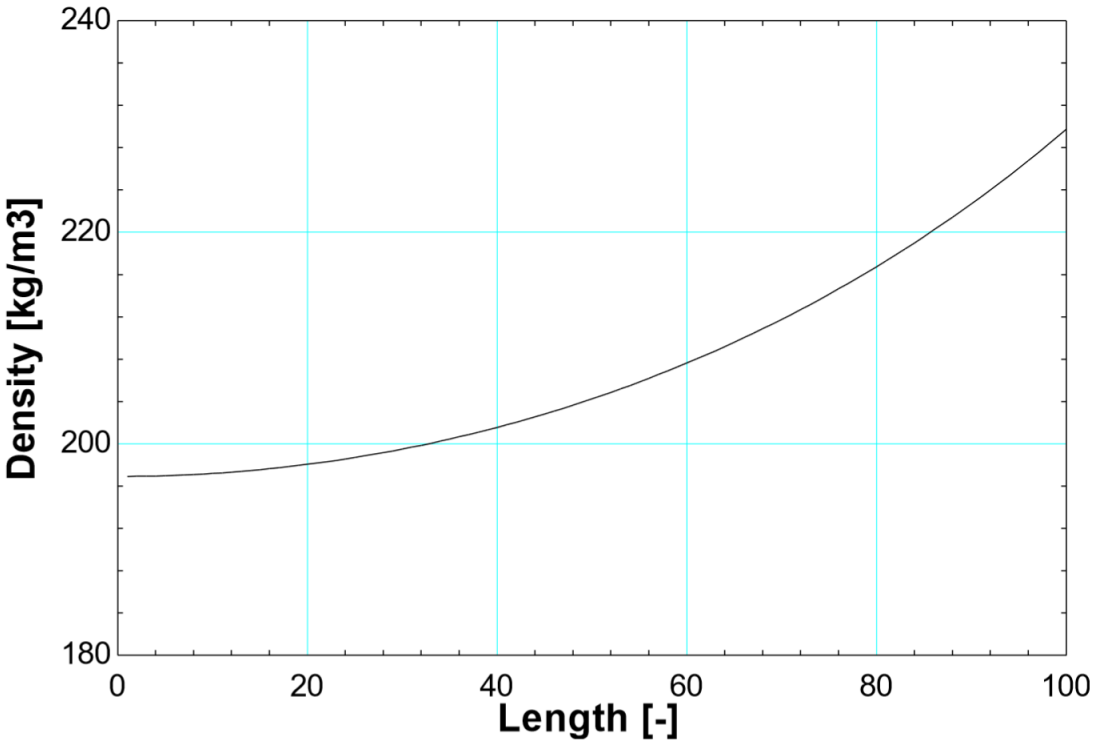

Figure 5.13: Ejector bulk fluid density along the diffuser length

A notation for the cross section view and top view of the impeller blades is defined in Figures 5.14 and 5.15.

The area of the impeller channel inlet can be defined in accordance with Figure

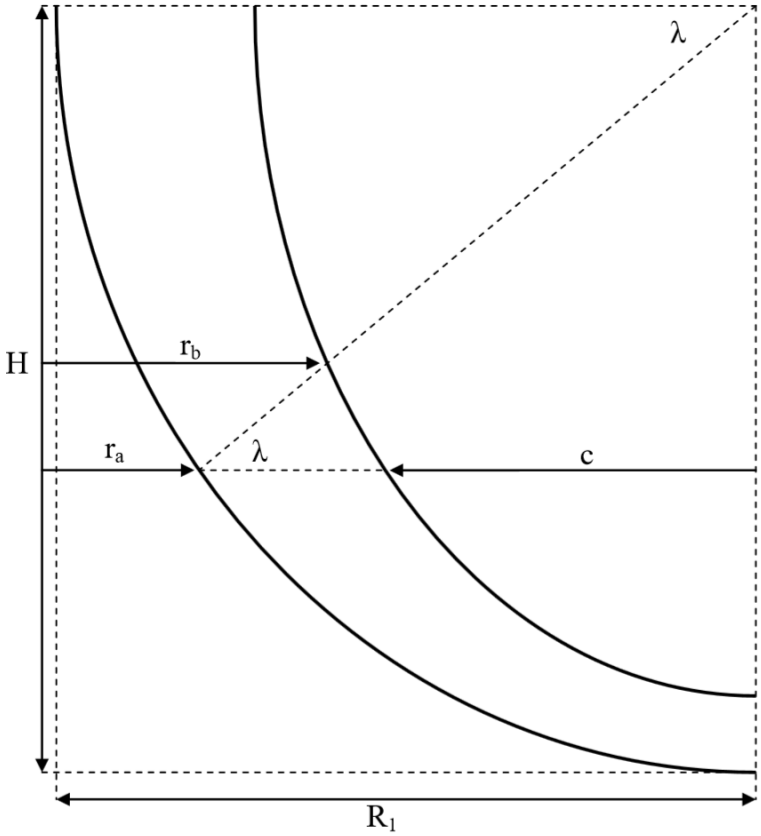

Figure 5.14: Cross sectional view and notation of compressor impeller blade profile

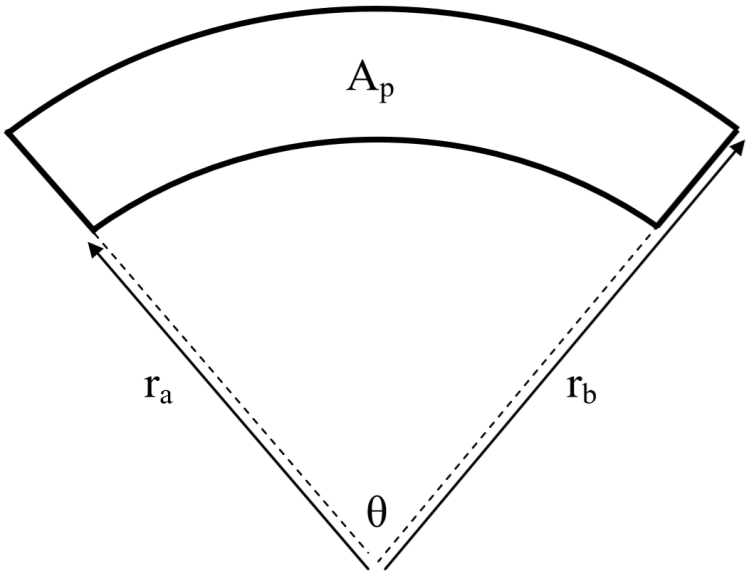

Figure 5.15: Top view and notation of compressor impeller blade profile for the intake area

5.15 and Equation 5.18.

$$A_p = \pi(r_b^2 - r_a^2)\frac{\theta}{2\pi} = \frac{\theta}{2}((r_b^2 - r_a^2) \tag{5.18}$$

Assuming that the lower curve on Figure 5.14 is circular (i.e. $H = R_1$), and therefore the channel has an arc shape, the cross sectional area of the channel can be defined as:

$$A_p = \frac{\theta}{2}((r_b^2 - r_a^2)\frac{1}{cos\lambda}\,, \qquad \forall\theta, \theta \neq 0, \theta \neq \frac{\pi}{2} \tag{5.19}$$

Given that $r_a = R_1 - c$, it can be deduced that:

$$c = \frac{1}{2}2R_1 sin\left(\frac{2(\pi - \lambda)}{2}\right) = R_1 cos\lambda \tag{5.20}$$

Now, r_a can be defined as $R_1(1 - cos\lambda)$, and therefore:

$$A - p = \frac{\theta}{2cos\lambda}\left[r_b^2 - (R_1(1 - cos\lambda))^2\right] \tag{5.21}$$

This can be re-arranged to enable r_b to be calculated, as follows:

$$r_b = \left[A_p\frac{2cos\lambda}{\theta} + (R_1(1 - cos\lambda))^2\right]^{\frac{1}{2}} \tag{5.22}$$

The impeller blade inlet and outlet geometry has been calculated as is included in the Appendix. For the sake of brevity, it has not been included in the main body of the thesis, given the established nature of research in this area. However, of particular note is the very compact size of the impeller, due to the high density

of supercritical R744.

5.4.2 Gerotor

A gerotor is a type of positive displacement device, which is a type of trochoidal device (along with the Wankel engine). Gerotors are suitable as work expansion and compression devices where the working fluid is of a relatively high density (i.e. similar magnitude to that of water at Normal Conditions). Gerotors are commonly used as pumps, but there has been recent interest in exploring their use in refrigeration cycles, Organic Rankine Cycles and low temperature Brayton cycles [106–110]. Various methods for the generation of trochoidal device geometries are discussed in the literature [111–113], along with analyses of their performance and flow characteristics and optimisation [114–117]. An alternative method for the generation of a gerotor profile is presented later in this section.

Trochoidal devices are part of the family of planetary rotation machines and offer advantages over other types of machines; eg. reliability, simplicity, possibility of higher speeds and a wide variety of applications (pumps, compressors, expanders, blowers, engines) [118]. There are two major components in a trochoidal device; the rotor and the chamber (piston and cylinder), which are referred to as the trochoid and envelope, and vice versa. In a trochoidal type pump, such as a gerotor, the rotor is a trochoid and the chamber is an envelope, however in a Wankel engine the rotor is an envelope and the chamber is a trochoid.

The theory of trochoidal devices in summarised by Shung and Pennock. [118]. A trochoid is defined by the path created by a fixed point on a circle of radius $r_{t,m}$ with distance r_c to the cycle centre, which rolls on a fixed circle of radius $r_{t,f}$; the moving and fixed pitch circles, respectively [118]. If the moving pitch circle has a greater radius than the fixed pitch circle (ie. $r_{t,m} > r_{t,f}$), the trochoid is called an epitrochoid. If the moving pitch circle has a smaller radius than the fixed pitch circle (ie. $r_{t,m} < r_{t,f}$), the trochoid is called a hypotrochoid. If the moving pitch circle has the same radius as the fixed pitch circle (ie. $r_{t,m} = r_{t,f}$), the trochoid

is called a cycloid. Trochoids are further categorised into prolate, ordinary and curtate if they are smooth, have a cusp, or cross over themselves, respectively. Ordinary hypotrochoids and epitrochoids are also classified as epicycloids and hypocyloids, respectively. Observation of gerotors indicates that they are often generated using prolate hypotrochoids, or some variation thereof.

A notation system has been introduced to describe the geometry of the trochoids analytically [118]. The centers of the fixed and moving pitch circles are denoted $\mathbf{O}_{t,f}$ and $\mathbf{O}_{t,m}$, respectively. The reference line is defined as the line connecting the two centres, $\overrightarrow{\mathbf{O}_{t,f}\mathbf{O}_{t,m}}$. The reference line passes through the point of contact of the two circles, point P. The radii of the fixed and moving pitch circles are $r_{t,f}$ and $r_{t,m}$, respectively; the distance between the centres, referred to as the eccentricity, is denoted by $e_t =\mid r_{t,f} - r_{t,m} \mid$. The Cartesian reference frame attached to the fixed pitch circle is denoted by the vectors $\overrightarrow{\mathbf{O}_{t,f}\mathbf{X}_t}$ and $\overrightarrow{\mathbf{O}_{t,f}\mathbf{Y}_t}$, representing the X_t and Y_t axis respectively, and is referred to as the trochoid frame. The cartesian reference frame attached to the moving pitch circle is denoted by the vectors $\overrightarrow{\mathbf{O}_{t,m}\mathbf{X}'_t}$ and $\overrightarrow{\mathbf{O}_{t,m}\mathbf{Y}'_t}$, representing the X'_t and Y'_t axis respectively, and is refered to as the reference frame. When the reference line $(\overrightarrow{\mathbf{O}_{t,f}\mathbf{O}_{t,m}})$ rotates at an angle α to the X_t axis, the generating frame turns at an angle $\frac{\alpha}{k_t}$ relative to the same axis, where k_t is referred to as the angular velocity ratio for the trochoid. A positive value of k_t implies an epitrochoid, whilst a negative value of k_t implies a hypotrochoid.

The trochoid generation point, $\mathbf{C}$, is located on the X'_t axis at a radius of r_c from the moving pitch circle centre $\mathbf{O}_{t,f}$. The coordinates of the generation point $\mathbf{C}$ is defined by equations 5.23 5.24. Figure 5.16 gives a visual representation of the geometry and notation used in the generation of a trochoid, using a peritrochoid as an example.

The generation point of the trochoid is defined by Equations 5.23 and 5.24, which are expressed in relative to the trochoid frame ($\overrightarrow{\mathbf{O}_{t,f}\mathbf{X}_t}$ and $\overrightarrow{\mathbf{O}_{t,f}\mathbf{Y}_t}$).

$$X_t = e_t \cos\alpha + r_c \cos\frac{\alpha}{k_t} \tag{5.23}$$

$$Y_t = e_t \sin\alpha + r_c \sin\frac{\alpha}{k_t} \tag{5.24}$$

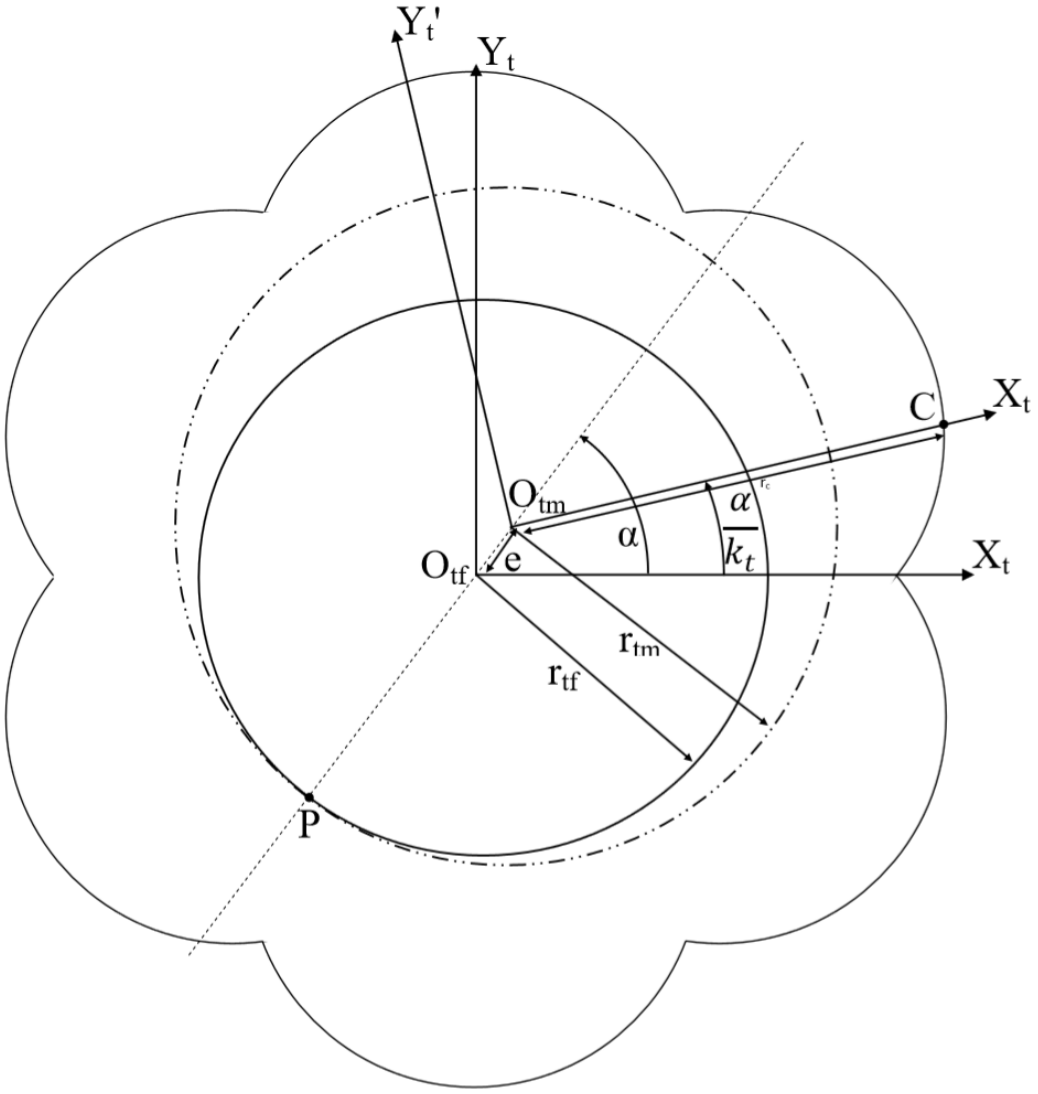

Figure 5.16: Geometry of a trochoid (peritrochoid) [118]

There are two types of conjugate envelopes that can be generated using a trochoidal profile; an inner envelope and and outer envelope, which are located inside and outside the trochoid profile, respectively. The conjugate envelope is defined by the maximum inner or minimum outer envelope for which there is no interference throughout one entire motion; the contact force between the trochoid

and the envelope is zero when they are static. Further, and most crucially for a positive displacement device, the compartment sealing is inherently optimised by the geometry of the two parts.

The generation of the conjugate envelope can be best visualised by imagining that the trochoid is initially surrounded by lots of tiny beads, and as it undergoes planetary motion (as guided by the moving and fixed pitch circles) the beads are pushed outwards by the trochoidal lobes, resulting in the identification of the outer conjugate envelope profile. The same principle can be used to explain the generation an inner conjugate envelope, except the beads are inside the trochoid and the moving and fixed pitch circles are reversed.

The geometry used to describe the conjugate envelope is much the same as the geometry used to describe the trochoid. The centers of the fixed and moving pitch circles are denoted $\mathbf{O}_{e,f}$ and $\mathbf{O}_{e,m}$, respectively. The reference line is defined as the line connecting the two centres, $\overrightarrow{\mathbf{O}_{e,f}\mathbf{O}_{e,m}}$. The reference line passes through the point of contact of the two circles, point P. The radii of the fixed and moving pitch circles are $r_{e,f}$ and $r_{e,m}$, respectively; the distance between the centres, referred to as the eccentricity, is denoted by $e_e =\mid r_{e,f} - r_{e,m} \mid$. The Cartesian reference frame attached to the fixed pitch circle is denoted by the vectors $\overrightarrow{\mathbf{O}_{e,f}\mathbf{X}_e}$ and $\overrightarrow{\mathbf{O}_{e,f}\mathbf{Y}_e}$, representing the X_e and Y_e axis respectively, and is referred to as the trochoid frame. The Cartesian reference frame attached to the moving pitch circle is denoted by the vectors $\overrightarrow{\mathbf{O}_{e,m}\mathbf{X}_t}$ and $\overrightarrow{\mathbf{O}_{e,m}\mathbf{Y}_t}$, representing the X_t and Y_t axis respectively, and is referred to as the reference frame. When the reference line ($\overrightarrow{\mathbf{O}_{e,f}\mathbf{O}_{e,m}}$) rotates at an angle α to the X_e axis, the generating frame turns at an angle $\frac{\beta}{k_e}$ relative to the same axis, where k_t is referred to as the angular velocity ratio for the envelope. A positive value of k_t implies an that the angular displacement of the reference line $\overrightarrow{\mathbf{O}_{e,f}\mathbf{O}_{e,m}}$ is in the same direction as the angular displacement of the trochoid frame. Figure 5.17 gives a visual representation of the geometry and notation used in the generation of the envelope.

The rotor profile can be defined according to Equations 5.25 and 5.25, which

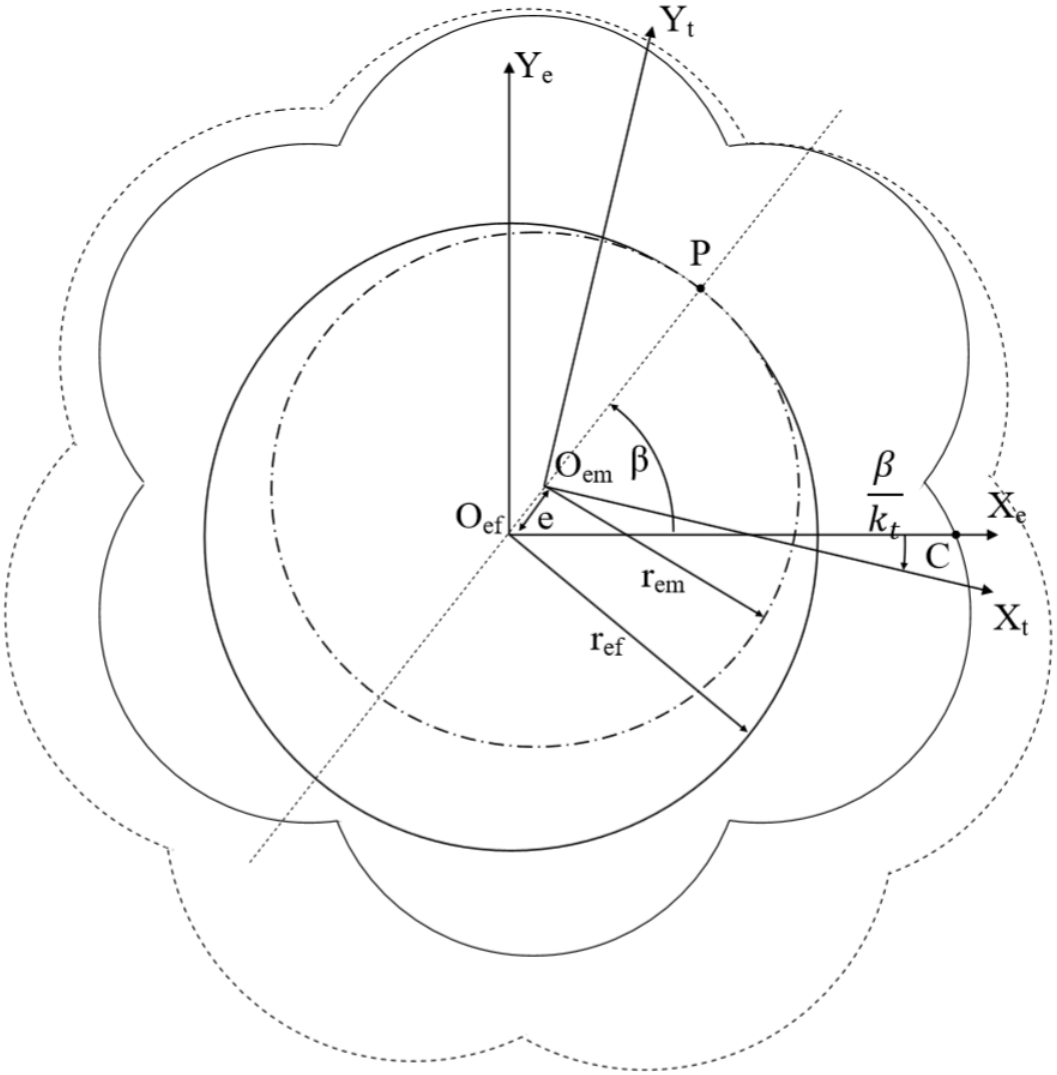

Figure 5.17: Geometry of a trochoid envelope [118]

calculate the coordinates of any point on the rotor.

$$X_e = e_e \cos\beta + X_t \cos\left(\frac{\beta}{k_e}\right) - Y_t \cos\left(\frac{\beta}{k_e}\right) \tag{5.25}$$

$$Y_e = e_e \sin\beta + X_t \sin\left(\frac{\beta}{k_e}\right) - Y_t \sin\left(\frac{\beta}{k_e}\right) \tag{5.26}$$

Substituting Equation 5.23 into 5.25 and Equation 5.24 into 5.26, the coordinates of the generating point are now:

$$X_e = e_e \cos\beta + e_t \cos\left(\alpha + \frac{\beta}{k_e}\right) - r_c \cos\left(\frac{\alpha}{k_t} + \frac{\beta}{k_e}\right) \tag{5.27}$$

$$Y_e = e_e \sin\beta + e_t \sin\left(\alpha + \frac{\beta}{k_e}\right) - r_c \sin\left(\frac{\alpha}{k_t} + \frac{\beta}{k_e}\right) \tag{5.28}$$

According to Shund and Pennock [118], the condition for a Type 2 conjugate envelope defined by Equations 5.29, 5.30, 5.31, 5.32 & 5.33:

$$k_e = k_t - 1 \tag{5.29}$$

$$X_t = -2\frac{r_c}{k_t}\cos\left(1 - \frac{2}{k_t}\right)\mu\cos\mu + r_c\cos\frac{2\mu}{k_t} \tag{5.30}$$

$$Y_t = -2\frac{r_c}{k_t}\cos\left(1 - \frac{2}{k_t}\right)\mu\sin\mu + r_c\sin\frac{2\mu}{k_t} \tag{5.31}$$

$$\mu = \frac{1}{2}\left[\alpha + \left(\frac{k_t}{k_t - 1}\right)\beta\right] \tag{5.32}$$

$$\nu = \frac{1}{2}\left[\alpha + \left(\frac{2 - k_t}{k_t - 1}\right)\beta\right] \tag{5.33}$$

An alternative method of generating a trochoid inner rotor and outer rotor is presented below, beginning with the outer rotor. The number of lobes that the inner rotor has is denoted, N, such that the angle of rotation of the inner rotor, θ_i is defined by:

$$\theta_i = \theta_o \frac{N}{N+1} \tag{5.34}$$

where θ_o is the angle of rotation of the outer rotor. Therefore, we can define the rotation of the contact point frame, θ_c, is $N\theta_o$.

Denoting r as the fixed pitch circle diameter and E as the distance between the fixed and the moving pitch circles, it can be deduced that the radius of the fixed pitch circle (outer rotor), r_3, is defined by rE. Likewise, the radius of the moving pitch circle (inner rotor), r_2, is defined by $r_2 = E(N+1)$, according

to Kennedy's theorem. Figure 5.18 shows the geometry and notation for the coordinate systems, and contact point, C.

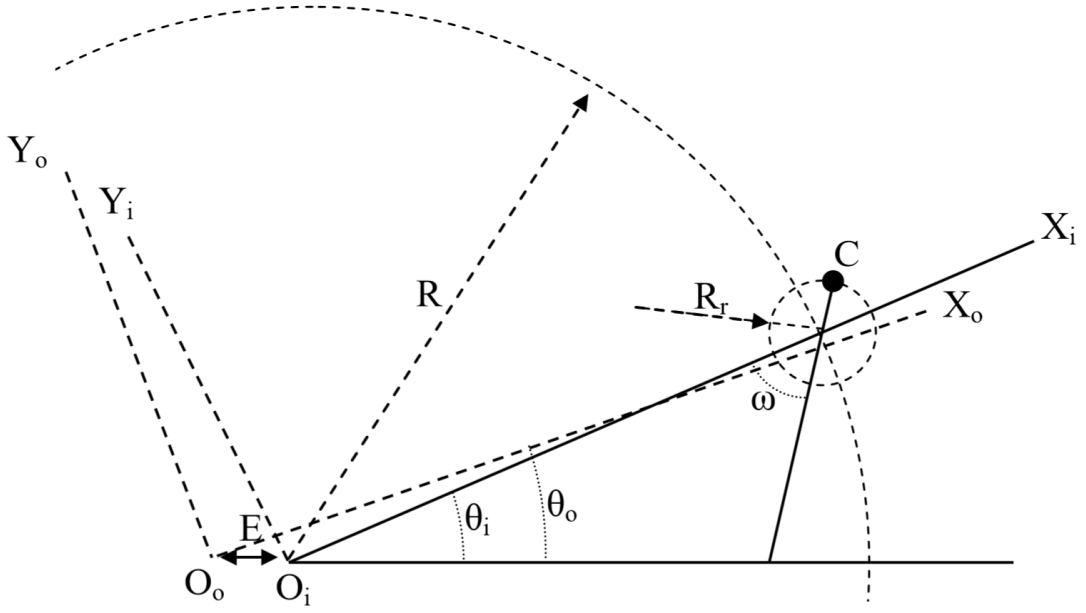

Figure 5.18: Coordinate systems and contact point for the outer rotor

It is possible to define ω on Figure 5.18 using Equation 5.35:

$$\omega = tan^{-1}\left(\frac{sin\theta}{\frac{R}{rE} - cos\theta}\right) \tag{5.35}$$

The x and y Cartesian coordinates of the inner rotor are defined by Equations 5.36 and 5.37:

$$X_o = Rcos\theta + R_c cos(\theta + \omega) + Ecos(N\theta) \tag{5.36}$$

$$Y_o = Rsin\theta + R_c sin(\theta + \omega) + Esin(N\theta) \tag{5.37}$$

Figure 5.19 illustrates the profile of a typical outer rotor, calculated using this method.

Now the inner rotor can be defined, beginning with Equation 5.39 for the coordinate system, $X_{i,c}$ and $Y_{i,c}$ of the inner rotor for when $\alpha_i < \kappa < \alpha_{i+1},\ \forall i,\ i = (1, 2, 3, ..., N) \cdot \frac{2\pi}{N}$, where:

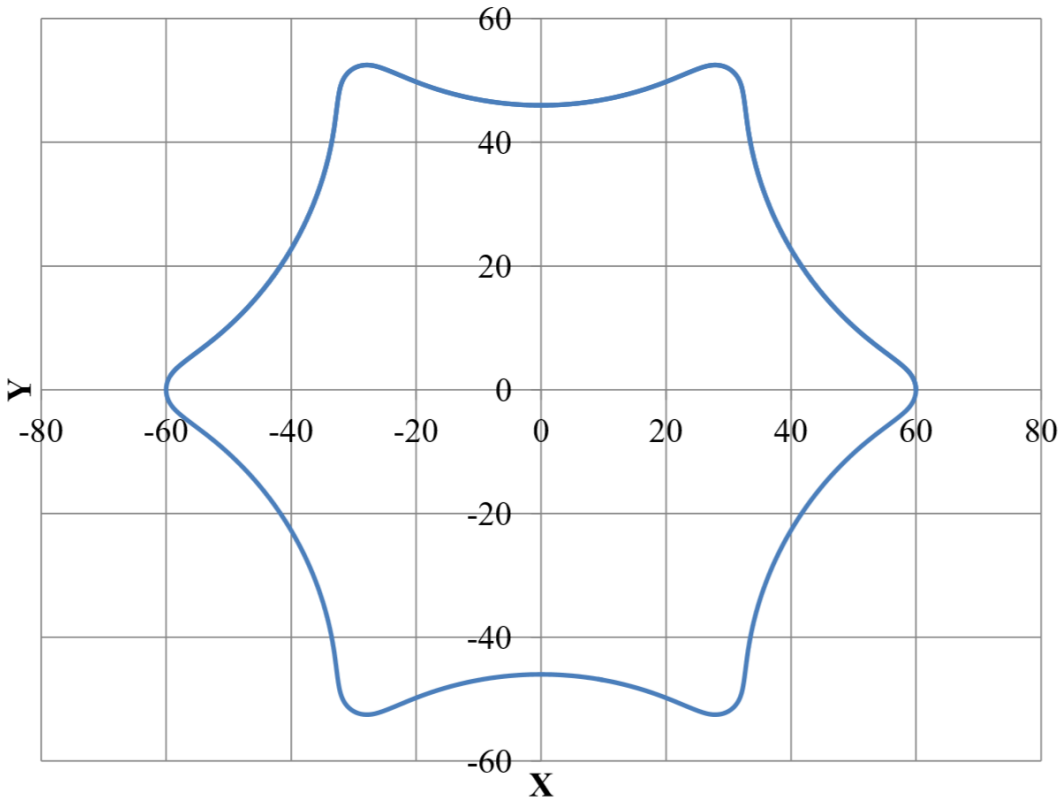

Figure 5.19: Illustration of a typical outer rotor profile

$$\kappa = tan^{-1}\left(\frac{Y_{i,c}}{X_{i,c}}\right) \tag{5.38}$$

and:

$$\begin{aligned} X_{i,c} &= X_o - E \\ Y_{i,c} &= Y_o \end{aligned} \tag{5.39}$$

It can now be derived that the radius of the inner rotor can be described using the following Equations:

$$r = Rcos(\kappa - \alpha_i) + \sqrt{R_r^2 - R^2 + R^2 cos^2(\kappa - \alpha_i)} \tag{5.40}$$

and

$$r = \delta cos(\kappa - (\alpha_i + \frac{\pi}{N})) - \sqrt{R_b^2 - l_f^2 + l_f^2 \left(cos^2(\kappa - (\alpha_i + \frac{\pi}{N}))\right)} \tag{5.41}$$

where

$$\delta = Rcos\frac{\pi}{N} + \sqrt{Rcos^2\frac{\pi}{N} - R^2 + (R_b + R_r)^2)} \tag{5.42}$$

and

$$r = Rcos(\kappa - \alpha_{i+1}) + \sqrt{R_r^2 - R^2 + R^2cos^2(\kappa - \alpha_{i+1})} \tag{5.43}$$

R_b is a user definable quantity, which adjust the profile of the inner rotor between the lobes, thereby affecting the volume of the enclosed control volume between the outer and inner rotors.

Equations 5.40, 5.41 and 5.43 are calculated N number of times (i.e. the number of lobes on the inner rotor), where $\alpha_i = \frac{2\pi}{N} \cdot i,\ \forall i,\ i = (1, 2, 3, ..., N)$

Figure 5.20 illustrates the profile of a typical inner rotor, along with its respective outer rotor calculated using this method.

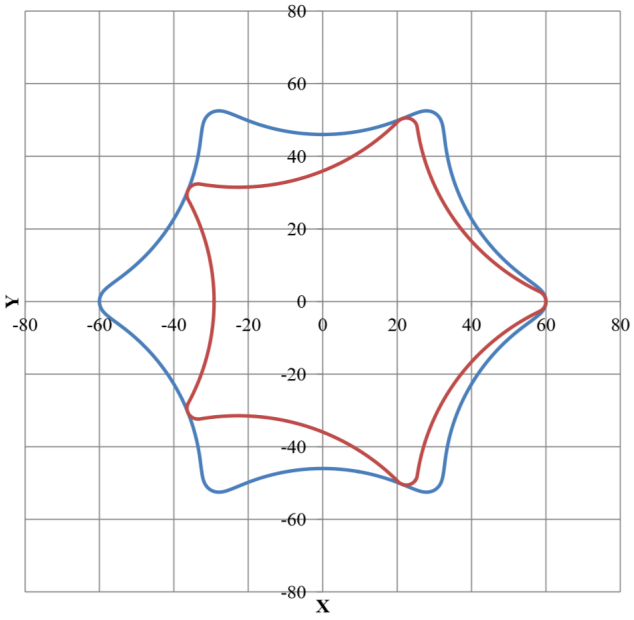

Figure 5.20: Illustration of a typical inner and outer rotor profile

An illustration of the gerotor rotating through $\frac{2\pi}{N}$ is shown in Figure 5.21.

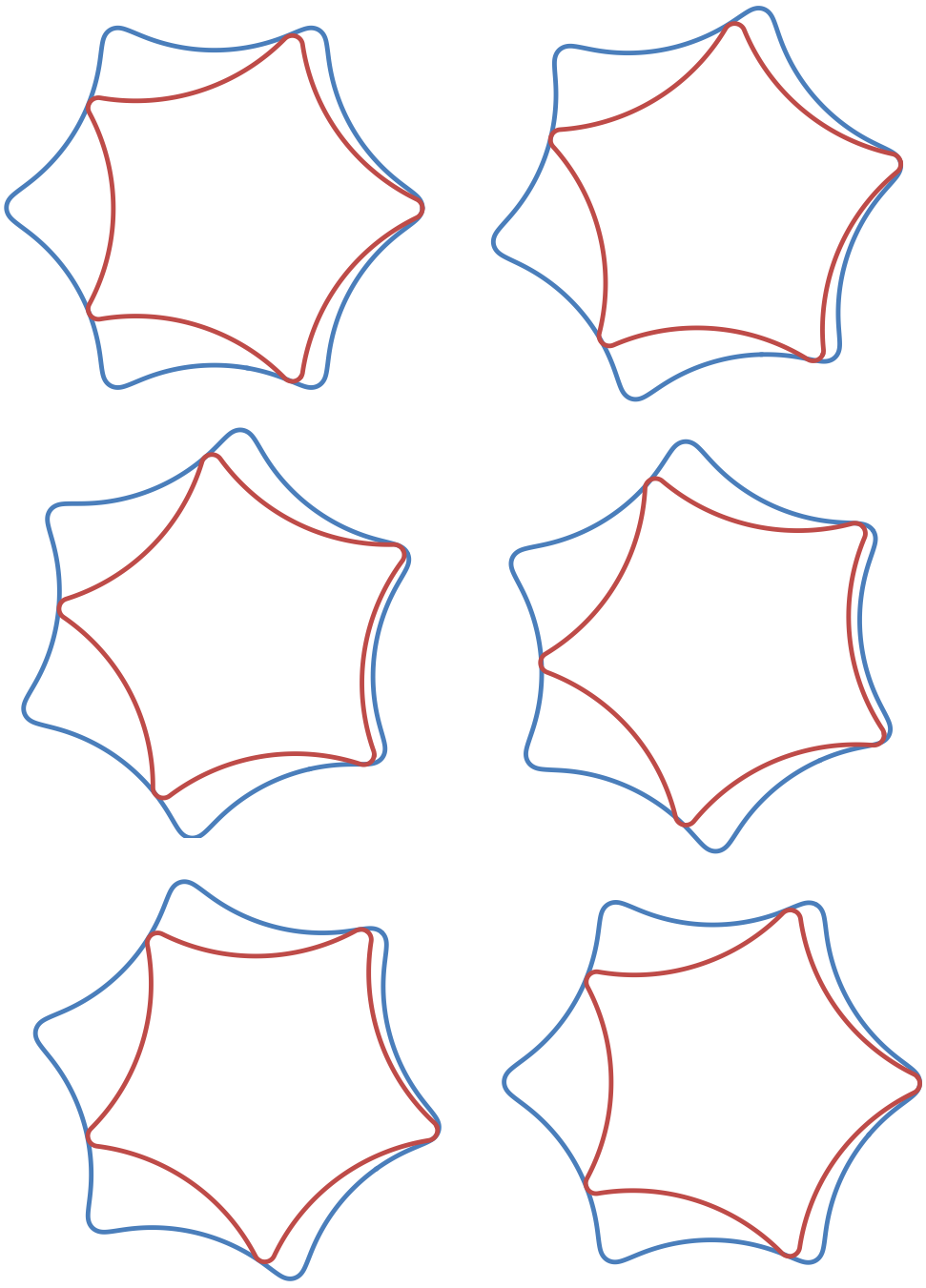

Figure 5.21: Illustration a typical gerotor rotating through $\frac{2\pi}{N}$ of a turn

5.5 Conclusions

This Chapter has set out a high level preliminary design of a number of components within the novel thermally activated R744 simultaneous heating and cooling

heat pump conceptualised in Chapter 4. A design methodology for R744 heat exchangers (both R744 - R744 and R744 - water) have been provided. This was used to give an estimation of the size, number and length of tubes required in a shell and tube heat exchanger, for both the internal heat recuperator and the twin - parallel, two - stage hot water generator.

The two - phase ejector has been modelled, and this model was primarily used in the simulation of Cycle 2 in Chapter 4. The methodology and calculation process behind the ejector model has been explained, along with a preliminary assessment of the ideal motive flow nozzle and combined flow diffuser profiles for ensuring linear acceleration / deceleration of the fluid. The ideal motive flow nozzle was found to be particularly elongated in shape, which is due to the substantial decrease in density once the fluid drops into the saturation region.

It was intended to continue analysing the optimum shape of the ejector using a 2 or 3 dimensional fluid dynamics package. A database of R744 thermophysical properties was created, which was formatted into a manner compatible with ANSYS CFX. However, the author was unable to make the software accept the database in the time available, despite repeated attempts. Therefore, 2 or 3 dimensional analysis was not possible.

Potential design methodologies for the compressors and work expanders have been explored, including: a centrifugal compressor and a trochoidal gerotor pump. A centrifugal compressor impeller design methodology has been presented, and this is included with Appendix B. The basic theory trochoidal devices has been discussed, and a methodology for the generation of an outer and inner rotor profile is given. The author's intention was to continue this area of research by analysing centrifugal compressor concepts and gerotor concepts in a fluid dynamics package, but this was not possible.

Chapter 6

Overall Conclusions

Worldwide demand for air conditioning is predicted to increase by 72 % by the year 2100, primarily due to the increase in economic productivity of south east Asia and Africa, which will result in an improvement in living standards and a consequent increase in demand for air conditioning. It is predicted that this effect will be compounded by climate change. Therefore, the efficient, low carbon and low cost provision of chilled water for air conditioning systems is both a huge challenge and opportunity. Trigeneration (the combined generation of electricity, heating and cooling) is a progression of cogeneration (the combined generation of electricity and heating), which will enable this goal to be reached.

This Thesis begins by providing an overview of trigeneration system design, thermal storage technologies and trigeneration control strategies. Trigeneration is shown to deliver an improved EUF over a system where electricity, heating and cooling are produced separately [21, 28–30]. Trigeneration control and operation strategies are discussed and analysed at length in a number of studies [23, 25, 26, 33, 36, 37], which conclude that the ideal control and operation strategy is dependent upon climatic conditions and the performance parameters of the trigeneration system.

Thermally activated heat pumps which can be integrated into trigeneration systems are identified as a key research topic. Chapter 2 begins with a review of single component and multi component, zeotropic and azeotropic refrigerants.

Natural refrigerants such as R744 and R717 are identified as featuring heavily in research over the past decade, owing to a continued move towards low GWP and low ODP refrigerants, driven in part by the Montreal protocol. The use of highly zeotropic refrigerant mixtures, such as LiBr - H_2O and H_2O - NH_3, in thermally activated absorption heat pumps is discussed, and a number of concepts and recent advances to increase the COP are presented. These include: multi - stage / multi - effect cycles, generator - absorber exchanger cycles and vapour recompression cycles. Triple - stage triple - effect absorption chillers are capable of achieving a COP_c of approximately 1.6, but suffer from corrosion in the upper generator due to the high temperatures [48]. The COP is both a function of the upper generation temperature, chilled water temperature, load conditions and the flow arrangement. A brief review of multi - bed and multi - stage adsorption heat pumps, and sorbent and sorbate pairs demonstrates that COP of this technology is still far below that of absorption heat pumps. A review of R744 Mechanical Vapour Compression (MVC) heat pumps along with a review advances Supercritical Carbon Dioxide (S-CO2) power cycle concepts is provided. It is evident from the review of literature that there is a small scope for innovations in multi - stage multi - effect absorption heat pump cycle design, and a significant scope for innovations in R744 heat pump cycle design. Therefore, the analysis of multi - stage multi - effect absorption heat pump cycle and R744 heat pump cycle concepts form the key contributions to research presented within this Thesis.

Chapter 3 explores two types of thermally activated absorption heat pumps: multi - effect / multi - stage H_2O - NH_3 absorption heat pumps and multi - effect / multi - stage LiBr - H_2O compression - absorption heat pumps. It is demonstrated that the double - stage / triple - effect H_2O - NH_3 absorption heat pump cycle can achieve a COP_c equivalent to a triple - stage / triple - effect LiBr - H_2O absorption heat pump, but with one fewer stage.

The sequence of internal heat recuperation devices within the cycle is shown to be vital to the performance. The double - stage / triple - effect H_2O - NH_3 ab-

sorption heat pump cycle is able to achieve a theoretical COP_c of 1.765. A triple - stage / quintuple - effect cycle is conceptualised, but temperature required in the upper generator is too high for the thermophysical properties of the ammonia and water mixture to be resolved.

Whilst the double - stage / triple - effect H_2O - NH_3 absorption heat pump cycle appears to be promising, a number of patents for similar concepts already exist or have existed [52, 53]. Therefore this cycle is not considered suitable for further research and development.

Singe - stage / single - effect, double - stage / double - effect and triple - stage / triple - effect LiBr - H_2O compression - absorption heat pump cycles are demonstrated to achieve a significant improvement in COP_c over their conventional absorption heat pump cycle counterparts. The triple - stage / triple - effect LiBr - H_2O compression - absorption heat pump is shown to achieve a $COP_{c,th}$ of 2.0, when the steam compressor has a pressure ratio of 2.0. The net effect of the addition of the compressor to the evaporator outlet is not only an increase in $COP_{c,th}$, but also a reduction in generation temperature. The corresponding $COP_{c,th}$ is demonstrated to be over 16.0 in all scenarios analysed.

Whilst the triple - stage / triple - effect LiBr - H_2O absorption - compression heat pump cycle appears to be a promising area for future research, the extremely low pressure and density of the steam exiting the evaporator means that the very high volumetric flowrate through the compressor would result in it being almost impracticably large. (6.1 m^3/s for 100 kW of cooling output). Therefore the absorption - compression cycle is not considered as a topic of further research.

Chapter 4 identifies three novel thermally and mechanically or pure thermally activated transcritical R744 heat pump cycles which are conceptualised, modelled and analysed. Each of these cycles are capable of providing simultaneous heating and cooling, and are designed to use the thermal energy in the exhaust gases from a Primary Generation Unit (PGU), in this instance a gas turbine. Cycle 2 is identifed as the preferred heat pump cycle as it provides a higher COP_c and

COP_h than Cycle 1. Cycle 3 is a minor evolution of Cycle 2 and is capable of providing mechanical work output as well as producing hot water and chilled water, however the small magnitude of the mechical work output and complexity of a split flow compressor meant that Cycle 3 is not pursued further. Cycle 2 is capable of providing coolth (10 °C) at a $COP_{c,th}$ of 1.58 and hot water (65 °C) at a $COP_{h,th}$ 2.41, with a first stage expander inlet temperature of 350 °C.

These performance figures for COP_c are very similar to those theoretically achieved by triple - stage LiBr - H_2O absorption chillers. However, Cycle 2 is capable also simultaneously producing hot water at 65 °C. Cycle 2 requires half the number of processes of a triple - stage LiBr - H_2O absorption chiller and uses a single working fluid, further simplifying the system and the control.

It is demonstrated that Cycle 2 performs considerably better than a 'separates system' of a supercritical CO_2 Brayton cycle linked to a R744 MVC heat pump cycle, achieving a 65% and 145% increase in $COP_{c,th}$ and $COP_{h,th}$ respectively, with an expander inlet temperature of 250 °C. It is also demonstrated that when integrated within a trigeneration system with a gas turbine as the PGU, the optimum first stage work expander inlet temperature is between 240°C and 275 °C. The cycle is able achieve a maximum COP_c of 0.84, and maximum COP_c of 1.45 in this scenario (i.e. for every 1 kWh of exhaust heat, 0.84 kWh of coolth and 1.45 kWh of hot water are produced).

Three novel thermally and mechanically or pure thermally activated transcritical R744 heat pump cycles have been conceptualised, modelled and analysed. Each of these cycles are capable of providing simultaneous heating and cooling, and is designed to use the thermal energy in the exhaust gases from a Primary Generation Unit (PGU), in this instance a gas turbine. Cycle 2 was identifed as the preferred heat pump cycle as it provides a higher COP_c and COP_h than Cycle 1. Cycle 3 is a minor evolution of Cycle 2 and is capable of providing mechanical work output as well as producing hot water and chilled water, however the small magnitude of the mechical work output and complexity of a split flow compressor

meant that Cycle 3 was not pursued further. Cycle 2 is capable of providing coolth (10 °C) at a $COP_{c,th}$ of 1.58 and hot water (65 °C) at a $COP_{h,th}$ 2.41, with a first stage expander inlet temperature of 350 °C.

These performance figures for COP_c are very similar to those theoretically achieved by triple - stage LiBr - H_2O absorption chillers, as demonstrated earlier (n.b. typically $COP_c = 1.6$). However, Cycle 2 is capable also simultaneously producing hot water at 65 °C. Cycle 2 requires half the number of processes of a triple - stage LiBr - H_2O absorption chiller and uses a single working fluid, further simplifying the system and the control. Chapter 5 provides an overview of an initial component analysis and design for key components of Cycle 2, such as: the internal heat recuperator, ejector, work expander and supercritical fluid cooler.

It was then shown that Cycle 2 performance considerably better than a 'separates system' of a supercritical CO_2 Brayton cycle linked to a R744 MVC heat pump cycle, achieving a 65% and 145% increase in $COP_{c,th}$ and $COP_{h,th}$ respectively, with an expander inlet temperature of 250 °C.

Lastly, it has been demonstrated that when integrated within a trigeneration system with a gas turbine as the PGU, the optimum first stage work expander inlet temperature is between 240°C and 275 °C. The cycle is capable achieve a maximum COP_c of 0.84, and maximum COP_c of 1.45 in this scenario (i.e. for every 1 kWh of exhaust heat, 0.84 kWh of coolth and 1.45 kWh of hot water are produced).

Chapter 5 documents and initial component analysis and design for key components of Cycle 2, including: the internal heat recuperator, ejector, work expander and supercritical fluid cooler. A design and calculation methodology is presented with the purpose of forming the continuation of this research from a Technology Readiness Level[1] of 2 (technology concept and / or application formulated) to a Technology Readiness Level of 3 (analytical and experimental critical function and / or characteristic proof - of - concept).

[1]Technology Readiness Level is a widely used concept to estimate the maturity of specific technologies

References

[1] Stan Cox. *Loosing Our Cool: Uncomfortable Truths About Our Air-Conditioned World*. New Press, 2010.

[2] Morna Isaac and Detlef P. van Vuuren. Modeling global residential sector energy demand for heating and air conditioning in the context of climate change. *Energy Policy*, 37(2):507–521, February 2009.

[3] K. Edem NTsoukpoe, Hui Liu, Nolwenn Le Pierrès, and Lingai Luo. A review on long-term sorption solar energy storage. *Renewable and Sustainable Energy Reviews*, 13(9):2385–2396, December 2009.

[4] D Wu and R Wang. Combined cooling, heating and power: A review. *Progress in Energy and Combustion Science*, 32(5-6):459–495, September 2006.

[5] Frank de Bruijn. The current status of fuel cell technology for mobile and stationary applications. *Green Chemistry*, 7(3):132, 2005.

[6] Antoni Gil, Marc Medrano, Ingrid Martorell, Ana Lázaro, Pablo Dolado, Belén Zalba, and Luisa F. Cabeza. State of the art on high temperature thermal energy storage for power generation. Part 1Concepts, materials and modellization. *Renewable and Sustainable Energy Reviews*, 14(1):31–55, January 2010.

[7] H Michels and R Pitzpaal. Cascaded latent heat storage for parabolic trough solar power plants. *Solar Energy*, 81(6):829–837, June 2007.

[8] a Kandari. Thermal stratification in hot storage-tanks. *Applied Energy*, 35(4):299–315, 1990.

[9] U Herrmann. Two-tank molten salt storage for parabolic trough solar power plants. *Energy*, 29(5-6):883–893, May 2004.

[10] B Zalba. Review on thermal energy storage with phase change: materials, heat transfer analysis and applications. *Applied Thermal Engineering*, 23(3):251–283, February 2003.

[11] Doug Brosseau, Mike Edgar, John W. Kelton, Kye Chisman, Daniel Ray, and Blaine Emms. Testing of Thermocline Filler Materials and Molten-Salt Heat Transfer Fluids for Thermal Energy Storage Systems in Parabolic Trough Power Plants. *Solar Energy*, (July):587–595, 2004.

[12] Francis Agyenim, Neil Hewitt, Philip Eames, and Mervyn Smyth. A review of materials, heat transfer and phase change problem formulation for latent heat thermal energy storage systems (LHTESS). *Renewable and Sustainable Energy Reviews*, 14(2):615–628, February 2010.

[13] a Sharma, V Tyagi, C Chen, and D Buddhi. Review on thermal energy storage with phase change materials and applications. *Renewable and Sustainable Energy Reviews*, 13(2):318–345, February 2009.

[14] E. Halawa and W. Saman. Thermal performance analysis of a phase change thermal storage unit for space heating. *Renewable Energy*, 36(1):259–264, January 2011.

[15] V. M. van Essen, H. a. Zondag, J. Cot Gores, L. P. J. Bleijendaal, M. Bakker, R. Schuitema, W. G. J. van Helden, Z. He, and C. C. M. Rindt. Characterization of MgSO4 Hydrate for Thermochemical Seasonal Heat Storage. *Journal of Solar Energy Engineering*, 131(4):041014–1 – 041014–7, 2009.

[16] Franziska Schaube, Antje Wörner, and Rainer Tamme. High temperature thermo-chemical heat storage for CSP using gas-solid reactions. In *System*.

[17] Bunsen Wong, Lloyd Brown, Franziska Schaube, Rainer Tamme, and Christian Sattler. Oxide based thermochemical heat storage. In *Lloydia (Cincinnati)*, pages 1–8.

[18] R Weber and V Dorer. Long-term heat storage with NaOH. *Vacuum*, 82(7):708–716, March 2008.

[19] Chris Bales and Svante Nordlander. TCA Evaluation - Lab Measurements, Modelling and Systems Simulations. Technical Report December, 2005.

[20] Maria Mottillo. Modelling an Adsorption System for the Seasonal Storage of Heat in Residential Buildings. Technical report, Department of Building, Civil and Environmental Engineering, Concordia University, Montréal, Canada, 2002.

[21] Mohammad Ameri, Ali Behbahaninia, and Amir Abbas Tanha. Thermodynamic analysis of a tri-generation system based on micro-gas turbine with a steam ejector refrigeration system. *Energy*, 35(5):2203–2209, May 2010.

[22] H Li, L Fu, K Geng, and Y Jiang. Energy utilization evaluation of CCHP systems. *Energy and Buildings*, 38(3):253–257, March 2006.

[23] Jiang-Jiang Wang, You-Yin Jing, and Chun-Fa Zhang. Optimization of capacity and operation for CCHP system by genetic algorithm. *Applied Energy*, 87(4):1325–1335, April 2010.

[24] Aiying Rong, Henri Hakonen, and Risto Lahdelma. An efficient linear model and optimisation algorithm for multi-site combined heat and power production. *European Journal of Operational Research*, 168(2):612–632, January 2006.

[25] a Rong, R Lahdelma, and P Luh. Lagrangian relaxation based algorithm for trigeneration planning with storages. *European Journal of Operational Research*, 188(1):240–257, July 2008.

[26] K.C. Kavvadias, a.P. Tosios, and Z.B. Maroulis. Design of a combined heating, cooling and power system: Sizing, operation strategy selection and parametric analysis. *Energy Conversion and Management*, 51(4):833–845, April 2010.

[27] N Fumo, P J Mago, and L M Chamra. Hybrid-cooling, combined cooling, heating, and power systems. *Proceedings of the Institution of Mechanical Engineers, Part A: Journal of Power and Energy*, 223(5):487–495, August 2009.

[28] S Tassou, I Chaer, N Sugiartha, Y Ge, and D Marriott. Application of tri-generation systems to the food retail industry. *Energy Conversion and Management*, 48(11):2988–2995, November 2007.

[29] S Acha, G Mavromatidis, V Caritte, and N Shah. Effective low-cost energy saving strategies in supermarkets: An uk case study. *Proceedings of the 26th International Conference on Efficiency, Cost, Optimization, Simulation and Environmental Impact of Energy Systems, ECOS 2013*, 2013.

[30] G Mavromatidis, S Acha, and N Shah. Diagnostic tools of energy performance for supermarkets using artificial neural network algorithms. *ENERGY AND BUILDINGS*, 62:304–314, 2013.

[31] Sau Man Lai and Chi Wai Hui. Feasibility and flexibility for a trigeneration system. *Energy*, 34(10):1693–1704, October 2009.

[32] Sau Man Lai and Chi Wai Hui. Integration of trigeneration system and thermal storage under demand uncertainties. *Applied Energy*, 87(9):2868–2880, September 2010.

[33] J Miguez. Feasibility of a new domestic CHP trigeneration with heat pump: I. Design and development. *Applied Thermal Engineering*, 24(10):1409–1419, July 2004.

[34] E. Cardona and a. Piacentino. A methodology for sizing a trigeneration plant in mediterranean areas. *Applied Thermal Engineering*, 23(13):1665–1680, September 2003.

[35] E Cardona, a Piacentino, and F Cardona. Matching economical, energetic and environmental benefits: An analysis for hybrid CHCP-heat pump systems. *Energy Conversion and Management*, 47(20):3530–3542, December 2006.

[36] P.J. Mago and L.M. Chamra. Analysis and optimization of CCHP systems based on energy, economical, and environmental considerations. *Energy and Buildings*, 41(10):1099–1106, October 2009.

[37] P.J. Mago, L.M. Chamra, and J. Ramsay. Micro-combined cooling, heating and power systems hybrid electric-thermal load following operation. *Applied Thermal Engineering*, 30(8-9):800–806, June 2010.

[38] Piers Forster and Venkatachalam Ramaswamy. Changes in Atmospheric Constituents and in Radiative Forcing. Technical report.

[39] Kyoto Protocol to the United Nations Framework Convention on Climate Change, 1998.

[40] Directive 2006/40/EC of the European Parliament and of the Council, 2006.

[41] L Kairouani and E Nehdi. Cooling performance and energy saving of a compressionabsorption refrigeration system assisted by geothermal energy. *Applied Thermal Engineering*, 26(2-3):288–294, February 2006.

[42] Douglas M. Robinson and Eckhard a. Groll. Efficiencies of transcritical

CO2 cycles with and without an expansion turbine. *International Journal of Refrigeration*, 21(7):577–589, November 1998.

[43] Jahar Sarkar and Souvik Bhattacharyya. Thermodynamic analyses and optimization of a transcritical N2O refrigeration cycle. *International Journal of Refrigeration*, 33(1):33–40, January 2010.

[44] H Kruse and H Russmann. The natural fluid nitrous oxidean option as substitute for low temperature synthetic refrigerants. *International Journal of Refrigeration*, 29(5):799–806, August 2006.

[45] P Srikhirin. A review of absorption refrigeration technologies. *Renewable and Sustainable Energy Reviews*, 5(4):343–372, December 2001.

[46] DeVault. Triple effect absorption chiller utilising two refrigeration circuits, 1993.

[47] Y Kaita. Simulation results of triple-effect absorption cycles. *International Journal of Refrigeration*, 25(7):999–1007, November 2002.

[48] Leilei Wang, Shijun You, Huan Zhang, and Xianli Li. Simulation of gas-fired triple-effect LiBr/water absorption cooling system with exhaust heat recovery generator. *Transactions of Tianjin University*, 16(3):187–193, May 2010.

[49] G Grossman and R DeVault. Simulation and Performance Analysis of a 4-Effect Lithium Bromide-Water Absorption Chiller under Contract No . DE-AC05-840R21400 Prepared by the Dl SCLAl MER Portions of this document may be illegible in electronic image products . Images are produced fro. In *Simulation*, 2008.

[50] Yousef S H Najjar. Pergamon. *Applied Thermal EngineeringThermal Engineering*, 16(2), 1996.

[51] S Adewusi. Second law based thermodynamic analysis of ammonia?water absorption systems. *Energy Conversion and Management*, 45(15-16):2355–2369, September 2004.

[52] R DeVault. Seven-effect absorption refrigeation, 1989.

[53] R DeVault. Dual-circuit, multiple-effect refrigeration system and method, 1995.

[54] Hajizadeh Aghdam, F. Ranjbar, and S.M. Seyed Mahmoudi. Performance Comparison of Triple-Effect Parallel Flow and Series Flow Absorption Refrigeration Systems. *Journal of Applied Sciences*, 8(16):2913–2918, December 2008.

[55] Hongxi Yin, Ming Qu, and David H. Archer. Model based experimental performance analysis of a microscale LiBrH2O steam-driven double-effect absorption Chiller. *Applied Thermal Engineering*, 30(13):1741–1750, September 2010.

[56] Sam V Shelton, Central Park West, and Laura A Schaefer. Modelling and Analysis of the Air Cooled Ammonia-Water Triple Effect Cycle. Technical report, 1995.

[57] D Boer, M Valles, and A Coronas. Performance of double effect absorption compression cycles for air-conditioning using methanolTEGDME and TFETEGDME systems as working pairs. *International Journal of Refrigeration*, 21(7):542–555, November 1998.

[58] H Lee, K Koo, S Jeong, J Kim, and Y Oh. Thermodynamic design data and performance evaluation of the water + lithium bromide + lithium iodide + lithium nitrate + lithium chloride system for absorption chiller. *Applied Thermal Engineering*, 20:707–720, 2000.

[59] C Park, J Koo, and Y Kang. Performance analysis of ammonia absorption

GAX cycle for combined cooling and hot water supply modes. *International Journal of Refrigeration*, 31(4):727–733, June 2008.

[60] Y Kang. An advanced GAX cycle for waste heat recovery: WGAX cycle. *Applied Thermal Engineering*, 19(9):933–947, September 1999.

[61] a. Rameshkumar, M. Udayakumar, and R. Saravanan. Heat transfer studies on a GAXAC (generator-absorber-exchange absorption compression) cooler. *Applied Energy*, 86(10):2056–2064, October 2009.

[62] J Kim. Simulation of the compressor-assisted triple-effect H2O/LiBr absorption cooling cycles. *Applied Thermal Engineering*, 22(3):295–308, March 2002.

[63] Keith E Herold, Lawrence A Howe, and Reinhard Radermacher. Analysis of a hybrid compression-absorption cycle using lithium bromide and water as the working fluid. *International Journal of Refrigeration*, 14:264–272, 1991.

[64] R. Ventas, a. Lecuona, a. Zacarías, and M. Venegas. Ammonia-lithium nitrate absorption chiller with an integrated low-pressure compression booster cycle for low driving temperatures. *Applied Thermal Engineering*, 30(11-12):1351–1359, August 2010.

[65] R. Ayala, C.L. Heard, and F.a. Holland. Ammonia/lithium nitrate absorption/compression refrigeration cycle. Part II. experimental. *Applied Thermal Engineering*, 18(8):661–670, August 1998.

[66] R. Ayala, C.L. Heard, and F.a. Holland. Ammonia/lithium nitrate absorption/compression refrigeration cycle. Part I. Simulation. *Applied Thermal Engineering*, 17(3):223–233, March 1997.

[67] Y Kang. Recherche avancée : analyse de la performance des cycles hybrides GAX (HGAX). *International Journal of Refrigeration*, 27(4):442–448, June 2004.

[68] W Worek. Enhancement of a double-effect absorption cooling system using a vapor recompression absorber. *Energy*, 28(12):1151–1163, October 2003.

[69] Daniele Ludovisi, William M Worek, and Milton Meckler. Simulation of a Double-Effect Absorber Cooling System Operating at Elevated Vapor Recompression Levels Simulation of a Double-Effect Absorber Vapor Recompression Levels. *HVAC&R Research*, 12(3):533–547, 2006.

[70] Milton Meckler. Enhanced lithium bromide absorption cycle water vapor recompression absorber.pdf, 1998.

[71] B Saha. Solar/waste heat driven two-stage adsorption chiller: the prototype. *Renewable Energy*, 23(1):93–101, May 2001.

[72] T.X. Li, R.Z. Wang, J.K. Kiplagat, L.W. Wang, and R.G. Oliveira. A conceptual design and performance analysis of a triple-effect solidgas thermochemical sorption refrigeration system with internal heat recovery. *Chemical Engineering Science*, 64(14):3376–3384, July 2009.

[73] P. Muthukumar and M. Groll. Metal hydride based heating and cooling systems: A review. *International Journal of Hydrogen Energy*, 35(8):3817–3831, April 2010.

[74] Gustav Lorentzen. Revival of carbon dioxide as a refrigerant. *International Journal of Refrigeration*, 17(January):292–302, 1994.

[75] Jahar Sarkar. Review on Cycle Modifications of Transcritical CO 2 Refrigeration and Heat Pump Systems. *Advanced Research in Mechanical Engineering*, 1:22–29, 2010.

[76] J Sarkar, S Bhattacharyya, and M Gopal. Simulation of a transcritical CO2 heat pump cycle for simultaneous cooling and heating applications. *International Journal of Refrigeration*, 29(5):735–743, August 2006.

[77] Yang Chen. *Thermodynamic Cycles using Carbon Dioxide as Working Fluid*. PhD thesis, 2011.

[78] Steven A Wright, Ross F Radel, Milton E Vernon, Gary E Rochau, and Paul S Pickard. Operation and Analysis of a Supercritical CO2 Brayton Cycle. Technical Report September, Sandia National Laboratories, 2010.

[79] J. Sarkar and Souvik Bhattacharyya. Optimization of recompression S-CO2 power cycle with reheating. *Energy Conversion and Management*, 50(8):1939–1945, August 2009.

[80] Masanori Aritomi, Takao Ishizuka, Yasushi Muto, and Nobuyoshi Tsuzuki. Performance Test Results of a Supercritical CO2 Compressor Used in a New Gas Turbine Generating System. *Journal of Power and Energy Systems*, 5(1):45–59, 2011.

[81] Motoaki Utamura. Thermodynamic Analysis of Part-Flow Cycle Supercritical CO2 Gas Turbines. *Journal of Engineering for Gas Turbines and Power*, 132(11):111701, 2010.

[82] Craig S Turchi. Supercritical CO 2 for Application in Concentrating Solar Power Systems. In *Supercritical CO2 Power Cycle Symposium*, number Figure 1, pages 1–5, 2009.

[83] H Yamaguchi, X Zhang, K Fujima, M Enomoto, and N Sawada. Solar energy powered Rankine cycle using supercritical CO2. *Applied Thermal Engineering*, 26(17-18):2345–2354, December 2006.

[84] Zhiwen Ma and Craig S Turchi. Advanced Supercritical Carbon Dioxide Power Cycle Configurations for Use in Concentrating Solar Power Systems Preprint. In *Supercritical CO2 Power Cycle Symposium*, number March, 2011.

[85] Li Jing, Pei Gang, and Ji Jie. Optimization of low temperature solar thermal

electric generation with Organic Rankine Cycle in different areas. *Applied Energy*, 87(11):3355–3365, November 2010.

[86] J Sarkar. Optimization of a transcritical CO2 heat pump cycle for simultaneous cooling and heating applications. *International Journal of Refrigeration*, 27(8):830–838, December 2004.

[87] D Li and E Groll. Transcritical CO2 refrigeration cycle with ejector-expansion device. *International Journal of Refrigeration*, 28(5):766–773, August 2005.

[88] J Nickl, G Will, H Quack, and W Kraus. Integration of a three-stage expander into a CO2 refrigeration system. *International Journal of Refrigeration*, 28(8):1219–1224, December 2005.

[89] R. Chacartegui, J.M. Muñoz de Escalona, D. Sánchez, B. Monje, and T. Sánchez. Alternative cycles based on carbon dioxide for central receiver solar power plants. *Applied Thermal Engineering*, 31(5):872–879, April 2011.

[90] B Saha. Performance evaluation of a low-temperature waste heat driven multi-bed adsorption chiller. *International Journal of Multiphase Flow*, 29(8):1249–1263, August 2003.

[91] Skander Jribi, Anutosh Chakraborty, Ibrahim I El-sharkawy, Bidyut Baran Saha, and Shigeru Koyama. Thermodynamic Analysis of Activated Carbon-CO 2 based Adsorption Cooling Cycles. Technical report, 2009.

[92] R Wang and R Oliveira. Adsorption refrigerationAn efficient way to make good use of waste heat and solar energy. *Progress in Energy and Combustion Science*, 32(4):424–458, 2006.

[93] By Shenyi Wu. *INVESTIGATION OF EJECTOR RE-COMPRESSION*. PhD thesis, University of Nottingham, 1999.

[94] Simona Steiu, Daniel Salavera, Joan Carles Bruno, and Alberto Coronas. A basis for the development of new ammoniawatersodium hydroxide absorption chillers. *International Journal of Refrigeration*, 32(4):577–587, June 2009.

[95] J Fernandezseara. Heat and mass transfer analysis of a helical coil rectifier in an ammonia?water absorption system. *International Journal of Thermal Sciences*, 42(8):783–794, August 2003.

[96] J Fernández-Seara. Study and control of the optimal generation temperature in NH3H2O absorption refrigeration systems. *Applied Thermal Engineering*, 21(3):343–357, February 2001.

[97] S. Deng, Y.J. Dai, R.Z. Wang, T. Matsuura, and Y. Yasui. Comparison study on performance of a hybrid solar-assisted CO2 heat pump. *Applied Thermal Engineering*, February 2011.

[98] Ding-Yu Peng and Donald B. Robinson. A New Two-Constant Equation of State. *Industrial & Engineering Chemistry Fundamentals*, 15(1):59–64, February 1976.

[99] JongSik Oh, Giridhari L. Agrawal, and Charles William BUckley. High efficiency R744 refrigeration system and cycle, 2010.

[100] M Kim. Fundamental process and system design issues in CO2 vapor compression systems. *Progress in Energy and Combustion Science*, 30(2):119–174, 2004.

[101] Jian Min Yin, Clark W Bullard, and Predrag S Hrnjak. R-744 gas cooler model development and validation. *International Journal of Refrigeration*, 24:692–701, 2001.

[102] B.S. Petukhov. Heat Transfer and Friction in Turbulent Pipe Flow with Variable Physical Properties. *Advances in Heat Transfer*, 6:503–564, 1970.

[103] P Simoes, J Fernandes, and J Mota. Dynamic model of a supercritical carbon dioxide heat exchanger. *The Journal of Supercritical Fluids*, 35(2):167–173, September 2005.

[104] Masafumi Nakagawa, Ariel R. Marasigan, and Takanori Matsukawa. Experimental analysis on the effect of internal heat exchanger in transcritical CO2 refrigeration cycle with two-phase ejector. *International Journal of Refrigeration*, pages 1–10, March 2010.

[105] S Elbel and P Hrnjak. Experimental validation of a prototype ejector designed to reduce throttling losses encountered in transcritical R744 system operation. *International Journal of Refrigeration*, 31:411–422, August 2007.

[106] Mark Holtzapple and Andrew Rabroker. Gerotor Apparatus for a Quasi-Isothermal Brayton Cycle Engine, 2010.

[107] Mark Holtzapple and George Rabroker. Gerotor apparatus for a quasi-isothermal Brayton cycle engine, 2010.

[108] James a. Mathias, Jon R. Johnston, Jiming Cao, Douglas K. Priedeman, and Richard N. Christensen. Experimental Testing of Gerotor and Scroll Expanders Used in, and Energetic and Exergetic Modeling of, an Organic Rankine Cycle. *Journal of Energy Resources Technology*, 131(1):012201–012210, 2009.

[109] Mark Holtzapple, George Rabroker, Michael Ross, Steven Atmur, and Gary Noyes. Gerotor apparatus for a quasi-isothermal Brayton cycle engine, 2010.

[110] Huijuan Chen, D. Yogi Goswami, and Elias K. Stefanakos. A review of thermodynamic cycles and working fluids for the conversion of low-grade heat. Technical report, July 2010.

[111] Jia Yan, Daniel C. H. Yang, and Shih-Hsi Tong. A New Gerotor Design Method With Switch Angle Assignability. *Journal of Mechanical Design*, 131(1):011006, 2009.

[112] Giovanni Mimmi, Università Pavia, Meccanica Strutturale, and Via Ferrata. On Design and Performance of Internal Epitrochoidal Pumps. In *ASME International Design Engineering Technical Conferences*, pages 1–8, 2006.

[113] Yii-Wen Hwang and Chiu-Fan Hsieh. Geometric Design Using Hypotrochoid and Nonundercutting Conditions for an Internal Cycloidal Gear. *Journal of Mechanical Design*, 129(4):413, 2007.

[114] G Bonandrini, G Mimmi, and C Rottenbacher. Theoretical analysis of internal epitrochoidal and hypotrochoidal machines. In *Proceedings of the Institution of Mechanical Engineers, Part C: Journal of Mechanical Engineering Science*, volume 223, pages 1469–1480, June 2009.

[115] C-F Hsieh. Non-undercutting region and property evaluation of epitrochoidal gerotor geometry. *Proceedings of the Institution of Mechanical Engineers, Part C: Journal of Mechanical Engineering Science*, 224(2):473–481, January 2010.

[116] D C H Yang, J Yan, and S-H Tong. Flowrate formulation and displacement analyses for deviation function-based gerotor pumps. *Proceedings of the Institution of Mechanical Engineers, Part C: Journal of Mechanical Engineering Science*, 225:480–487, January 2010.

[117] Chiu-Fan Hsieh. Influence of Gerotor Performance in Varied Geometrical Design Parameters. *Journal of Mechanical Design*, 131(12), 2009.

[118] Great Bnutin and Mechanical Engineering. Geometry for Trochoidal-Type Machines with Conjugate Envelopes. *Mechanism and Machine Theory*, 29(I):25–42, 1994.

Appendix A

R744 Heat Pump Cycle Early Concepts

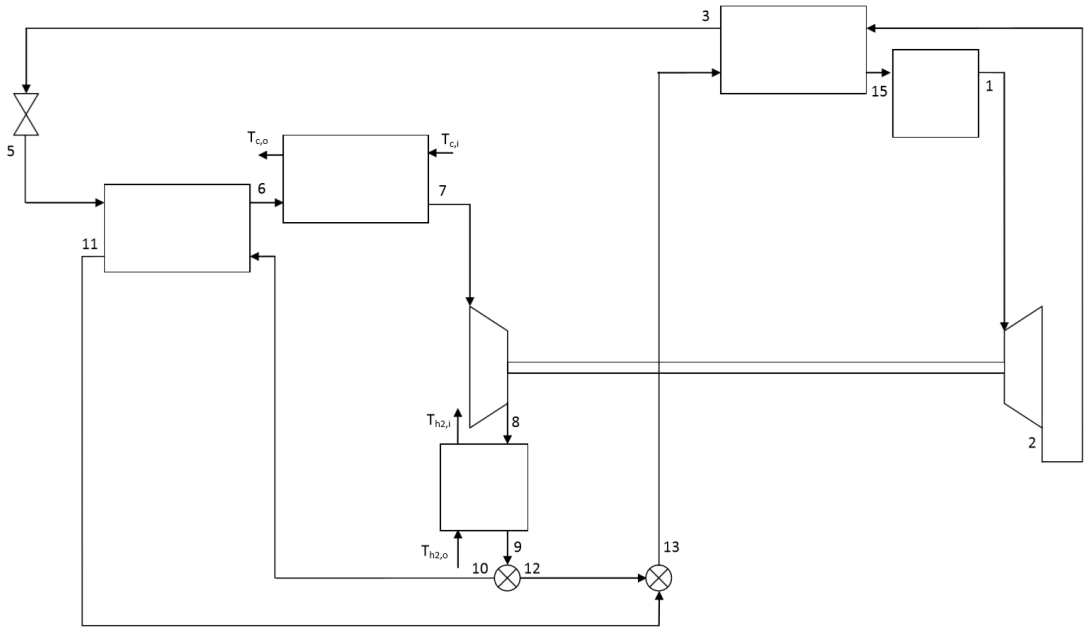

Figure A.1: Process flow diagram of R744 heat pump cycle concept 'Cycle A'

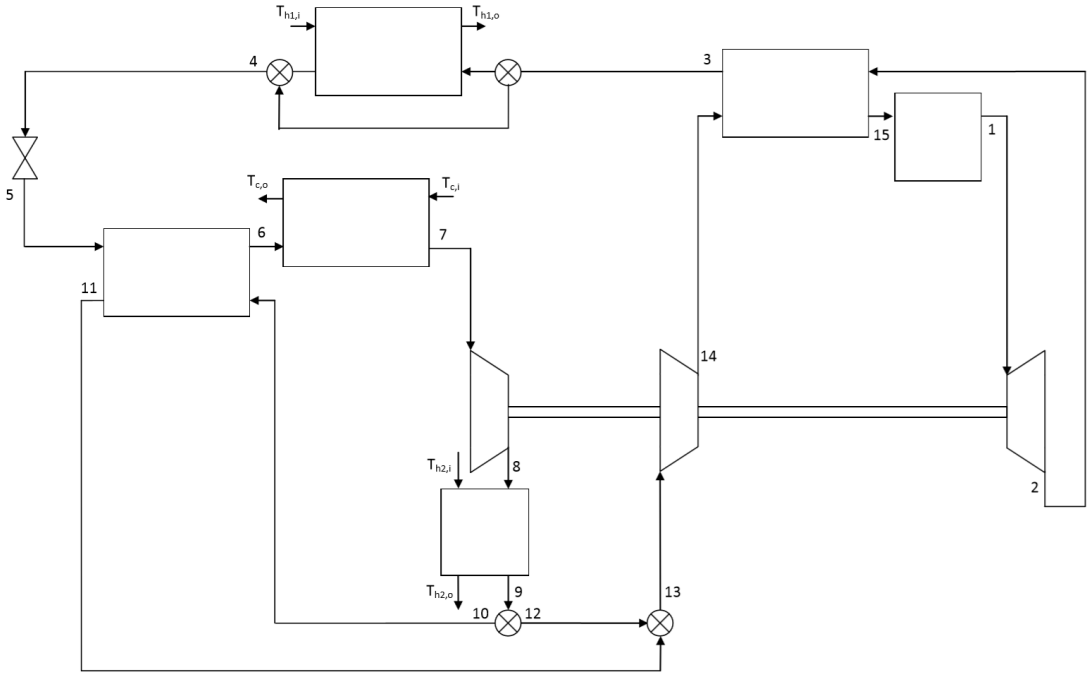

Figure A.2: Process flow diagram of R744 heat pump cycle concept 'Cycle B'

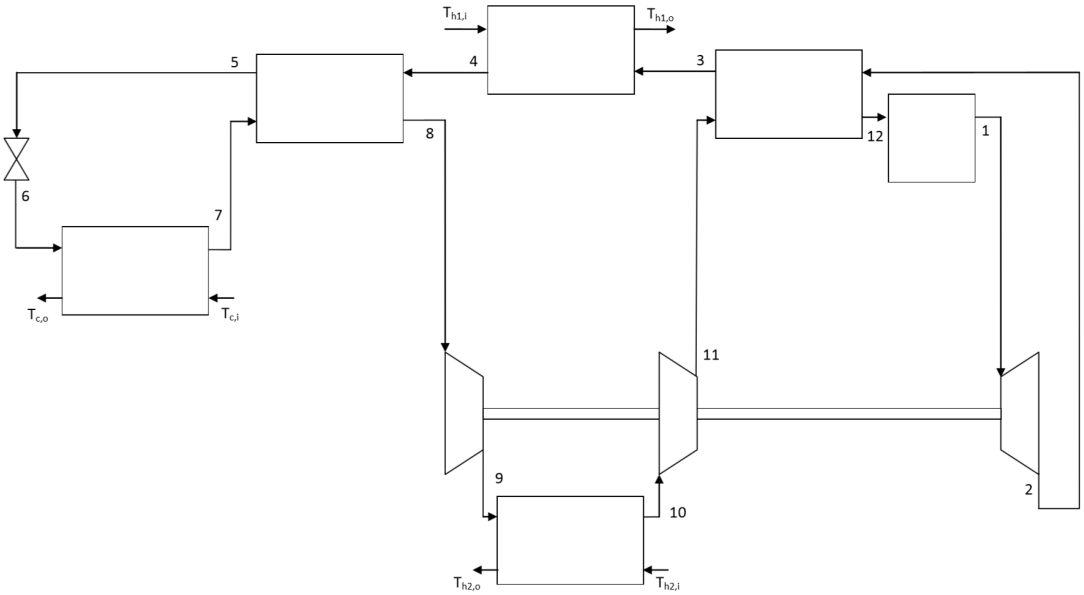

Figure A.3: Process flow diagram of R744 heat pump cycle concept 'Cycle C'

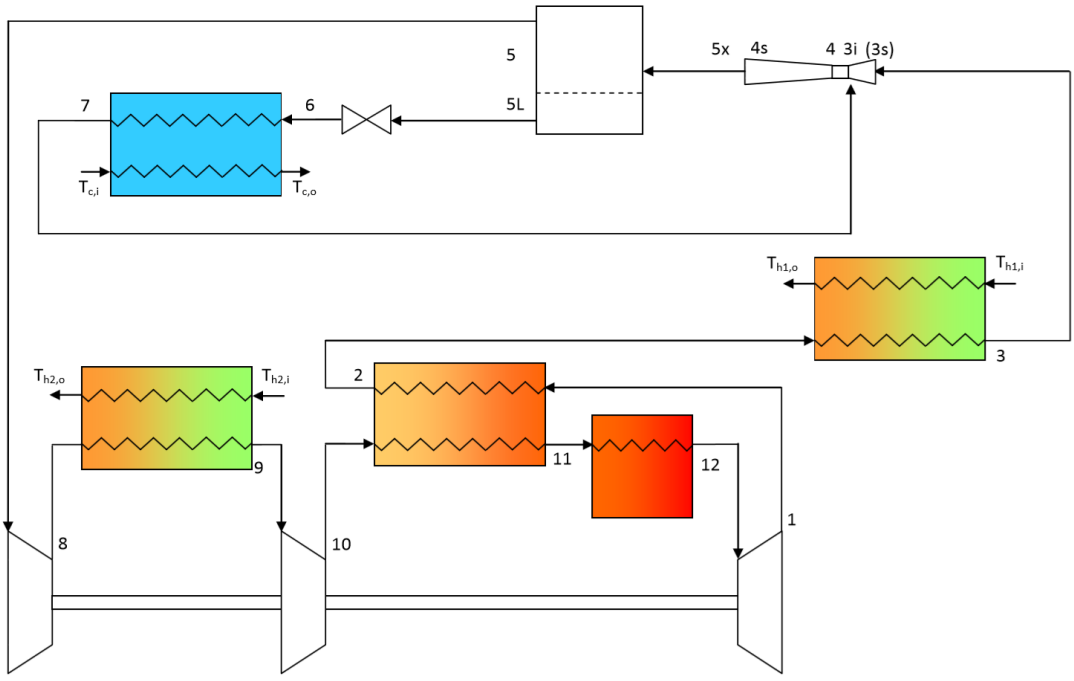

Figure A.4: Process flow diagram of R744 heat pump cycle concept 'Cycle D'

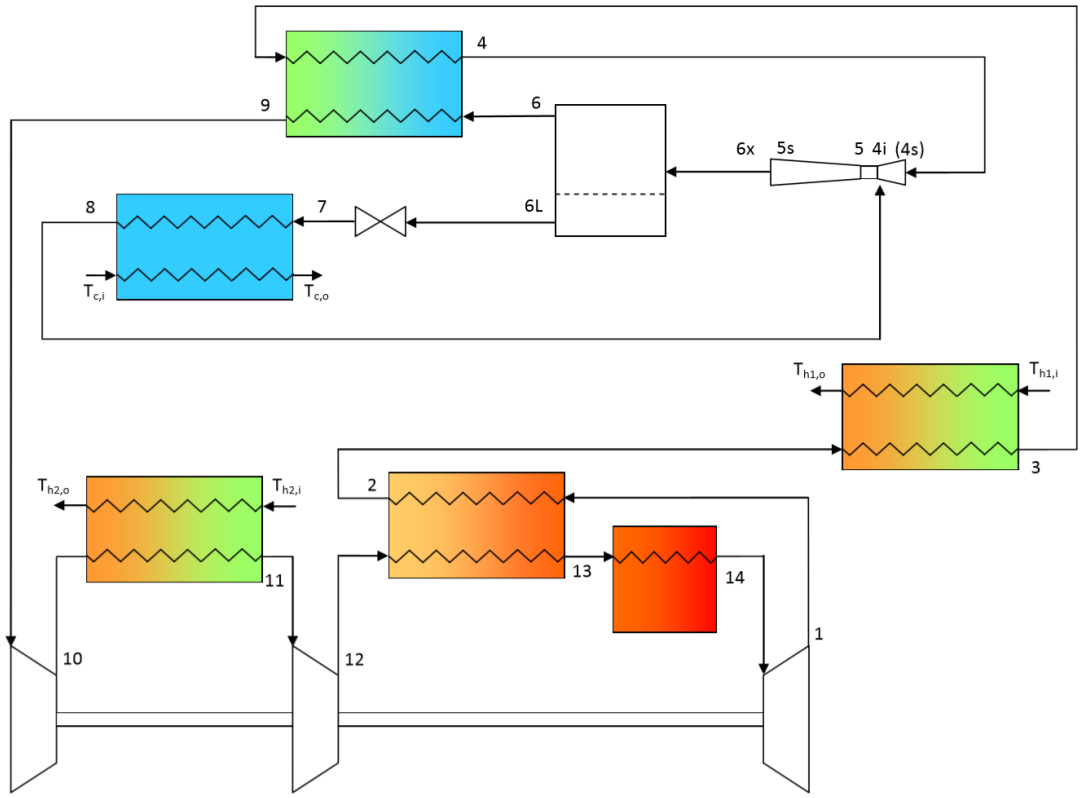

Figure A.5: Process flow diagram of R744 heat pump cycle concept 'Cycle E'

Appendix B

R744 Centrifugal Compressor Impeller Blade Geometry

Velocity triangles are given below.

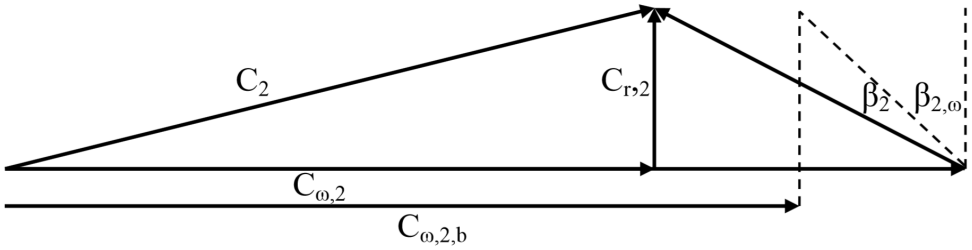

Figure B.1: Impeller outlet velocity triangle

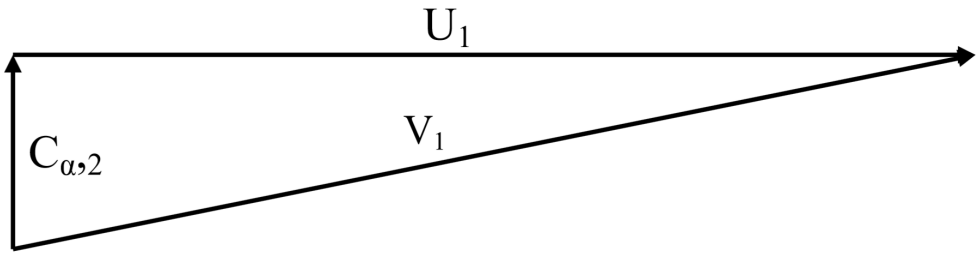

Figure B.2: Impeller inlet velocity triangle

The output of the computational code used to calculate the velocity triangles is given below.

$$R\$ = \text{'R744'} \tag{B.1}$$

$$N_{blade} = 6 \tag{B.2}$$

$$N_{splitter} = 6 \tag{B.3}$$

$$N = 50000 \tag{B.4}$$

$$b_1 = 0.01 \tag{B.5}$$

$$R_1 = 0.015 \tag{B.6}$$

$$\beta_{2,b} = 60 \tag{B.7}$$

$$\eta = 0.8 \tag{B.8}$$

$$m = 10 \tag{B.9}$$

$$P_{01} = 150 \tag{B.10}$$

$$P_{03} = 250 \tag{B.11}$$

$$T_{01} = 350 \tag{B.12}$$

$$\rho_{01} = \rho\left(R\$,\ \mathrm{T} = T_{01},\ \mathrm{P} = P_{01}\right) \tag{B.13}$$

$$S_{01} = \mathrm{s}\left(R\$,\ \mathrm{T} = T_{01},\ \mathrm{P} = P_{01}\right) \tag{B.14}$$

$$H_{01} = \mathrm{h}\left(R\$,\ \mathrm{T} = T_{01},\ \mathrm{P} = P_{01}\right) \tag{B.15}$$

$$S_{03,is} = S_{01} \tag{B.16}$$

$$H_{03,is} = \mathrm{h}\left(R\$,\ \mathrm{S} = S_{03,is},\ \mathrm{P} = P_{03}\right) \tag{B.17}$$

$$\rho_{03} = \rho\left(R\$,\ \mathrm{T} = T_{03},\ \mathrm{P} = P_{03}\right) \tag{B.18}$$

$$S_{03} = \mathrm{s}\left(R\$,\ \mathrm{T} = T_{03},\ \mathrm{P} = P_{03}\right) \tag{B.19}$$

$$H_{03} = H_{01} + \frac{H_{03,is} - H_{01}}{\eta} \tag{B.20}$$

$$T_{03} = \mathrm{T}\left(R\$,\ \mathrm{H} = H_{03},\ \mathrm{P} = P_{03}\right) \tag{B.21}$$

$$Work_{in} = (H_{03} - H_{01}) \cdot 1000 \tag{B.22}$$

$$U_2 = \frac{\frac{Work_{in}}{1.04 \cdot \sigma}}{C_{w,2}} \tag{B.23}$$

$$R_2 = U_2/\omega \tag{B.24}$$

$$U_1 = \omega \cdot R_1 \tag{B.25}$$

$$Q_1 = m/\rho_{01} \tag{B.26}$$

$$\omega = 2 \cdot 3.1415 \cdot N/60 \tag{B.27}$$

$$A_{1,annulus} = 3.1415 \cdot \left(\left((R_1)^2\right) - \left((R_1 - b_1)^2\right)\right) \tag{B.28}$$

$$A_{1,volute} = 3.1415 \cdot \left(\left((R_1)^2\right) - \left((R_1 - b_1)^2\right)\right) \cdot (\sin(\alpha_1)) \tag{B.29}$$

$$A_{1,volute,check} = 3.1415 \cdot b_1 \cdot (\sin(\alpha_1)) \cdot (\mathrm{Cos}(3.1415/N)) \cdot ((2 \cdot R_1) - b_1) \tag{B.30}$$

$$A_2 = 2 \cdot 3.1415 \cdot R_2 \cdot b_2 \tag{B.31}$$

$$A_{2,volute} = 2 \cdot 3.1415 \cdot R_2 \cdot b_2 \cdot (\mathrm{Cos}(\beta_2)) \tag{B.32}$$

$$\Delta P = P_{03} - P_{01} \tag{B.33}$$

$$\Delta T = T_{03} - T_{01} \tag{B.34}$$

$$\Delta H = H_{03} - H_{01} \tag{B.35}$$

$$Head = \delta P \cdot 9.81 \tag{B.36}$$

$$Ns = (2 \cdot 3.1415 \cdot N/60) \cdot \frac{(m/\rho_{01})^{0.5}}{(\Delta H \cdot 1000)^{0.75}} \tag{B.37}$$

$$T_{1,1} = T_{01} \tag{B.38}$$

$$P_{1,1} = P_{01} \tag{B.39}$$

$$\rho_{1,1} = \rho_{01} \tag{B.40}$$

$$C_{a,1,1} = \frac{m}{\rho_{1,1} \cdot A_{1,annulus}} \tag{B.41}$$

$$Cp_{1,2} = \mathrm{c_p}\,(R\$,\ \mathrm{T} = T_{1,1},\ \mathrm{P} = P_{1,1}) \tag{B.42}$$

$$Cv_{1,2} = \mathrm{c_v}\,(R\$,\ \mathrm{T} = T_{1,1},\ \mathrm{P} = P_{1,1}) \tag{B.43}$$

$$\gamma_{1,2} = \frac{Cp_{1,2}}{Cv_{1,2}} \tag{B.44}$$

$$T_{1,2} = T_{01} - \frac{C_{a,1,1}^2}{2 \cdot Cp_{1,2} \cdot 1000} \tag{B.45}$$

$$P_{1,2} = P_{01} \cdot \left(\left(\frac{T_{1,2}}{T_{1,1}}\right)^{\frac{GAMMA1_2}{\gamma_{1,2}-1}}\right) \tag{B.46}$$

$$\rho_{1,2} = \rho\left(R\$,\ \mathrm{T} = T_{1,2},\ \mathrm{P} = P_{1,2}\right) \tag{B.47}$$

$$C_{a,1,2} = \frac{m}{\rho_{1,2} \cdot A_{1,annulus}} \tag{B.48}$$

$$C_{a,1} = C_{a,1,2} \tag{B.49}$$

$$V_1 = \sqrt{\left(C_{a,1}^2\right) + \left(U_1^2\right)} \tag{B.50}$$

$$\alpha_1 = \arctan\left(C_{a,1}/U_1\right) \tag{B.51}$$

$$C_{r,2} = C_{a,1} \tag{B.52}$$

$$C_{w,2,b} = U_2 - C_{r,2} \cdot \tan\left(\beta_{2,b}\right) \tag{B.53}$$

$$\sigma = 1 - \left(\frac{\sqrt{\mathrm{Cos}(\beta_{2,b})}}{\left(N_{splitter} + N_{blade}\right)^{0.7}}\right) \tag{B.54}$$

$$C_{w,2} = \sigma \cdot C_{w,2,b} \tag{B.55}$$

$$C_2 = \sqrt{\left(C_{w,2}^2\right) + \left(C_{r,2}^2\right)} \tag{B.56}$$

$$V_2 = \sqrt{\left(\left(U_2 - C_{w,2}\right)^2\right) + \left(C_{r,2}^2\right)} \tag{B.57}$$

$$\beta_2 = \arctan\left(\frac{U_2 - C_{w,2}}{C_{r,2}}\right) \tag{B.58}$$

$$\eta_c = 0.8 \tag{B.59}$$

$$\eta_i = \sqrt{\eta_c} \tag{B.60}$$

$$Cp_2 = \mathrm{c_p}\left(R\$,\ \mathrm{P} = P_{02},\ \mathrm{T} = T_{02}\right) \tag{B.61}$$

$$Cv_2 = \mathrm{c_v}\left(R\$,\ \mathrm{P} = P_{02},\ \mathrm{T} = T_{02}\right) \tag{B.62}$$

$$\gamma_2 = Cp_2/Cv_2 \tag{B.63}$$

$$\Delta H_{imp,is} = \eta_i \cdot \Delta H \tag{B.64}$$

$$H_{02,is} = H_{01} + \Delta H_{imp,is} \tag{B.65}$$

$$S_{02,is} = S_{01} \tag{B.66}$$

$$P_{02} = \mathrm{P}\left(R\$,\ \mathrm{H} = H_{02,is},\ \mathrm{S} = S_{02,is}\right) \tag{B.67}$$

$$T_{02} = T_{03} \tag{B.68}$$

$$T_2 = T_{02} - \left(\frac{C_2^2}{2 \cdot Cp_2 \cdot 1000}\right) \tag{B.69}$$

$$P_2 = P_{02} \cdot \left((T_2/T_{02})^{\frac{\gamma_2}{\gamma_2 - 1}}\right) \tag{B.70}$$

$$\rho_2 = \rho\left(R\$,\ \mathrm{T} = T_2,\ \mathrm{P} = P_2\right) \tag{B.71}$$

$$A_2 = \frac{m}{(\rho_2 \cdot C_{r,2})} \quad \textbf{Calculate } \mathbf{b_{2!}} \tag{B.72}$$

Solution

$\alpha_1 = 24.24\,[\mathrm{deg}]$ $A_{1,annulus} = 0.0006283\,[\mathrm{m^2}]$

$A_{1,volute} = 0.0002579\,[\mathrm{m^2}]$ $A_{1,volute,check} = 0.0002579\,[\mathrm{m^2}]$

$A_2 = 0.0004941\,[\mathrm{m^2}]$ $A_{2,volute} = 0.0002004\,[\mathrm{m^2}]$

$\beta_2 = 66.07\,[\mathrm{deg}]$ $\beta_{2,b} = 60$

$b_1 = 0.01\,[\mathrm{m}]$ $b_2 = 0.001963\,[\mathrm{m}]$

$Cp_2 = 2.087\,[\mathrm{kJ/kgK}]$ $Cv_2 = 0.9024\,[\mathrm{kJ/kgK}]$

$C_2 = 134.8\,[\mathrm{m/s}]$ $C_{a,1} = 35.36\,[\mathrm{m/s}]$

$C_{r,2} = 35.36\,[\mathrm{m/s}]$ $C_{w,2} = 130.1\,[\mathrm{m/s}]$

$C_{w,2,b} = 148.6\,[\mathrm{m/s}]$ $\Delta H = 24.87\,[\mathrm{kJ/kg}]$

$\Delta H_{imp,is} = 22.24\,[\mathrm{kJ/kgK}]$ $\Delta P = 100\,[\mathrm{bar}]$

$\Delta T = 34.2\,[\mathrm{K}]$ $\eta = 0.8$

$\eta_c = 0.8$ $\eta_i = 0.8944$

$\gamma_2 = 2.312\,[\text{-}]$ $Head = 981\,[\mathrm{m}]$

$H_{01} = 403.4\,[\mathrm{kJ/kg}]$ $H_{02,is} = 425.6\,[\mathrm{kJ/kg}]$

$H_{03} = 428.2\,[\mathrm{kJ/kg}]$ $H_{03,is} = 423.3\,[\mathrm{kJ/kg}]$

$m = 10\,[\mathrm{kg/s}]$

$N = 50000$

$Ns = \mathbf{0.3945}\,[\mathrm{kg^{0.75}\text{-}m^{1.5}/s^{0.5}\text{-}kJ^{0.75}}]$

$N_{blade} = 6$

$N_{splitter} = 6$

$\omega = 5236$

$P_{01} = 150\,[\mathrm{bar}]$

$P_{02} = 263\,[\mathrm{bar}]$

$P_{03} = 250\,[\mathrm{bar}]$

$P_2 = 257.8\,[\mathrm{bar}]$

$Q_1 = 0.02226\,[\mathrm{m^3/s}]$

$R\$ = \text{'R744'}$

$\rho_{01} = 449.2\,[\mathrm{kg/m^3}]$

$\rho_{03} = 540.4\,[\mathrm{kg/m^3}]$

$\rho_2 = 572.4\,[\mathrm{kg/m^3}]$

$R_1 = 0.015\,[\mathrm{m}]$

$R_2 = 0.04007\,[\mathrm{m}]$

$\sigma = 0.8758$

$S_{01} = 1.601\,[\mathrm{kJ/kgK}]$

$S_{02,is} = 1.601\,[\mathrm{kJ/kgK}]$

$S_{03} = 1.614\,[\mathrm{kJ/kgK}]$

$S_{03,is} = 1.601\,[\mathrm{kJ/kgK}]$

$T_{01} = 350\,[\mathrm{K}]$

$T_{02} = 384.2\,[\mathrm{K}]$

$T_{03} = 384.2\,[\mathrm{K}]$

$T_2 = 379.8\,[\mathrm{K}]$

$U_1 = 78.54\,[\mathrm{m/s}]$

$U_2 = 209.8\,[\mathrm{m/s}]$

$V_1 = 86.13\,[\mathrm{m/s}]$

$V_2 = 87.18\,[\mathrm{m/s}]$

$Work_{in} = 24866\,[\mathrm{W}]$